

Electronic readout of DNA amplification in nanoliter chambers. Strategies towards highly parallel semiconductor-based nucleic acid amplification testing.

Présentée le 3 mars 2023

Faculté des sciences et techniques de l'ingénieur
Chaire Swiss-up en ingénierie - Laboratoire d'électronique pour les sciences du vivant
Programme doctoral en microsystemes et microélectronique

pour l'obtention du grade de Docteur ès Sciences

par

Saurabh TOMAR

Acceptée sur proposition du jury

Prof. C. S. Brès, présidente du jury
Prof. C. Guiducci, directrice de thèse
Prof. K. Shepard, rapporteur
Prof. P. Georgiou, rapporteur
Prof. G. Villanueva, rapporteur

Acknowledgments

For the lack of proper words, I fear this acknowledgment may be an understatement to the contributions of the people who have helped me reach this goal. Nevertheless, I will try my best.

Before anything else, I am incredibly grateful to my supervisor Prof. Carlotta Guiducci for allowing me to pursue my thesis at her laboratory. I appreciate her confidence in my abilities to take on such a complex endeavor. Thank you for your precious scientific advice and ideas and for reorienting me in my times of confusion. I appreciate your full confidence in my ideas and your allowing me complete freedom to explore them.

I would also like to thank the jury members, Prof. Camille Sophie Brès, Prof. Kenneth Shepard, Prof. Pantelis Georgiou and Prof. Guillermo Villanueva, for taking time out of their busy schedule to evaluate this work and provide their valuable feedback and comments on further improving the manuscript.

I am deeply indebted to my collaborators, without whom I would not have made it. I am really grateful to Barbora Lavickova for all the help with tackling the problems with molecular biology and for helping me realize a major part of my thesis. I cannot thank Charlotte Lasne, Auriane Cozic, Domenico Catucci and Amir Miran Zadeh enough, who helped me solve various challenging problems throughout this thesis. Their excellent scientific contributions to this work cannot be overstated. I also want to thank Antonios Kritikos and Dr. Anthony Croxatto for collaborating on detecting antibiotic-resistant bacteria. Their insight helped me discover new avenues where I can apply my research. I would also like to thank Prof. Polly Fordyce and Prof. Subhasish Mitra from Stanford University for hosting me in their labs. I am incredibly grateful to my collaborator Adam K. White at Fordyce Lab, for further expanding my understanding of molecular biology for diagnostics.

I am thankful to my CLSE colleagues who made this journey much easier and worth remembering. My Ph.D. twin Pierre, thanks for introducing me to hiking and teaching me how to swim! My office neighbor Till, thanks for all the encouragement and video game sessions! And Gloria, who kept rolling her eyes at all my poor jokes! My immense thanks to Heather, Monica, Sylvain, Enrico, Loulia and Erick for helping me with things I was not very good at. I want to thank Alessandro Novello and Camille Gilbert, with whom my collaboration was short but still led to a valuable contribution to the thesis. I want to acknowledge the valuable assistance of the staff at the center of microfabrication at EPFL (CMi) during the fabrication and development of new processes.

A special thanks to Widad for always being there for me and making me smile.

और अंत में मेरे प्रिय माँ और पिताजी। मुझे पता है कि मेरी कृतज्ञता पर्याप्त नहीं होगी, लेकिन मैं आपको उन सभी बलिदानों के लिए धन्यवाद देना चाहता हूँ जो आपने मुझे यहां तक पहुंचाने के लिए किए हैं। आप मेरे लिए निरंतर समर्थन के स्रोत रहे हैं। चरण स्पर्श!

Saurabh Tomar

Abstract

Polymerase chain reaction (PCR) has been the most significant driver in the field of nucleic acid testing (NAT) since its invention. Popularized as an abbreviation by the Covid-19 pandemic, PCR-based methods are the gold standard in the field of diagnostics and research. Constantly maturing on the technical front, PCR has already achieved the ultimate goal where it can detect the presence of a single nucleic acid molecule in the reaction mixture. However, such technological capability proved less than optimal during the outbreak of the Covid-19 pandemic. In fact, it led to the revelation that the next generation of NAT needs solutions that are low-cost, high-throughput and decentralized. The last decade and a half have already seen trends in a similar direction, only to be vindicated and accelerated by the emergence of the Covid-19 pandemic. One of the major reasons for the high cost and centralized nature of NAT is the use of optical labels as a readout method. High material costs, requiring complex optics for readout and being prone to deterioration in ambient conditions have restricted optical-NAT methods to specialized laboratory settings.

Steps to ameliorate these shortcomings have led to the development of label-free isothermal NAT methods. These readout methods sense chemical species like H^+ or pyrophosphates, which are formed as by-products of the biochemical reactions used to amplify nucleic acids. Sensing accumulation of H^+ ions or change in the reaction pH is one of the most popular label-free methods as its readout can be carried out electrically on relatively inexpensive CMOS chips. The principle is widely used by Ion Torrent in their next-generation sequencing solution, where they use millions of ion-sensitive field effect transistors (ISFET), fabricated by CMOS technology to sense H^+ by incorporation of a nucleotide. ISFET-based NAT solutions offer the unique advantage of compact size, high parallelism, integrated readout and low-cost per chip due to highly optimized manufacturing technology. Being a general method, readout based on H^+ sensing can be adapted to any amplification method, thereby reducing the complexity of the assay. The extremely high sensitivity of ISFETs, when combined with ultra-low volume partitioning microfluidics has the potential to offer low-cost and rapid NAT platforms that offer a wide range of assay choices, all on a centimeter-sized footprint.

However, to realize such solutions technological bottlenecks, specific to ISFETs need to be addressed. This thesis aims to address these challenges and lays down strategies for the realization of highly parallel semiconductor NAT devices. To avoid negatively affecting the signal-to-noise ratio of ISFET and minimize evaporation losses in ultra-low volumes, two molecular assays that can be operated at low temperatures have been developed. This work demonstrates a new microfluidic packaging strategy that requires no post-CMOS processing and allows for large-scale microfluidic integration on CMOS chips. The thesis concludes with a demonstration of DNA amplification readout via ISFETs in a nanoliter-sized volume, which can be scaled up in density to realize high-through non-optical digital-PCR-like solutions.

Keywords: ISFET, DNA, DNA amplification, PCR, label-free, reference electrode, SU-8, microfluidics, RPA, LAMP, microfluidic packaging, nucleic acid testing, evaporation, ultra-low volume, surface-to-volume ratio, nanowire, FET.

Résumé

L'amplification en chaîne par polymérase (PCR) a été un catalyseur de l'essor des tests d'amplification des acides nucléiques (TAAN). Popularisées comme abréviation par la pandémie du Covid-19, les méthodes basées sur la PCR sont la référence dans le domaine du diagnostic et de la recherche. En évolution constante sur le plan technique, la PCR est déjà parvenue à atteindre le but ultime : détecter la présence d'une seule molécule d'acide nucléique dans le mélange réactionnel. Cependant, une telle précision s'est avérée sous-optimale durant la pandémie du Covid-19. L'explosion du nombre de la fréquence des tests PCR a révélé le besoin de décentralisation de la prochaine génération de TAAN, tout en maintenant des coûts faibles. La dernière décennie s'inscrit dans cette direction, avec une accélération notable due à l'émergence de la pandémie du Covid-19. L'une des principales raisons du coût élevé et de la nature centralisée du TAAN est l'utilisation des marqueurs optiques comme méthode de lecture. Les coûts élevés des matériaux, la nécessité d'optiques complexes pour la lecture et la détérioration des capteurs dans les conditions ambiantes, ont cantonné les méthodes optiques de TAAN à des laboratoires spécialisés.

Les mesures visant à améliorer ces problèmes ont conduit au développement des méthodes TAAN isothermes sans marquage. Ces méthodes de lecture détectent les espèces chimiques comme les ions H^+ ou les pyrophosphates, tous deux sous-produits des réactions biochimiques utilisées pour amplifier les acides nucléiques. La détection de l'accumulation d'ions H^+ , qui se traduit par un changement du pH réactionnel, est l'une des méthodes sans marquage les plus populaires car sa lecture peut être effectuée électriquement sur des puces CMOS relativement peu coûteuses. Le principe est largement utilisé par Ion Torrent dans sa prochaine génération de solution de séquençage, qui utilise des millions de transistors à effet de champ sensibles aux ions (ISFET), fabriqués avec la technologie CMOS, pour détecter les ions H^+ par incorporation d'un nucléotide. Les solutions TAAN basées sur la technologie ISFET offrent de nombreux avantages : une taille compacte, un parallélisme élevé, une lecture intégrée et un faible coût par puce grâce à une technologie de fabrication hautement optimisée. La lecture basée sur la détection d'ions H^+ est une méthode générale qui peut être adaptée à n'importe quelle méthode d'amplification, réduisant ainsi la complexité de l'analyse. La sensibilité extrêmement élevée des ISFET, combinée à l'introduction de canaux microfluidiques avec une partition à ultra-faible volume, a le potentiel d'offrir des plates-formes TAAN rapides et à faible coût offrant ainsi un large éventail de choix de dosage, le tout sur une empreinte centimétrique.

Cependant, pour réaliser de telles solutions, des obstacles technologiques, spécifiques aux ISFET, doivent être surmontés. Cette thèse vise à aborder ces défis et établit des stratégies pour la réalisation des dispositifs TAAN à semi-conducteurs hautement parallèles. Pour éviter d'affecter négativement le rapport signal sur bruit de l'ISFET et pour minimiser les pertes par évaporation dans des volumes ultra-faibles, deux dosages moléculaires pouvant fonctionner à basse température ont été développés. Ce travail démontre une nouvelle stratégie d'intégration microfluidique qui ne nécessite aucun traitement post-CMOS et permet une intégration microfluidique à grande échelle sur des puces CMOS. La thèse se termine par une démonstration de la lecture de l'amplification de l'ADN via des ISFET dans un volume de la taille d'un nanolitre, qui

peut être hautement parallélisé pour réaliser des solutions de type PCR numérique non optique à haut débit.

Keywords: ISFET, ADN, amplification de l'ADN, PCR, amplification sans marquage, électrode de référence, SU-8, microfluidique, RPA, LAMP, intégration microfluidique, test ADN, évaporation de matériaux, volumes très faibles, ratio surface/volume, nanowire, FET.

Contents

Acknowledgments	1
Abstract	3
Résumé	5
Contents	7
List of Figures	9
List of Tables	11
Chapter 1 Technologies and applications of Nucleic Acid Testing	12
1.1 Introduction	12
1.2 Technological evolution of NA testing based on amplification	12
1.3 Technological evolution in sequencing for NAT	14
1.4 Rationale and objective of the thesis	15
Chapter 2 Label-free chemical sensing of DNA Amplification	17
2.1 Introduction	17
2.2 Recombinase Polymerase Amplification	20
2.2.1 Experimental design	21
2.2.2 RPA with commercial TwistDx™ kits	22
2.2.3 RPA in different reaction buffers	23
2.2.4 RPA in minimally buffered conditions	25
2.2.5 Summary	29
2.3 Loop-Mediated Isothermal Amplification	31
2.3.1 Experimental design	31
2.3.2 LAMP in minimally buffered conditions	32
2.3.3 LAMP at low temperatures	35
2.3.4 Summary	41
2.4 Conclusion	42
Chapter 3 Hybrid microfluidic packaging with integrated reference electrode	43
3.1 Introduction	44
3.2 Microfluidic module: Fabrication and Characterization	46
3.2.1 Microfabrication process	46
3.2.2 Metal-coated multi-layer SU-8 pillars	47
3.2.3 Through-PDMS-Vias	50

3.2.4	CMOS Chip and silicon nanowire ISFETs	51
3.3	Discussion of choices related to the process	52
3.3.1	Negative Microchannel Mold	52
3.3.2	Gold electrode lines	53
3.3.3	Metal-coated SU-8 pillars	54
3.3.4	Integration of pseudo-RE in PDMS microfluidics	56
3.4	Evaporation in low volume	57
3.4.1	Vapor barrier	57
3.4.2	Hydration channels	58
3.5	Conclusion	58
Chapter 4	Label-free detection of DNA amplification in small volumes	60
4.1	Introduction	60
4.2	QUASR LAMP	61
4.3	Translating LAMP assay from tube to micro-channels	63
4.3.1	Experimental design and setup	63
4.3.2	On-Chip QUASR-LAMP	64
4.4	On-chip chemical sensing of amplification	68
4.4.1	Experimental design and setup	68
4.4.2	Electronic readout of DNA amplification on-chip in ultra-low volumes	70
4.4.3	Conclusion	75
Chapter 5	Conclusions and prospective	76
5.1	Main Achievements	76
5.1.1	pH-based readout of isothermal nucleic acid amplification	76
5.1.2	Design of scalable microfluidic module with integrated reference electrode	76
5.1.3	Fabrication of “through-PDMS-via” using 1 mm high SU-8 structures	76
5.1.4	pH-based DNA amplification readout in nanoliter volume via semiconductor devices	77
5.2	Prospective Outlook	77
5.2.1	Technology	77
5.2.2	Rapid antibiotic susceptibility testing	78
5.2.3	Towards ISFET-based digital quantification system	79
Chapter 6	Appendices	81
6.1	Composition of isothermal amplification reaction buffers	81
6.2	Fabrication of Ag/AgCl electrode in microfluidic module	82
References		84
Curriculum Vitae		90

List of Figures

FIGURE 2.1. MECHANISM OF H ⁺ GENERATION IN DNA AMPLIFICATION ASSAYS.	19
FIGURE 2.2. SCHEMATIC DEPICTION OF THE RECOMBINASE POLYMERASE AMPLIFICATION PROCESS.	21
FIGURE 2.3. PH READOUT WITH COMMERCIAL RPA KITS IN DIFFERENT CONDITIONS.	23
FIGURE 2.4. RPA IN VARIOUS REACTION BUFFERS.	25
FIGURE 2.5. RPA IN ATP-ONLY ASSAY.	26
FIGURE 2.6. RPA IN MINIMALLY BUFFERED CONDITIONS.	27
FIGURE 2.7. PH CHANGE OF CHLORIDE BUFFER WITH DIFFERENT PPI CONCENTRATIONS UPON HCL TITRATION.	28
FIGURE 2.8. SCHEMATIC DEPICTION OF LOOP-MEDIATED ISOTHERMAL AMPLIFICATION.	30
FIGURE 2.9. LAMP IN MINIMALLY BUFFERED CONDITIONS.	32
FIGURE 2.10. SPECIFICITY AND ROBUSTNESS OF LAMP.	33
FIGURE 2.11. PH-BASED LAMP WITH DIFFERENT INCUBATION TIME.	34
FIGURE 2.12. STANDARD CURVE FOR PH-BASED LAMP.	35
FIGURE 2.13. OPTIMIZATION OF Mg ²⁺ FOR LOW TEMPERATURE LAMP.	36
FIGURE 2.14. OPTIMIZED LAMP AT LOW-TEMPERATURE.	37
FIGURE 2.15 PHOSPHOROTHIOATED OLIGONUCLEOTIDE.	37
FIGURE 2.16. LAMP WITH PHOSPHOROTHIOATE-MODIFIED PRIMERS.	38
FIGURE 2.17. EFFECT OF ET-SSB AND UREA ON LAMP.	39
FIGURE 2.18. LOW-TEMPERATURE LAMP WITH PRE-INCUBATION AT 60°C.	41
FIGURE 3.1 SCHEMATIC OF HYBRID MICROFLUIDIC PACKAGING.	45
FIGURE 3.2. WAFER LEVEL PROCESS STEPS FOR FABRICATION OF THE MICROFLUIDIC MODULE FEATURING PSEUDO-RE AND TPV.	46
FIGURE 3.3. FABRICATION OF MICROCHANNEL MOLD.	47
FIGURE 3.4. PROCESS FLOW STEPS FOR MULTI-LAYER SU-8 LITHOGRAPHY.	49
FIGURE 3.5. TYPICAL TWO-POINT RESISTANCE MEASUREMENT BETWEEN ONE PAIR OF SU-8 PILLARS.	50
FIGURE 3.6. MICROFLUIDIC MODULE AND CONFORMAL PSEUDO-RE.	51
FIGURE 3.7. ELECTRICAL CHARACTERIZATION OF THE PSEUDO-RE AND ISFET.	52
FIGURE 3.8. SEM MICROGRAPH AFTER IBE OF GOLD.	53
FIGURE 3.9. SEM IMAGES OF PSEUDO-RE AND PROTECTIVE TITANIUM LAYER.	54
FIGURE 3.10. PROCESSING OF SU-8 PILLARS.	55
FIGURE 3.11. AD-HOC SETUP SCREW VICES TO BOND PDMS LAYERS UNDER PRESSURE.	56
FIGURE 3.12. VARIOUS SCHEMES FOR MINIMIZING EVAPORATION IN PDMS MICROFLUIDICS.	58
FIGURE 4.1. SCHEMATIC DEPICTION OF QUASR LAMP.	63
FIGURE 4.2. SCHEMATIC DESIGN OF THE MICROREACTOR CHIP TO PERFORM ON-CHIP QUASR LAMP.	64
FIGURE 4.3. NON-IDEAL ARTIFACTS IN ON-CHIP QUASR LAMP.	65
FIGURE 4.4. ON-CHIP QUASR LAMP.	66
FIGURE 4.5. STANDARD CURVE FOR DIFFERENT CONCENTRATIONS OF LAMBDA DNA.	67
FIGURE 4.6. DNA AMPLIFICATION IN LOW COPY NUMBER REGIME.	68
FIGURE 4.7. EXPERIMENTAL SETUP FOR LABEL-FREE READOUT OF DNA AMPLIFICATION.	69
FIGURE 4.8. ON-CHIP SAMPLING MEASUREMENT OF DIFFERENT POST-AMPLIFICATION MIXTURES.	70
FIGURE 4.9 ON-CHIP READOUT OF LAMP WITH LOW VARIABILITY AMONG ISFETS. A.	72
FIGURE 4.10. ON-CHIP READOUT OF LAMP WITH HIGH VARIABILITY AMONG ISFETS.	72
FIGURE 4.11. REAL-TIME AMPLIFICATION CURVE OF LAMBDA DNA (100 NG) IN THE PRESENCE OF HELA GENOMIC DNA (100 NG).	73
FIGURE 4.12. EFFECT OF VOLUME ON PH-BASED READOUT OF LAMP.	74
FIGURE 5.1. FUTURE ITERATIONS OF THE FLUIDIC MODULE FOR MULTIPLEX READOUT.	78
FIGURE 5.2. ANTIBIOTIC HYDROLYSIS BY RESISTANT BACTERIA.	79
FIGURE 6.1. COMPOSITION OF DIFFERENT REACTION BUFFERS UTILIZED FOR RPA.	81
FIGURE 6.2. COMPOSITION OF DIFFERENT ENERGY SOURCES FOR RECOMBINASE ACTIVITY IN RPA.	81
FIGURE 6.3. COMPOSITION OF REACTION BUFFERS THAT ARE TITRATED WITH HCL TO MEASURE THEIR BUFFERING POWER.	82

FIGURE 6.4. FABRICATION OF Ag/AgCl ELECTRODE IN MICROFLUIDIC MODULE..... 83

List of Tables

TABLE 2.1. PRIMER SEQUENCES USED IN RPA OF CITRINE DNA.....	22
TABLE 2.2. PRIMER SEQUENCES USED IN LAMP OF BACTERIOPHAGE LAMBDA DNA.....	32
TABLE 2.3. LAMP PRIMER SEQUENCES WITH PHOSPHOROTHIOATE MODIFICATIONS.....	38
TABLE 3.1. PARAMETERS FOR 1 MM HIGH SU-8 PILLARS VIA THREE-LAYER COATING AND EXPOSURE AND A SINGLE DEVELOPMENT.....	48
TABLE 4.1. LABELED OLIGONUCLEOTIDE SEQUENCES USED IN QUASR LAMP OF BACTERIOPHAGE LAMBDA DNA.....	62

Chapter 1 Technologies and applications of Nucleic Acid Testing

1.1 Introduction

Deoxyribonucleic acid (DNA) and ribonucleic acid (RNA) are biopolymers that carry genetic instructions for the development, growth, functioning and reproduction of all known forms of life. When things go well with these processes, they offer important insights into the origin and evolution of these perturbations. Even though DNA was discovered in 1869 by Friedrich Miescher, its composition in 1978 by Albrecht Kossel and its double-helix structure in 1953 by James Watson and Francis Crick, its use as a biomarker for disease diagnostics and genetics did not take off until later in the 1980s. The primary reason was the rarity of nucleic acids (NAs). Typically, nucleic acids of interest are present in trace amounts in the biological samples, which makes their characterization difficult and unfeasible. As a result, various methods and tools had to be developed to detect minute quantities of nucleic acids in media from complex sources. After extraction and isolation of the trace amounts of NAs, the basic premise of these methods involves generating a sufficient quantity of duplicate copies for subsequent analysis. Historically duplication of NAs was done via a process called “DNA cloning” The technique involves the insertion of the gene of interest into bacterial cells, which during proliferation by cell division, will also replicate the NA of interest. At the end of the bacterial culture, the colony will contain many identical cells, each carrying one or more copies of the inserted DNA. The amplified DNA is extracted and purified from the colony. DNA cloning via cell culture is a time-consuming and tedious process and was the primary method of DNA amplification until the invention of polymerase chain reaction (PCR) by Kary Mullis in 1983.

1.2 Technological evolution of NA testing based on amplification

PCR made quantum improvements to the means of DNA replication by significantly reducing the time and simplification of the process. Made possible by the discovery of thermophilic *Taq* polymerase from the bacteria *Thermus aquaticus*, PCR uses multiple cycles of DNA denaturation at 95°C, followed by annealing of the primers to the denatured strands at 55°C and finally, an extension of the primers by the *Taq* polymerase at 72°C to achieve a copy of the DNA strand. This three-step process, repeated multiple times, achieves exponential amplification of DNA in less than 1.5 hours. By the early 1990s, patient-level genetic tests based on PCR became available for detecting the presence of hereditary breast and ovarian cancers. However, the widespread use of NAT only came about with the use of RNA polymerase in a reverse transcription-polymerase chain reaction (RT-PCR) in the mid to late 1990s. RT-PCR uses RNA as a template instead of DNA in PCR, allowing NAT on viral sources of NA. At the height of the AIDS epidemic, the high incidences of HIV and HCV infections via blood transfusion, especially among hemophiliacs, lead to the widespread adoption of RT-PCR for blood donor screening [1].

The high sensitivity of PCR also brought its own drawbacks. Being able to amplify from very small copies of DNA made PCR very prone to contamination from its own amplicons. Detection of amplified DNA required opening the PCR tubes and running the amplicons through the agarose gel matrix. This post-PCR handling of amplicons led to their spread into the laboratory space via aerosol and contaminated gloves. This problem was virtually solved by the invention of real-time PCR, where amplicon could be detected without opening the reaction tubes [2]. Post-processing of amplicons was avoided by putting the amplicon reporters directly with the PCR mixture and monitoring their signal over the course of amplification. The signal reporters are molecules (ethidium bromide, SYBR Green, etc.) that fluoresce when they intercalate between the bases or the grooves of the double-stranded DNA helix. Due to the inherent advantages, blood banks were the first to adopt real-time PCR as an alternative to traditional PCR for their in-house NAT [3].

By the late nineties, the invention of closed-tube real-time PCR led to an increased degree of automation leading to an increase in throughput and a reduction in the cost of NAT. The demand for automation in NAT was led by blood banks, where the sample numbers per day were quite high. This led to the development of whole-process automation nucleic acid detection systems, which include NA extraction, amplification and NA amplification analysis modules. These modular sections are relatively independent and are controlled via mechanical automation. With minimal hands-on time, these systems offer the advantages of high automaticity, reduced biosafety risk and high throughput.

As evident, these high-throughput automated systems have a large footprint, making them suitable only for large centralized testing facilities like blood banks. Around the beginning of the 2000s, the focus in the field of NAT shifted towards decentralized testing, mainly to reduce the time to result. Increased interest in tests that can be performed near the patient led to the emergence of point-of-care (POC) testing. Introduced in 2000 by Cepheid, GeneXpert could perform on-site real-time PCR within half hour with minimal training. The approach towards an all-in-one cartridge that can do sample preparation, PCR amplification of NA and subsequent analysis proved revolutionary and marked the birth of POC for molecular diagnostics. Since then, multiple companies have introduced similar systems for POC molecular diagnostics. These solutions mostly differ in design and operate on the same principle, i.e. they can generally analyze single patient samples, use PCR to amplify DNA and fluorescently read out the amplification. Over time, improvements to assay time and detection limit have occurred mainly by gradual optimization of thermocycling technology and a more sensitive optical readout setup.

Whether in a laboratory or POC setting, single-volume molecular assays form the bulk of diagnostic methods that are in use today. However, the concept of Digital PCR (dPCR) where molecular amplification assays are performed in a large number of small volume partitions instead of a singular big one, is steadily gaining interest [4]. Though proposed in the early 1990s, dPCR has only recently seen a resurgence due to improvements in the field of software and manufacturing [5][6]. Instead of using reference amplification for quantification as in qPCR, dPCR uses the statistical distribution of template DNA in a large number of small volumes to provide absolute quantification of DNA up to a single copy level. Only the presence or absence of amplification is necessary to derive a meaningful conclusion, hence the moniker "digital". The ultrasensitive dPCR is particularly useful for low abundance targets, targets in complex backgrounds and single nucleotide polymorphism. The key feature of dPCR is the partitioning technology. Current, commercial products employ either patterned micro-wells (Fluidigm, Quantstudio, Digital LightCycler) or two-phase droplet generation (Bio-Rad, RainDance) to realize sample parcellation. dPCR being a new technology brings its own issues. Working in tiny volumes with single-molecule concentrations is a challenging feat and can lead to exclusion of rare samples during the analysis or signal from false positives can overwhelm the signal from

the rare alleles of interest. dPCR is a specialist approach and is still in the state of maturation. Most of the commercial solutions are not approved for diagnostics and are used only for research.

1.3 Technological evolution in sequencing for NAT

Apart from the invention of PCR, Taq polymerase also enabled the development of a method of sequencing, which can be used to determine the base sequence of any NA. Developed by Fredrick Sanger in 1977, Sanger sequencing uses chain-terminating nucleotides to generate amplicons with different lengths and read them out via electrophoresis on a polyacrylamide gel [7]. Sanger sequencing greatly simplified the sequencing process and remained the standard method to sequence NA for nearly four decades. Sanger sequencing was the primary method used in Human Genome Project to sequence the whole human genome. Despite the powerful ability of to be able to sequence any NA, sequencing did not find much usage in NAT for diagnostics due to extremely high costs and limited throughput. Sequencing remained confined to research and academia until the mid-2000s when a new generation of sequencing methods came up that provided a massively parallel readout of the NA sequence, thereby dramatically bringing down the costs. These next-generation sequencing (NGS) methods rely on the localization of fragmented NA sequences in millions of clusters and read their sequences simultaneously. Subsequently, using computational analysis, sequence alignment is performed on the raw data to generate the complete sequence of the pre-fragmented NA template.

Since the commercial introduction of 454 Life Sciences' pyrosequencing in 2005, a large number of sequencing solutions have emerged. These solutions are extremely diverse and differ from each other in library preparation, method of sequencing and readout. Independent of the supplier's technology, each NGS solution requires a series of steps to be performed: starting with the fragmentation of DNA template, followed by adapter ligation to generate initiation sites for sequencing. The template is then amplified via solid-phase amplification on a patterned flow cell (Illumina) or emulsion amplification on beads (Ion Torrent, Roche 454) to generate a large number of copies for sequencing. Template sequences can be read via hybridization and ligation of labeled probes (SOLiD, Complete Genomics), via synthesis of DNA strand by using optically labeled oligonucleotides (Illumina, Qiagen) or via detection of by-products due to strand elongation (Ion Torrent, Roche 454) [8]. Having a diverse choice for NGS is important to reduce platform-specific bias that can be introduced into the data due to over-reliance on one particular method. However, in theory, each platform can be used to perform sequencing, in practice factors such as throughput, cost, error profile and read length make one NGS method preferable over the other. For example, ligation base NGS methods have very high accuracy (>99.99%), as each base is probed multiple times but the maximum read lengths are less than 100 bp and have several days of run time. This limits their use for genome-wide applications and makes them more suitable for niche clinical applications like oncology. NGS solutions from Illumina are the most popular due to the maturity of the technology and wide range of platforms. Illumina technology has high throughput, is less susceptible to homopolymer errors and has increased read length up to 300 bp, albeit with reduced accuracy (>99.5%). Ion Torrent NGS offers superior read lengths (400 bp) due to the use of unmodified nucleotides. Instead of using photodetectors to capture an optical signal from the incorporation of labeled nucleotides, Ion Torrent uses ion-sensitive field effect transistor (ISFET) to detect H⁺ ions released as a normal by-product of nucleotide incorporation. The use of a CMOS chip for sequencing cuts down the equipment cost and makes readout faster. However, as the pH signal is not perfectly proportional to the number of nucleotides detected, Ion Torrent lacks single-base accuracy when reading homopolymers sequences larger than 6-8 bp [9].

Motivated by the need to resolve long repetitive elements in the genome and structural variation that are relevant to evolution, adaptation and disease, that are not addressed by short read lengths of the current NGS, the next iteration of NGS aims to improve upon the read length of its predecessors. Currently, there are two long-read sequencing technologies commercially available on the market. Pacific Bioscience's (PacBio) single-molecule real-time sequencing uses a polymerase molecule immobilized at the bottom of a small well called zero-mode waveguide, to continuously sequence a circular template (hairpin adapters at both ends of DNA) DNA. The readout is performed as polymerase incorporates a labeled nucleotide, whose optical signal can only be read at the bottom of the waveguide. This leads to continuous monitoring of nucleotides that are incorporated at the rate of polymerase activity. By using a circular template, multiple reads of a long DNA strand can be achieved. Another approach is offered by Oxford Nanopore Technology (ONT), where DNA to be sequenced is passed through a biological nanopore. As the DNA translocates through the nanopore, the ionic current through the pore modulates according to the base passing through the pore. The base-nanopore interaction has a distinct electrical signature that can be used to generate the sequence of translocating DNA molecules. The methods offer average read lengths of more than 10 kbp. However, as the technology is not mature enough, they suffer from significantly high error rates (15% for PacBio and 30% for ONT). However, these error rates are going to reduce as the technology matures.

Evidently, for sequencing, the time to result and prices have reduced significantly. However, NGS as an alternative candidate for routine NAT is still not viable due to complicated workflow and comparatively higher cost. NGS is ideal for pathogen monitoring and genetic testing but remains less preferable for routine NAT over amplification-based methods [1].

1.4 Rationale and objective of the thesis

As evident from the previous section, in the field of NAT there is no one-size-fits-all solution for molecular testing. The choice of the method is dictated by multiple factors like cost, accuracy, precision, speed, sensitivity etc. Therefore, newer technologies and methods continue to emerge that may not offer a quantum leap over existing solutions but are able to address a niche application very effectively. Moreover, current NAT platforms were made for the pre-Covid-19 era. The Covid-19 pandemic has brought forth the limitations of existing solutions and made it abundantly clear that NAT needs to expand outside specialized laboratories for efficient, low-cost, rapid and large-scale detection and monitoring of infectious diseases.

Over the past couple of decades, the development of isothermal amplification methods with label-free readout have tried to address the issues of cost and device simplicity. As a result, methods that use the detection of amplification by-products like H^+ rather than optical labels are becoming increasingly popular and finding commercial use. Label-free pH-based sequencing by Ion Torrent has demonstrated the viability of ion-sensitive field effect transistor (ISFET) as a readout device for the amplification of NAs. Unsurprisingly, ISFETs have already been used in varieties of NAT applications from genotyping [10] to the detection of pathogens [11]. The true potential of CMOS technology for NAT lies in the scalability, parallelism and sensitivity of ISFETs, which these solutions fail to take full advantage of. ISFETs have been shown to be sensitive to changes of a few hundred of electron charges [12]. This corresponds to the amplification of only a few DNA templates, thus offering unprecedented sensitivity when employed in very small volumes. As the current NAT methods have already achieved the ultimate goal of detecting a single DNA/RNA molecule present in the reaction tube, the future developments will be in highly flexible solutions that have increased the multiplexing capability and offer a wide range of assays. Due to the advantage of CMOS technology, ISFET-based NAT solutions are uniquely positioned to address these developments.

Before such solutions could be developed, technological bottlenecks that are unique to ISFETs need to be tackled. Realization of thousands of ISFET sensors that can monitor amplification reactions is obvious due to the well-established CMOS manufacturing process. However, realizing hundreds or thousands of unique amplification reactions in very small volumes, that are monitored by the array of ISFET sensors is not that trivial. The realization of a reference electrode in each reaction volume marks the primary bottleneck in the development of CMOS-based NAT platforms. Conventional NA amplification assays need to be adapted such that are susceptible to changes in pH, without sacrificing their efficacy. Moreover, for increased signal-to-noise ratio and reduced evaporation from low-volume reactions, amplification assays, unlike PCR should be able to operate at near room-temperature levels. In this thesis, we address these issues related to biochemistry, packaging and feasibility of pH-based amplification readout in ultra-low volumes, hoping to lay the foundation for the development of highly parallel semiconductor-based NA amplification testing solutions.

In chapter 2, we investigate two NA amplification methods and adapt them for pH-based readout at low temperatures. We examine in detail their biochemistry to determine the specificity of their pH readout and choose the one best suited for our application in the framework of this thesis. In the following chapter 3, we address packaging issues related to microfluidics for CMOS-based sensing solutions. We propose a fabrication method for the realization of a new design for reference electrodes that can be integrated in any kind of PDMS microfluidics. A key consequence of the design is that it eliminates the need to post-process the CMOS chip and leads to more compact fluidic layouts for high throughput applications. The process resulted in the development of an improved fabrication process for millimeter-high SU-8 structures. In chapter 4, we for the first time demonstrate a pH-based readout of DNA amplification in nanoliter-sized chambers via silicon nanowire ISFETs. We elucidate the effects of high-surface-to-volume ratio on the biochemistry of the amplification assays and steps to compensate for them. We discuss measurement strategies for amplification readout in case of variability in the sensor readout. Finally, we demonstrate a specific readout of DNA amplification in the presence of a non-specific template in nanoliter chambers. In the last chapter concluding remarks on the work of the thesis and possible future applications is given.

Chapter 2 Label-free chemical sensing of DNA Amplification

The work presented in this chapter is partially adapted from the article published in *Biosensors and Bioelectronics*, 2022.

Authors: Saurabh Tomar, Barbora Lavickova and Carlotta Guiducci.

Contributions: Saurabh Tomar contributed to conceptualization, methodology, validation, investigation, visualization, writing and editing.

Reference: Tomar, S.; Lavickova, B.; Guiducci, C. Recombinase polymerase amplification in minimally buffered conditions. *Biosensors and Bioelectronics*. 2022, 198, 113802.

2.1 Introduction

Polymerase chain reaction (PCR) has been the most popular technique to amplify and detect low-abundance nucleic acids. Popularized further by covid-19 pandemic due to its ability to detect pre-symptomatic infections, “PCR” has now become mainstream term. PCR’s requirement for thermocycling and extensive instrumentation makes it a technique mainly carried out in specialized settings of diagnostic laboratories. Point-of-care (POC) molecular diagnostics with sensitivities and specificity comparable to current gold standards can address the above issue. A PCR-based POC solution requires engineering considerations that are not limited to the material’s thermal constraints, the heat sensitivity of the enzymes used for diagnosis, the evaporation of water and complex thermal control instrumentation. Isothermal amplification methods simplify these constraints by requiring a constant temperature to amplify DNA. Instead of requiring high temperatures, isothermal methods use enzymes to perform strand separation. As a result, dozens of isothermal amplification methods employing various mechanisms to amplify DNA have emerged as promising alternatives to PCR with sensitivities comparable to PCR.

Typically, the readout of amplified product is performed by fluorescence detection of the double-stranded DNA (dsDNA) using either intercalating dyes or fluorophores. Traditionally, electrophoresis on agarose gel is used to identify amplicons at the end of the amplification reaction. When amplicons are moved through the agarose matrix under the influence of an electric field, the DNA is resolved based on its shape and charge. Real-time amplicon detection relies on changes in the fluorescence level resulting from either generation of target DNA or conformational change in the detection probes during NA amplification. Intercalating (Ethidium bromide) or groove binding (SYBR green) agents begin to fluoresce upon forming a complex with dsDNA, thereby leading to an increase in fluorescence as more and more DNA is generated during amplification. Detection probes are synthetic short oligonucleotides that can bind to the complementary regions on the amplifying DNA. The probe possesses a pair of fluorescing (fluorophore) and quenching (quencher) molecules, where the probe’s fluorescence depends on the distance between the pair. These probes are engineered such that the amplification of DNA leads to a change in spatial configuration between the fluorophore and quencher, leading to a change in emitted fluorescence. For example, the TaqMan[®] probe is the most commonly used method where the quencher becomes separated from the fluorophore due to the enzymatic activity of DNA polymerase, leading to an increase in fluorophore’s fluorescence. Apart from detecting amplified dsDNA, amplification by-products like aqueous hydrogen (H^+) [13] and pyrophosphate (PPi) can also serve as readout targets [14]. Colorimetric optical assays for endpoint detection use changes in the color of the reaction mix due to complex formation between inorganic cations and PPi [15].

As evident, optical methods require a tag or a label to be able to read the amplification of DNA. Eliminating labeling for readout of DNA offers the potential to develop simpler, rapid and low-cost assays. These advantages have led to the development of numerous techniques for label-free detection of DNA, like surface plasmon resonance [16], mass detection using cantilevers [17] and electrochemical measurement [18][19]. Electrical and electrochemical methods offer the unique advantage of label-free, simpler and miniaturized solutions that can be integrated into a small chip with the aid of complementary metal oxide (CMOS) technology. Advanced CMOS manufacturing process can be leveraged to deliver scalable, high-throughput analysis systems for POC applications. These methods directly sense the synthesized amplicon DNA or its by-products. The most popular of these methods is the direct sensing of local changes in the charge or pH because of the accumulation of H^+ in the amplification mixture. The technique exploits the production of aqueous hydrogen ions due to the incorporation of nucleotides by the polymerase in the elongating DNA strand (Figure 2.1) [13]. Over the course of DNA amplification, the accumulation of these by-products leads

to a change in the pH of the reaction mixture. The technique has been exploited to produce CMOS-based high-throughput DNA sequencing solutions commercially [20].

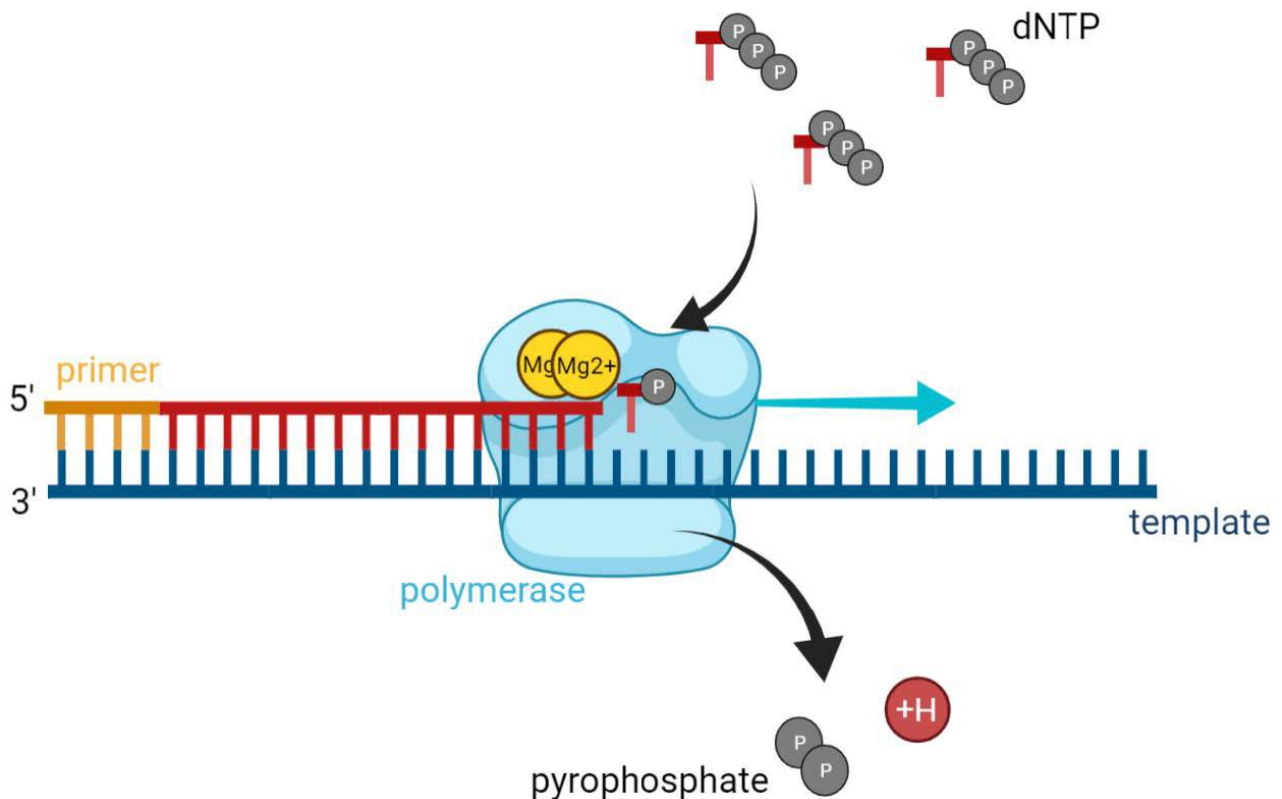


Figure 2.1. Mechanism of H^+ generation in DNA amplification assays. The polymerase binds to a primer sequence and incorporates dNTPs into the elongating strand, complementary to the template. At each step, it consumes two Mg^{2+} ions and releases a pyrophosphate ion and one proton.

Since the demonstration of readout of DNA amplification by sensing a change in pH, many traditional DNA amplification methods have been adapted to use it as a label-free method for the detection of DNA amplification. Apart from PCR [10], various isothermal amplification methods like loop-mediated amplification (LAMP) [10], strand displacement amplification (SDA) [21], rolling circle amplification (RCA) [22], multiple displacement amplification (MDA) [23] and recombinase polymerase amplification (RPA) [11] have been used to quantify nucleic acids via pH change. Due to the lack of thermal cycling, lower and constant operating temperatures, isothermal methods are the preferred assays for detection of the DNA amplification by pH readout. LAMP has been extensively employed in pH-based quantification of nucleic acids [10][24][25][26]. However, LAMP suffers from requirements of relatively higher temperature and complex assay design due to the need of multiple primers (up to 6). SDA [21] for pH-based assay also suffers from the same disadvantages. RCA can operate at lower temperatures but still requires an initial template denaturation at high temperatures to initiate amplification. In addition, the necessity of a circular template for RCA introduces additional preprocessing steps that increase the complexity of the assay. MDA can occur at low temperatures. However, it requires long amplification times to get a measurable pH change [23]. An ideal assay for pH-based nucleic acid detection needs to be isothermal, able to operate at relatively low temperatures and with a quick readout.

In this chapter, we investigate and adapt two isothermal assays for pH-based readout of DNA amplification at near room-temperature levels.

2.2 Recombinase Polymerase Amplification

RPA is a rapid (15 min to signal), simple (two primers, no specific template shape) and room temperature process, making it an ideal candidate for POC applications. Owing to these advantages, RPA has quickly become popular and has been successfully used for the identification of pathogens [27][28]; for example, single copy levels of SARS-CoV-2 have been detected with RT-RPA within 25 min [29].

RPA does not require the global melting of the DNA template and instead uses recombinase-assisted primer annealing for strand elongation. In RPA, a recombinase cooperatively binds to primers forming nucleoprotein complexes. This recombinase-primer complex scans the double-stranded template DNA for a complementary binding site. During this homology search, the displaced template DNA strand is stabilized by single-stranded DNA binding protein (SSB) to prevent primer ejection by branch migration. Upon recognition of the homologous site, the recombinase disassembles from the complex, facilitating primer binding via strand exchange. Then a strand displacing polymerase extends the primers at their 3' ends, resulting in a copy of the original template DNA (Figure 2.2a). This process is repeated to achieve exponential amplification [30]. In its nucleoprotein complex state, the recombinase continuously hydrolyses ATP [31]. Therefore, in RPA, a steady supply of ATP is ensured by using a "creatine kinase-creatine phosphate" regeneration system, which uses ADP (generated from ATP hydrolysis) to regenerate ATP (Figure 2.2a).

Therefore, RPA has two sources of H^+ , one from the nucleotide incorporation during amplification and the other from ATP hydrolysis by the recombinase. Hu et al. [11] hypothesized that H^+ derived from ATP hydrolysis is recycled back by creatine kinase (CK) in the presence of creatine phosphate (CP). Hence, the pH signal from RPA is generated only by nucleotide incorporation and not ATP hydrolysis.

The pH change upon DNA amplification can be detected either calorimetrically [21], where the color of a pH-sensitive dye in the mixture changes in response to pH or via solid state sensors like ion-sensitive field-effect transistors (ISFET), where a change in the mixture's pH is transduced into an electrical signal via field effect. The colorimetric method is not quantitative and can only be used for endpoint detection. Whereas ISFETs allow for real-time detection of DNA amplification with the benefits of scalability to a large number of sensors [10]. Hu and coworkers [11] used RPA in combination with thin-film ISFETs and showed a correlation between DNA amplification and ISFET signal. However, since the amplification was carried out with a fully buffered commercial kit (TwistDx's TwistAmp[®] exo), the exact mechanism that led to pH change in the amplifying mixture could not be clearly described. While the mechanism of pH change in polymerase-only assays is well understood [13], in the case of RPA the combined effect of additional proteins like recombinase, recombinase loading factor, single-strand binding (SSB) protein and creatine kinase on reaction's pH has not been described and elucidated.

Generally, the pH response in amplification assays is achieved via substantially reducing the concentrations of tris-like dedicated pH buffers. Minimal amount of pH buffer is retained to establish a pH value compatible with polymerase activity at the start of reaction. However, apart from tris-like buffers, other reaction constituents or reaction products can significantly buffer the pH [32].

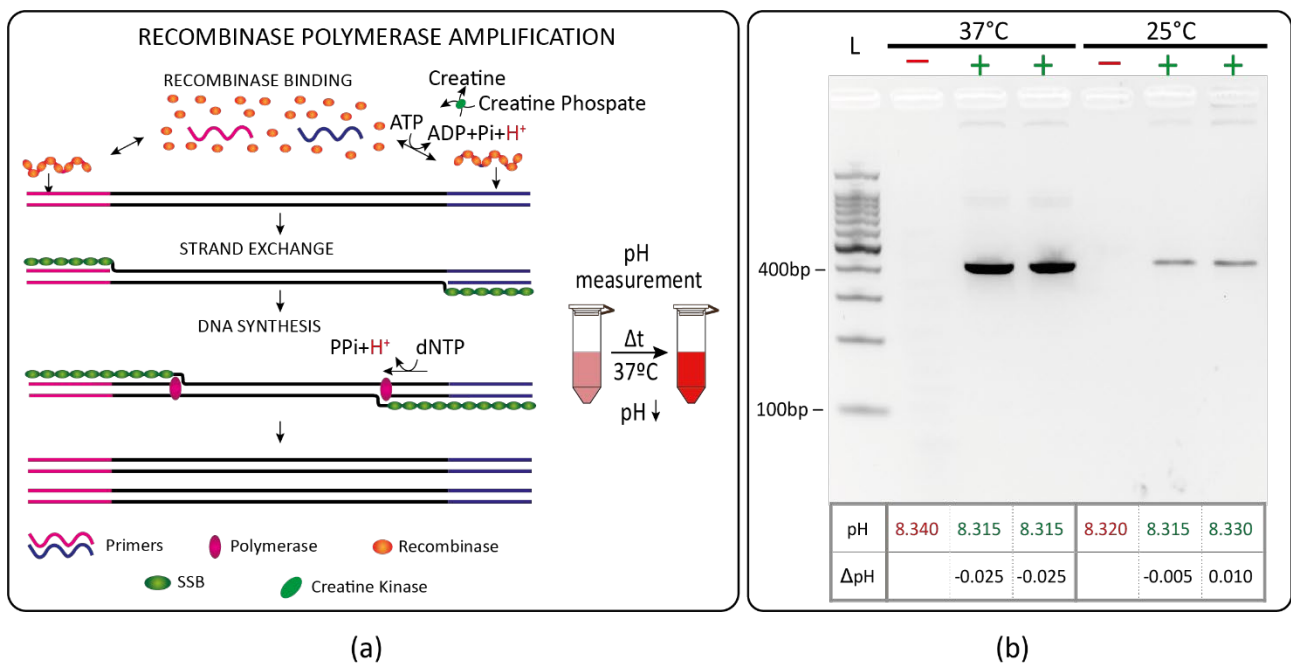


Figure 2.2. Schematic depiction of the Recombinase Polymerase Amplification process. (a) Recombinase binds to the primers forming recombinase-primer complexes, which continuously hydrolyze ATP. The resultant ADP is regenerated back into ATP by creatine kinase in the presence of creatine phosphate. Recombinase-primer complex scans the DNA strand for homologue site and upon encounter; the primer is inserted at the cognate site through the DNA strand-displacement process facilitated by the recombinase-primer complex disassembly. Single-strand binding protein (SSB) helps to stabilize the displaced strand as recombinase disassembles, allowing the polymerase to elongate the DNA. (b) Agarose gel electrophoresis of RPA with the commercial TwistAmp Liquid basic kit and at recommended 37°C and at 25°C, accompanied by a summary table with pH values after 30 min of amplification.

Our aim is to study the feasibility of the detection of DNA polymerization by RPA in minimally buffered conditions by measuring change in pH of reaction mixture. We hypothesized that, as opposed to a fully buffered kit like the one employed by Hu et al., RPA in minimally buffered conditions would further enhance the pH signal, positively affecting the sensitivity and limit of detection of RPA-based assays. Therefore, we reverse engineered TwistDx's RPA kit, and removed most of its pH buffer. We then titrated custom kit's constituents against different hydrogen ion concentrations to measure the constituents' intrinsic buffering capacity. Finally, we performed RPA such that the concentration of the constituents retains minimal buffering power while still allowing DNA amplification to occur. Finally, we also investigate effects of pyrophosphate (PPi) generation and accumulation on pH of RPA assay.

2.2.1 Experimental design

TwistAmp Liquid Basic and lyophilized TwistAmp Basic kits were sourced from TwistDx. Potassium acetate, dithiothreitol (DTT), polyethylene glycol (PEG) 20000, creatine phosphate disodium salt tetrahydrate were purchased from Sigma-Aldrich. ATP (adenosine 5' - triphosphate, NaOH titrated), dNTPs (deoxyribonucleotide triphosphate, NaOH titrated), GeneRuler 50bp DNA ladder were sourced from ThermoFisher Scientific. Potassium chloride and magnesium chloride were sourced from Invitrogen. Hydrochloric acid (25%), BenchTop 100bp DNA ladder and GelRed were purchased from Supelco, Promega and Biotium, respectively. Strain DH5alpha transformed with plasmid pKT0211 was grown at 37°C overnight in 5 mL lysogeny broth media supplemented with 100 µg/mL ampicillin. The plasmid was purified from the overnight culture using the QIAprep Spin Miniprep Kit, eluted in nuclease-free water instead of elution buffer. DNA concentration was measured by Nanodrop 1000 spectrophotometer (Thermo Fisher Scientific). Plasmid pKT0211 was a

gift from Kurt Thorn (Addgene plasmid #8734) (Sheff and Thorn, 2004). Primer sequences (IDT) are listed in Table 2.1.

Amplicon size	Forwards primer	Reverse primer
416 bp	5'-TTTGATGTGTTTTGCTAGATACCCAGA-3'	5'-TAGATTGATAGGATAAGTAATGGTTG-3'
324 bp	5'-TTTGATGTGTTTTGCTAGATACCCAGA-3'	5'-GAACCATCTTCAATGTTGTGTCTAATTTTG-3'
122 bp	5'-TTTGATGTGTTTTGCTAGATACCCAGA-3'	5'-TCTTGTAGTTACCGTCATCTTTGAAAAAAA-3'

Table 2.1. Primer sequences used in RPA of citrine DNA. Reverse primer determines the length of the amplicon, as forward primer is kept same.

The different reaction buffers and E-mix solutions are specified in Section 6.1. For commercial kits, the DNA amplification was carried out according to the manufacturer's protocol. Modified RPA conditions involving TwistAmp Liquid Basic kit consisted of either acetate or chloride buffers (Figure 6.1), either custom E-Mix or E-Mix_ATP (Figure 6.2), 1.8 mM dNTP, 0.48 μ M of each primer, 2.5 μ l of the "Core Reaction Mix" and either 14 mM of magnesium acetate or magnesium chloride. The target DNA concentration of 1.6 ng/ μ l was used in all RPA assays unless stated otherwise. The amplifications were carried out in thermocyclers (Swift Max-Pro, Esco healthcare or TC-3000, Techne) at 37°C for 30 min, unless indicated otherwise. The reactions were stopped by heating the reaction mixture at 95°C for 5 min. Agarose gel electrophoresis (1.5% agarose in TBE buffer) was carried out in Danaphor's Model 100 Standard gel plate and ThermoFischer's Owl EasyCast B2. GelRed was employed as nucleic acid staining dye. All gels were run at 120 V (EV261 power supply, Consort) and imaged with Gel Logic 100 imaging system (Kodak). The tested components were prepared at 1.25X dilution in KOH titrated MiliQ water (pH = 7.3) and titrated with different HCl concentrations. The final contraction of the measured reaction components was the same as in the RPA reaction (1X dilution). The exact compositions of different solutions tested are specified in figure captions and Figure 6.3. The pH measurements were carried with ISFET pH meter (Sentrons SI600) and a CupFET pH probe (Welling). A minimum 20 μ L was pipetted onto the pH sensor. The pH readings were allowed to stabilize for 2 min before being recorded.

2.2.2 RPA with commercial TwistDx™ kits

TwistDx™ provides various kit options for RPA. A freeze-dried TwistAmp Basic kit was used to recreate the original conditions used by Hu et al. [11]. The *E. coli* genomic DNA, associated primers and exo-probe were provided by Hywel Morgan (University of Southampton, UK). To see the influence of various factors on amplification and pH outcomes in the TwistAmp Basic kit, we tested the amplification with different templates, primers and amplification duration (Figure 2.3). However, any considerable and reproducible pH output differences between the Negative Template Control (NTC) and the Positive Template Control (PTC) were not detected. Exonuclease activity [30] in real-time RPA was found to have no effect on the pH of the reaction mixture (Figure 2.3c). To ensure that any resulting pH changes are not due to the implementation of different kits, we utilized the TwistAmp Liquid Basic kit throughout the study, as it provides greater flexibility in tailoring the ingredients.

To maximize the number of incorporated dNTPs and, therefore, the pH change, we chose to amplify DNA length (416 bp) within the maximal recommended fragment size for RPA (< 500 bp). Albeit testing all these different conditions, we did not observe any consistent pH differentiation between NTC and PTC (Figure 2.2b, Figure 2.3). Although these findings are in discrepancy with previous finding [11], they are in line with our hypothesis that a high buffering capacity of the commercially available kits due to the presence of dedi-

cated pH buffer is incompatible with a reproducible pH-based RPA-driven assay. Hence, to have a pH readout it is imperative to achieve RPA in minimally buffered conditions.

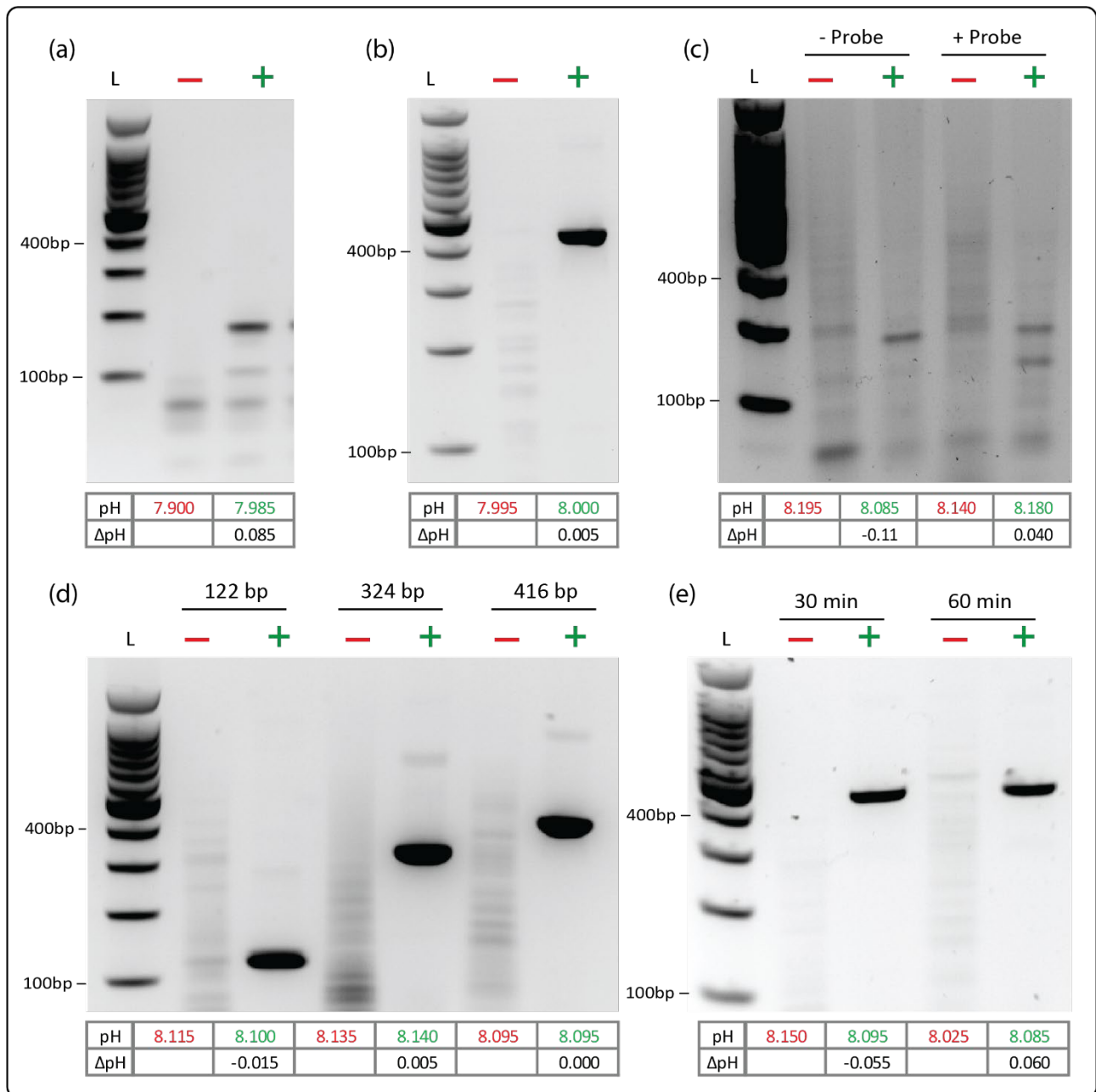


Figure 2.3. pH readout with commercial RPA kits in different conditions. RPA of two different DNA templates using TwistAmp Basic kit (a) *bla*_{CTX-M-15} gene in genomic DNA of NCTC13441 *E. coli* (0.2 pg/μl) and (b) Citrine, for 30 minutes at 39°C. (c) RPA of *bla*_{CTX-M-15} gene of NCTC13441 *E. coli* (0.2 pg/μl) by TwistAmp Liquid kit. In the presence of exo-probe, the exonuclease cleaves the DNA strand at tetrahydrofuran moiety, which shows up as a smaller DNA band on agarose gel. (d) RPA of Citrine DNA for amplicon lengths of 122 bp, 324 bp and 416 bp, using TwistAmp Basic kit for 30 minutes at 39°C. (e) RPA of Citrine DNA for different time durations, using TwistAmp Basic kit at 39°C. The table at the bottom of the images shows the pH at the end of the experiment.

2.2.3 RPA in different reaction buffers

The company does not disclose the composition of the RPA kit, which poses some challenges to modifying the mixtures to establish minimally buffered conditions. However, Piepenburg et al. [30] provide comprehensive strategies for performing DNA amplification using recombinant proteins. Based on their work, we generate all the kit elements except for the “Core Reaction Mix”, which contains all the enzyme compo-

nents. Though enzyme solutions are usually buffered, the amount of buffers carried over to the final reaction mixture is minimal and therefore has a negligible effect on the DNA amplification mixture's pH [21][23]. Besides testing the commercial "RPA buffer", which is acetate-based and contains tris buffer, we tested other variations of the reaction buffer: an acetate buffer (acetate anion based) and a chloride buffer (chloride anion based), both with and without tris (Figure 2.4a).

To evaluate the prepared buffers' properties, we tested their influence on the pH buffering capacity by titrating the buffers with different aqueous concentrations of hydrogen ion (H^+) (Figure 2.4b). We also tested DNA amplification levels (Figure 2.4c) after RPA in all the buffers. As expected, the reaction buffer containing tris and acetate salts showed a minimal change in pH upon the titration (Figure 2.4d), and the DNA amplification levels were identical to those of the commercial buffer. Removing tris did not influence either the DNA amplification or the pH behavior for the acetate buffer, due to the conjugate base property of acetate ions (CH_3COO^-). In the acetate buffer, the acetate anions and H^+ form a natural "conjugate base/weak acid" pH buffer. Therefore, the high concentration (50 mM) of the acetate ions will buffer any aqueous hydrogen added or produced during the reaction. The TwistDx kit's reaction buffer is acetate-based and contains tris buffer [33], making the commercial kit unsuitable for a pH-based amplification detection. By removing tris and replacing the acetate-ions with chloride-ions (chloride buffer), the reaction buffer becomes less resistant to pH changes while also maintaining high DNA amplification levels. Hence, for pH-based detection assays, chloride-based reaction buffer appears to be more suitable compared to acetate-based reaction buffer.

However, the pH change upon amplification was very small and did not change in a consistent way with any of the buffers employed. We hypothesized that in the absence of dedicated pH buffering agent, other reaction components or biochemical reactions could contribute to buffering of produced H^+ . In what follows we describe our attempts to minimize the pH buffering capacity of RPA by suppressing parasitic biochemical reactions and reducing concentration of pH buffering components.

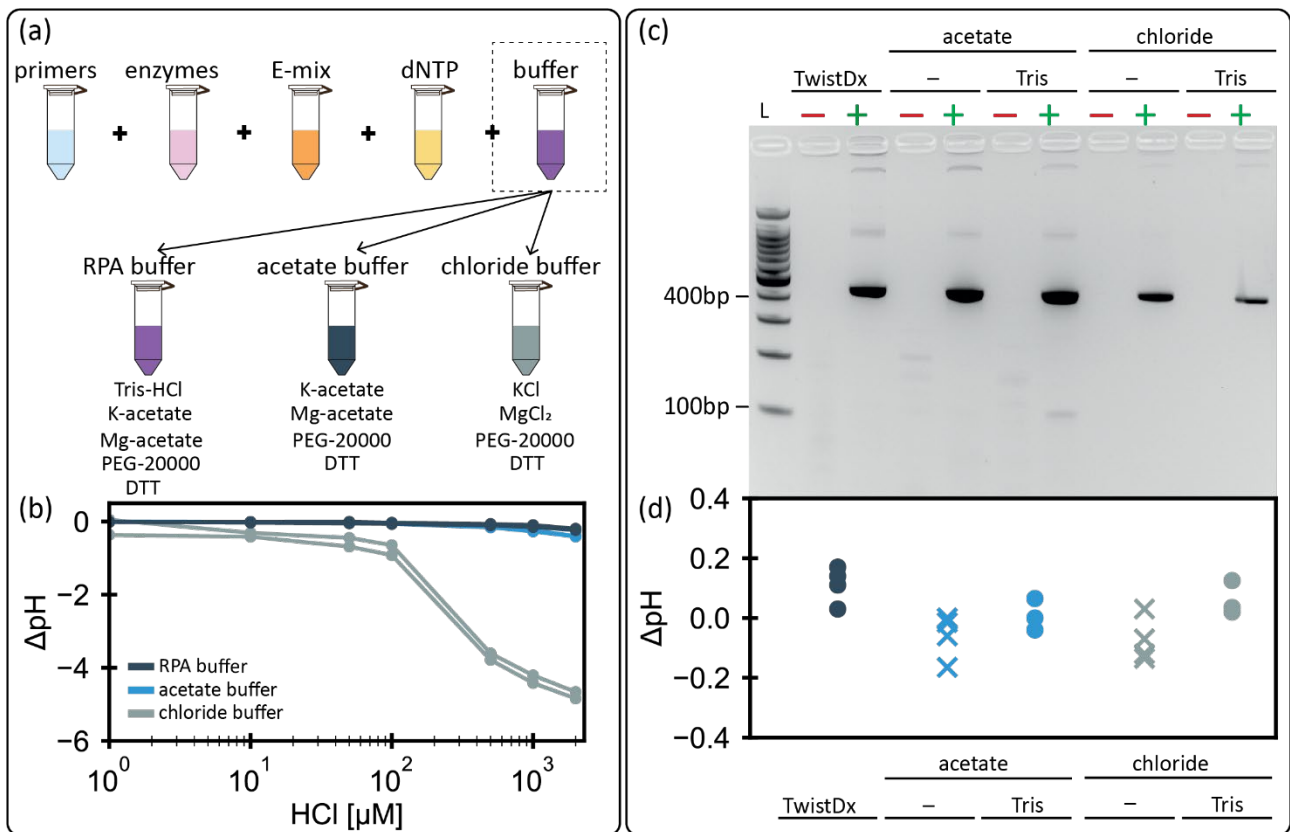


Figure 2.4. RPA in various reaction buffers. (a) Composition of different reaction buffers used. (b) pH changes in the different reaction buffers as a function of HCl titration. Reaction buffers were used at the same concentration as in RPA. Each buffer titration was replicated twice. (c) Agarose gel electrophoresis for RPA reactions carried out in various buffer conditions with the rest of the commercial kit unchanged. (d) Comparison of the pH change (ΔpH) between PTC (+) and its corresponding NTC (-) of the various buffer conditions. Data points for a particular reaction buffer are technical replicates. The RPA reactions were carried out at 37°C for 30 min.

2.2.4 RPA in minimally buffered conditions

Compared to other pH amplification assays, where the only source of H^+ is DNA synthesis, RPA has other source and sink of H^+ (Figure 2.2a), making any pH change and detection dependent on multiple factors. Ideally, these factors should be disjointed and studied separately to allow for advanced system comprehension and implementation.

2.2.4.1 RPA without ATP regeneration

The recombinase UvsX enzyme plays a vital role in the RPA primers attachment to the targeted site. The recombinase forms a nucleoprotein complex with primer and initiates primer annealing to the DNA strand. The sequential process of complex formation, homologue searching and strand transfer requires active hydrolysis ATP by recombinase, resulting in gradual accumulation of ADP, phosphate and H^+ . If the ATP concentration falls below the ADP concentration, the recombinase-primer nucleoprotein complex disassembles, preventing the primer annealing and DNA amplification. Therefore, a constant ATP supply, achieved by a creatine kinase-based regeneration system, is required. Creatine kinase regenerates ATP by utilizing ADP, H^+ and creatine phosphate (Figure 2.2a), thereby acting as H^+ sink. Accordingly, to investigate the pH effects of RPA without the reaction elements that act as H^+ sink, the ATP regeneration system was removed by omitting the creatine phosphate and replaced with higher ATP concentrations (Figure 2.5a).

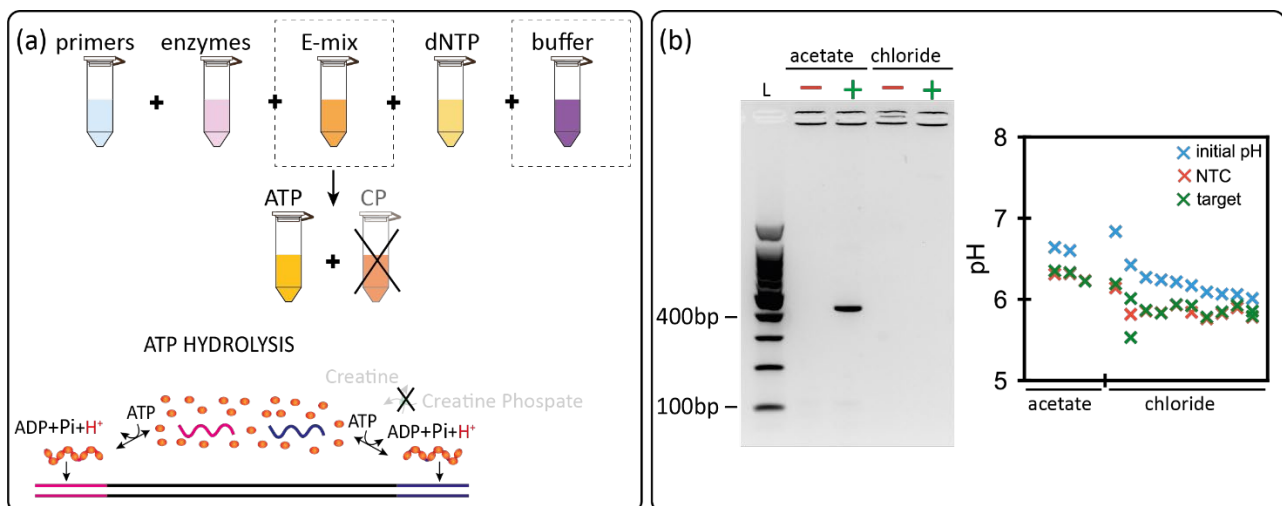


Figure 2.5. RPA in ATP-only assay. (a) Schematic depiction of an ATP-only RPA strategy, where creatine phosphate is removed to prevent ATP regeneration. ATP is hydrolyzed by recombinase when in nucleoprotein state with primers, resulting in generation of ADP and H⁺. The unmodified enzyme mixture still contains creatine kinase. (b) Agarose gel electrophoresis for RPA in the absence of creatine phosphate, 20 mM ATP and 40 mM Magnesium acetate/MgCl₂ were used. The initial pH (blue) of the reaction was adjusted with KOH to different levels. Variation in the pH of RPA mixture at the beginning of amplification reaction (blue) and at the end (orange and green) in the acetate and chloride reaction buffers. Each data point represents a technical replicate.

The ATP concentration (3 mM) used in RPA with the regeneration system is insufficient for DNA amplification when used in the absence of creatine phosphate. Due to the high ATP hydrolysis rate by recombinase [34], 3 mM of ATP is consumed before substantial amplification can take place. Therefore, elevated levels of ATP are required to sustain amplification for a longer time. However, an increase of negatively charged ATP leads to Mg²⁺ ions depletion and, consequently reaction malfunction. By increasing the Mg²⁺ ions concentration simultaneously with ATP, we were able to regain DNA amplification for RPA solely in the presence of ATP. However, amplification was seen only in the acetate-based buffer, whereas the chloride buffer assay showed a visible lack of amplification on the gel (Figure 2.5b). As expected, the reaction pH falls rapidly due to the hydrolysis of ATP by the recombinase, irrespective of the target DNA's presence. According to the manufacturer's protocol, RPA works optimally in a slightly basic pH condition (~pH 8). However, due to the intrinsic properties of ATP stability and its acid-based properties, the resulting starting pH for the ATP-only RPA reactions was lower than in the ATP-CP based assay. We hypothesized that due to the acetate buffer's intrinsic buffering capacity the reaction pH does not fall radically, therefore allowing regular polymerase and recombinase activity leading to DNA amplification. Whereas, in the chloride-based buffer, which lacks any pH buffering capability, the pH quickly falls to levels that inhibit RPA before any substantial DNA amplification can occur (Figure 2.5b) [35]. The ATP-only RPA also shows reduced amplification efficiency. As most of the pH change occurs due to the recombinase activity, the resulting pH behavior is similar in both NTC and PTC. Therefore, DNA amplification quantification by pH detection is not attainable in the ATP-only RPA reactions.

2.2.4.2 RPA with ATP regeneration

Having demonstrated that even after the removal of obvious buffer components, RPA did not yield pH changes suitable for pH-based amplification assay. We decided to explore the influence of other reaction components on the pH change and attempted to minimize their buffering power while maintaining the DNA amplification levels. ATP and dNTPs have numerous O⁻ sites of phosphodiester bonds that can act as protonating sites for H⁺. We anticipate that they would have a significant effect on the pH output [32]. We titrated various E-mix components in chloride buffer against different H⁺ concentrations and compared

them to the RCA buffer (Figure 6.3) from our previous study [23]. As expected, we observed varying degree of buffering effect from all the components (Figure 2.6b). dNTPs significantly buffered the pH when added to the buffer. We observed even higher buffering when ATP or creatine phosphate was added. Though creatine phosphate has only one phosphate group compared to three in ATP, comparable buffering among both is attributed to the higher concentration of creatine phosphate (50 mM) over ATP (3 mM). Similar buffering capacity was observed when CP and ATP were titrated together.

Given that, ATP and creatine phosphate form an inalienable part of RCA and significantly buffer the pH of DNA amplification reaction. We attempted to achieve pH-based read out by reducing ATP concentrations and creatine phosphate to levels that buffer the reaction minimally but are sufficient to retain the recombinase activity (Figure 2.6a). Although RCA retained its function and DNA amplification was obtained in various concentrations of CP and ATP in chloride buffer (Figure 2.6c), consistent pH change was not attained probably due to low yield of amplification product (Figure 2.6d). Unlike LAMP, the final amplified product in RCA is not high enough to generate levels of H^+ that can overcome its intrinsic buffering capacity [36]. Moreover, apart from DNA elongation due to polymerase activity, there are also unavoidable non-polymerase sources (UvsX recombinase) and sink (creatine kinase) for H^+ . Therefore, the net H^+ concentration depends on these enzymes' relative activity, making the pH signal not entirely specific to DNA amplification. Similar behavior can also be expected from amplification methods like Helicase Dependent Amplification (HDA) [37] that require ATP hydrolysis by ancillary proteins to amplify DNA.

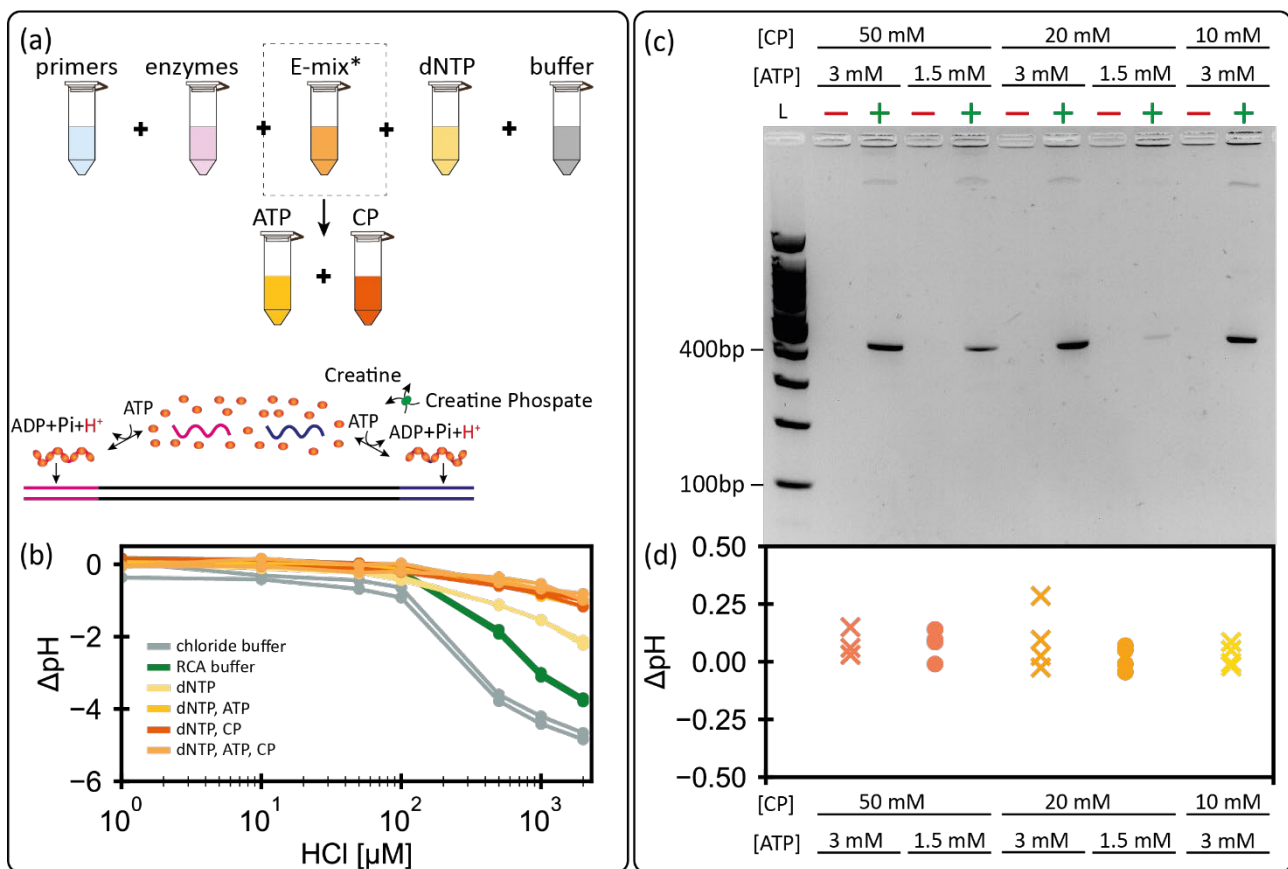


Figure 2.6. RPA in minimally buffered conditions. (a) Schematic depiction of RPA with ATP regeneration. H^+ generated from ATP hydrolysis is recycled back to regenerate ATP molecules by creatine kinase. (b) pH change in RCA buffer supplemented with dNTPs or in chloride buffer supplemented with various RPA constituents (dNTP, ATP, and CP) as a function of HCl titration. Each data point represents a technical replicate. (c) Agarose gel for RPA reaction augmented with different concentrations of CP (50 mM, 20 mM

and 10 mM) and ATP (3 mM and 1.5 mM). (d) Comparison of the pH change (ΔpH) between PTC (+) and its corresponding NTC (-) for different concentrations of CP and ATP. Each data point represents a technical replicate.

2.2.4.3 Effect of pyrophosphate precipitation on pH

Similar to RPA reactants, non- H^+ byproducts can also have similar effect on the pH of the amplification assay. Production of inorganic pyrophosphate (PPi) and its subsequent precipitation in LAMP assays has been shown to have an effect on the amplification mixture's conductivity [38]. The change in ionic strength due to PPI precipitation has been hypothesized [11] to also affect the pH of the mixture. Therefore, we explored the effect of PPI accumulation on the pH of the RPA mixture. In RPA, apart from nucleotide incorporation by polymerase, recombinase activity is also source of PPI. Hydrolysis of ATP by recombinase UvsX result in production of both ADP plus phosphate and AMP plus PPI [34]. Real-time monitoring of PPI in RPA was out of the scope of the present study. However, we tried to simulate the conditions at the end of RPA reaction by spiking chloride buffer with different concentrations of PPI and noting the effect on pH, both in presence and absence of magnesium (Figure 2.7). As expected, higher levels of PPI increase the pH buffering capacity of the chloride buffer (Figure 2.7a). In the presence of magnesium, the buffering capacity is significantly reduced due to the precipitation of PPI (Figure 2.7b). It was also noticed that with increased precipitation of PPI, the pH of the buffer also fell. However, even in the unlikely scenario where all of dNTP and ATP gets converted to PPI (~ 5 mM) and the reaction mixture is not intrinsically buffered against pH, the fall in pH (Figure 2.7c) due to PPI precipitation is still lower than the one reported in [11].

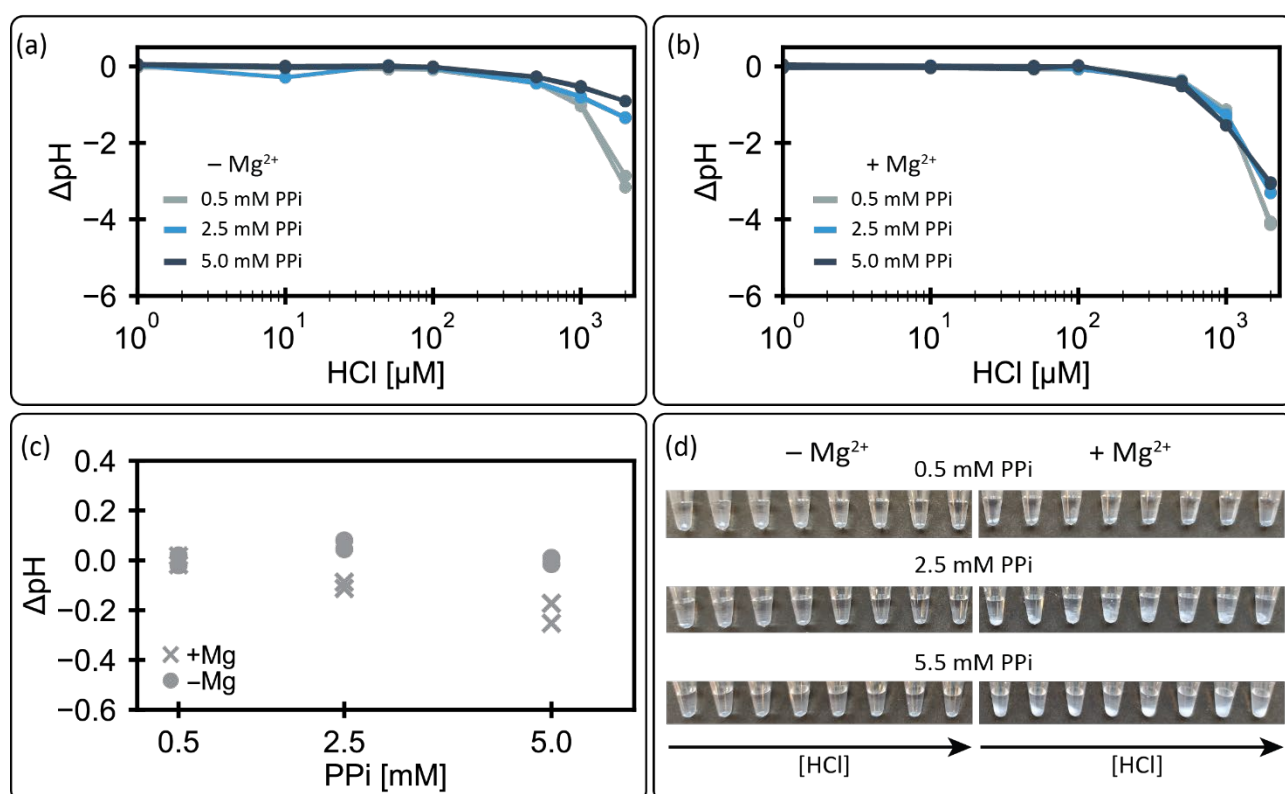


Figure 2.7. pH change of chloride buffer with different PPI concentrations upon HCl titration: (a) without magnesium chloride and (b) with 14 mM of magnesium chloride. (c) Effect of varying degrees of magnesium pyrophosphate precipitation on the pH. 14 mM of magnesium chloride was added to the solutions. (d) Different PPI concentrations (0.5 mM, 2.5 mM and 5 mM) with and without magnesium ions showing a varying degree of magnesium pyrophosphate precipitation in the presence of magnesium.

Precipitation of PPI can be observed visually due to an increase in turbidity of the reaction mixture. However, we did not observe a visible increase in the turbidity in any of our RPA experiments, signifying low levels of PPI production (Figure 2.7d). Low PPI generation is probably due to combination of two factors. Pri-

marily, the level of DNA amplification by RPA is not high enough to generate PPI levels that warrant its precipitation [39]. Secondly, TwistDx's commercial RPA formulations have been known to employ UvsY as loading factor [27], which is known to significantly suppress PPI/AMP generation from hydrolysis of ATP by UvsX [40]. Therefore, the amount of PPI generated in RPA and subsequently precipitated in RPA is not high enough to induce any significant and specific pH change.

2.2.5 Summary

After investigating the mechanism of pH change in recombinase polymerase amplification for possible applications in pH-based amplification assays, we have found that commercial RPA kits from TwistDx come buffered with tris and therefore do not produce any pH signal upon amplification. Even after removal of tris, the acetate ions in the reaction buffer mask any change in pH upon amplification. Upon switching to chloride-based reaction buffer, the pH change is still buffered by RPA specific constituents - ATP and creatine phosphate, due to presence of numerous phosphodiester sites that act as protonating sites for H^+ . No significant pH change was observed upon reducing the concentration of ATP and creatine phosphate, even though clear DNA amplification was observed on gel electrophoresis. This is probably due amplification level in RPA are not high enough to overcome the buffering capacity of the constituents and show a pH change. RPA can also be carried out, albeit with reduced efficiency, in the absence of creatine kinase-based ATP regeneration system by greatly increasing the amount of ATP. However, the amplification efficiency is reduced significantly in buffered conditions and no visible amplifications is seen in unbuffered conditions. PPI precipitation in amplification assay can also affect the pH of the mixture; however, amount of PPI generation and precipitation in RPA is not enough to overcome the systems intrinsic buffering capacity and translate in a change in pH.

Chemical detection of nucleic acid amplification relies on detection of amplification by-products like hydrogen ion and PPI. However, in RPA due to its unique chemistry, there are sources and sinks for these by-products that are not of polymerase origin, thereby adversely affecting the signal-to-noise ratio for chemical sensing of amplification. Moreover, even in the absence of dedicated pH buffering agents, RPA retains high intrinsic pH buffering capacity due to the very nature of its biochemistry, thereby buffering any H^+ generated due to DNA amplification. These limitations are common to amplification techniques like RPA, HDA and recombinase assisted LAMP [41] that require enzyme catalyzed nucleotide hydrolysis.

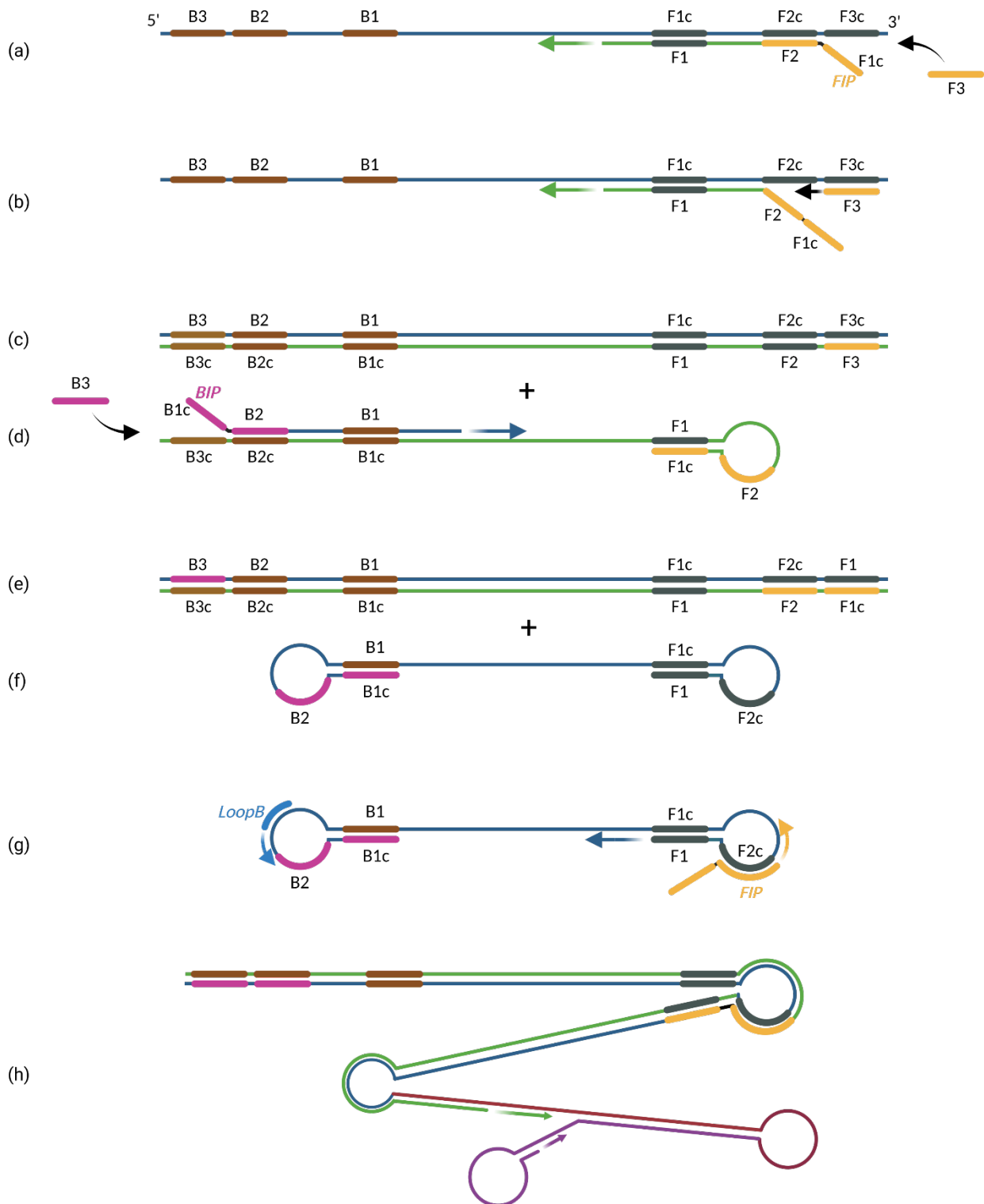


Figure 2.8. Schematic depiction of Loop-mediated isothermal amplification. (a) FIP/BIP primer starts the amplification by hybridizing to the template DNA. (b) The newly synthesized strand is displaced when the polymerase elongates from F3. (c) A hairpin is created at the 5' end of the displaced strand, while BIP primer recognizes its target at the 3' end. The new strand is displaced when B3 hybridizes. (e,f) Two loop structures are formed at the termini. (g) Amplification can continue from the F1 foldback at the 3' end, or after hybridization of FIP. In addition, loop primers recognize sequences in the hairpin. (h) The amplification products are shaped in cauliflower-like long chains of repeated template sequences linked by loops.

2.3 Loop-Mediated Isothermal Amplification

LAMP allows for sequence specific amplification of DNA using only one enzyme that performs the job of both strand elongation and strand displacement. LAMP takes advantage of the careful design of 6 primers to achieve a high degree of specificity. When coupled with highly strand displacing polymerase, LAMP can exponentially amplify DNA in very small amount of time. The process is schematically detailed in Figure 2.8.

The inner primers (forward: FIP and backward: BIP) are composed of two distinct sequences, one sense (F2 and B1c) and one antisense (F1c and B2). The outer primers (F3 and B3) are homologous to some regions outside the inner primers. The 3' end of the sense part (F2) hybridizes to the target and starts the reaction. At some point, the outer primer (F3) in lower concentration is also able to hybridize and launches the elongation of a new strand, displacing the previously formed in the process. This displaced strand spontaneously folds back to form a loop at one end, as the non-sense part of the FIP primer (F1c) binds to its complementary region. The same process happens at the 3'-end of this new strand, creating a new target DNA flanked by two loops. The ends of the foldback form double-stranded regions of DNA, which also act as primers. The polymerase binds to these sites, elongates and displaces the second loop at the 5'-end. Each new strand created and released contains this loop structure, and can therefore start a new reaction later on [42]. To sum up, the LAMP relies on the special design of the primers, folding back to create loops at the end of the DNA pieces and the strand-displacing polymerase able to elongate these structures. It is possible to add two loop primers, recognizing sequences between the inner and outer primers, in the loop. They multiply the number of elongation reactions occurring in parallel [43]. LAMP is an exponential amplification reaction with very high yield and can produce up to 10^9 amplification products from a few copies of the template in less than an hour. The reaction is ideally performed at 65°C by strong strand displacing polymerase (like *Bst*, *Bst 2.0*, *Bst 3.0*). This method accommodates target genes between 130 bp and 200 bp. [42]. The products are long chains of amplicons, linked by the loop structures in between each target sequence. The design of the primers is critical, and close attention should be given to the length, distances and melting temperatures.

2.3.1 Experimental design

The protocol for LAMP is adapted from New England Biolab's (NEB) general guidelines. Mesophilic DNA polymerase *Bst 2.0* from NEB was used in all our LAMP assays. For LAMP assays manufacturer recommend using the "Standard LAMP Buffer" (sold as Isothermal Amplification Buffer) supplied along with *Bst 2.0* polymerase. This buffer is then supplemented with 6 mM of $MgSO_4$ to reach an 8 mM total concentration. Custom L Buffer for our pH-based LAMP assay was made using the same composition as the kit, but removing the tris-HCl (20 mM) from the Standard LAMP buffer. Our Custom LAMP Buffer is composed of 10 mM $(NH_4)_2SO_4$, 50 mM KCl, 2 mM $MgSO_4$ and 0.1% Tween[®]20 in deionized water. The initial pH was adjusted to 8.0-8.5 with 10 mM KOH. $MgSO_4$ was directly set at the final concentration of 8 mM (optimized later to 6 mM).

The bacteriophage Lambda DNA (NEB) was used as the template, combined with the 6 LAMP primers (IDT) as designed by Nagamine and al. [43]. HeLa genomic DNA (NEB) was used as non-specific DNA template for specificity and negative control reactions. A 20X primer mix of the oligonucleotides (Table 2.2) was prepared with FIP (32 μ M), BIP primers (32 μ M), F3 (4 μ M), B3 primers (4 μ M), loop F (8 μ M) and loop B primers (8 μ M) in deionized water.

Primer	Sequence
FIP	5'-CAGCCAGCCGCGACGACGTTTCGCTCATAGGAGATATGGTAGAGCCGC-3'
BIP	5'-GAGAGAATTTGTACCACCTCCACCGGGCACATAGCAGTCCTAGGGACAGT-3'
F3	5'-GGCTTGGCTCTGCTAACACGTT-3'
B3	5'-GGACGTTTGTAAATGTCCGCTCC-3'
Loop F	5'-CTGCATACGACGTGTCT-3'
Loop B	5'-ACCATCTATGACTGTACGCC-3'

Table 2.2. Primer sequences used in LAMP of bacteriophage lambda DNA. [43]

Unless specified, the amplification mix is prepared by mixing the reaction buffer with the primer mix, dNTPs (5.6 mM total), *Bst* 2.0 polymerase (0.32 U/ μ L) and 1 μ L of template into deionized water. Unless stated otherwise, 25 μ L aliquots (STARLAB) were briefly spun down and incubated at 65°C for 30 minutes (Esco Healthcare). It was followed by 4 minutes at 95°C to end the reaction by denaturing the polymerase. For every experiment and condition, two reactions were performed in parallel: one aliquot was loaded with 1 μ L of DNA template, and the Negative Template Control (NTC) was loaded with 1 μ L of nuclease-free water. The signal (Δ pH) is obtained after subtracting the pH of NTC from the pH of amplified target mixture.

2.3.2 LAMP in minimally buffered conditions

Unlike RPA, which requires ancillary enzymes along with polymerase, LAMP's biochemistry is simpler, as it only requires single enzyme i.e. the polymerase to amplify DNA. Therefore, in LAMP the only source of H⁺ is the strand elongation activity of polymerase. Due to relatively less complex biochemistry, LAMP assay can be easily modified to work in minimally buffered conditions just by removal of dedicated tris-like pH buffers. With commercially available colorimetric kits (Warmstart Colorimetric LAMP 2X Master Mix from NEB), detection of DNA amplification via pH readout is well established and widely reported in literature. Tanner et al. provide a nice foundation to develop minimally buffered LAMP assays [21].

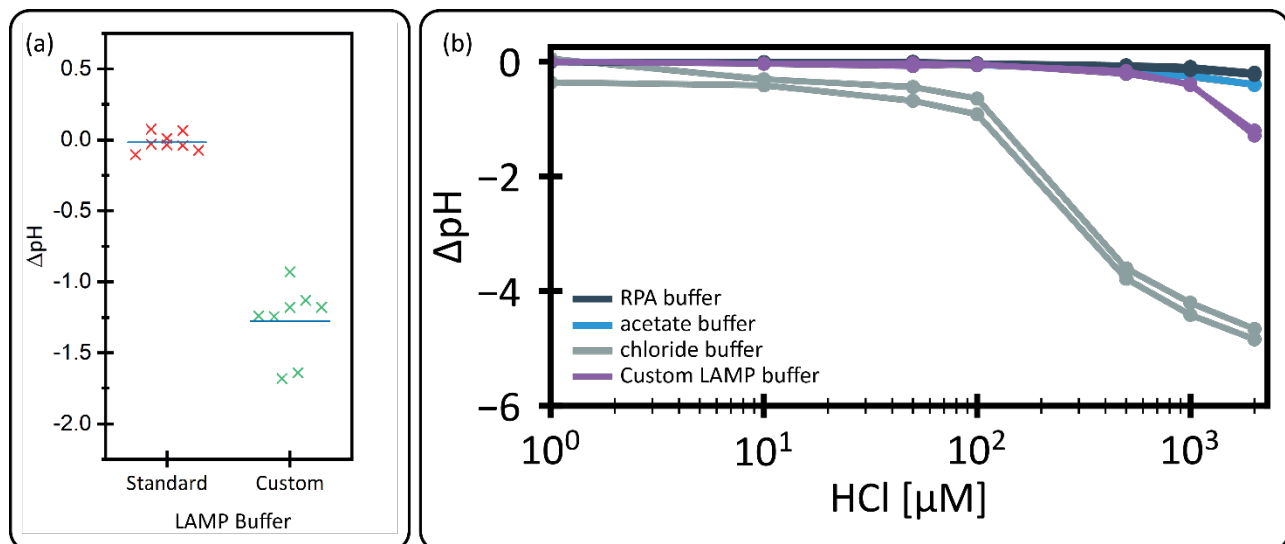


Figure 2.9. LAMP in minimally buffered conditions. (a) Change in pH (Δ pH) between the NTC and the target after amplification in different reaction buffers. Reaction mix were incubated for 30 minutes with 2.10^5 copies of lambda template or water (NTC). (b) Titration of LAMP custom buffer against increasing concentration of HCl showing relative buffering capacity of different reaction buffers. Each titration was performed in duplicate.

We created a minimally buffered Custom LAMP buffer by removing tris from the commercially supplied Standard LAMP buffer. We were able to amplify bacteriophage lambda DNA without any noticeable difference in amplification efficiency and achieve specific pH readout of DNA amplification (Figure 2.9a). When

titrated against various concentration of H^+ , Custom LAMP buffer showed more pH buffering capacity than RPA's chloride buffer (Figure 2.9b). This pH buffering capacity can be attributed to the presence of ammonium (NH_4^+) ions in the LAMP reaction buffer. Ammonium ions increase amplification yield and specificity by destabilizing weak hydrogen bonding between mismatched primer-template base pairing. The discrepancy in the pH signal of RPA in chloride buffer (Figure 2.6d) and LAMP in Custom buffer (Figure 2.9a) can be attributed to the high amplification yield of LAMP. LAMP is able to amplify DNA to the levels that it is able to overcome the buffering capacity of ammonium ions.

Some assays perform a pre-denaturation at $95^\circ C$, before adding the polymerase to help anneal the primers to the template and increase the specificity of the reaction [44]. We observed no significant change so this step was skipped, as it increases the complexity of the process and the risk of carry-over contamination.

2.3.2.1 Specificity and robustness

Reliance on a set of six different primers recognizing eight regions on the target confers LAMP a very high level of specificity [42]. The specificity of our LAMP assay was verified by applying the same protocol as above, using the lambda primers but spiked with HeLa genomic DNA (75 ng). A Positive Template Control (PTC), with lambda DNA template (10 pg or $2 \cdot 10^5$ copies) was run in parallel for comparison. No amplification was detected using HeLa genomic template and the pH remained constant ($\Delta pH = 0.03$), contrary to the PTC ($\Delta pH = -0.995$).

The robustness of our reaction was tested by verifying that it could amplify the target gene when mixed with other contaminant DNA. The reaction mix was supplemented with either water (NTC), lambda DNA (10 pg) (PTC), HeLa genomic DNA (10 pg) or lambda and HeLa genomic DNA (10 pg each). As shown in Figure 2.10, all and only the aliquots containing the target lambda gene amplified. Samples containing non-specific template were indistinguishable from positive controls in the gel and pH measures. Thus, this experiment shows that LAMP is robust enough to amplify the target gene within a sample containing human DNA.

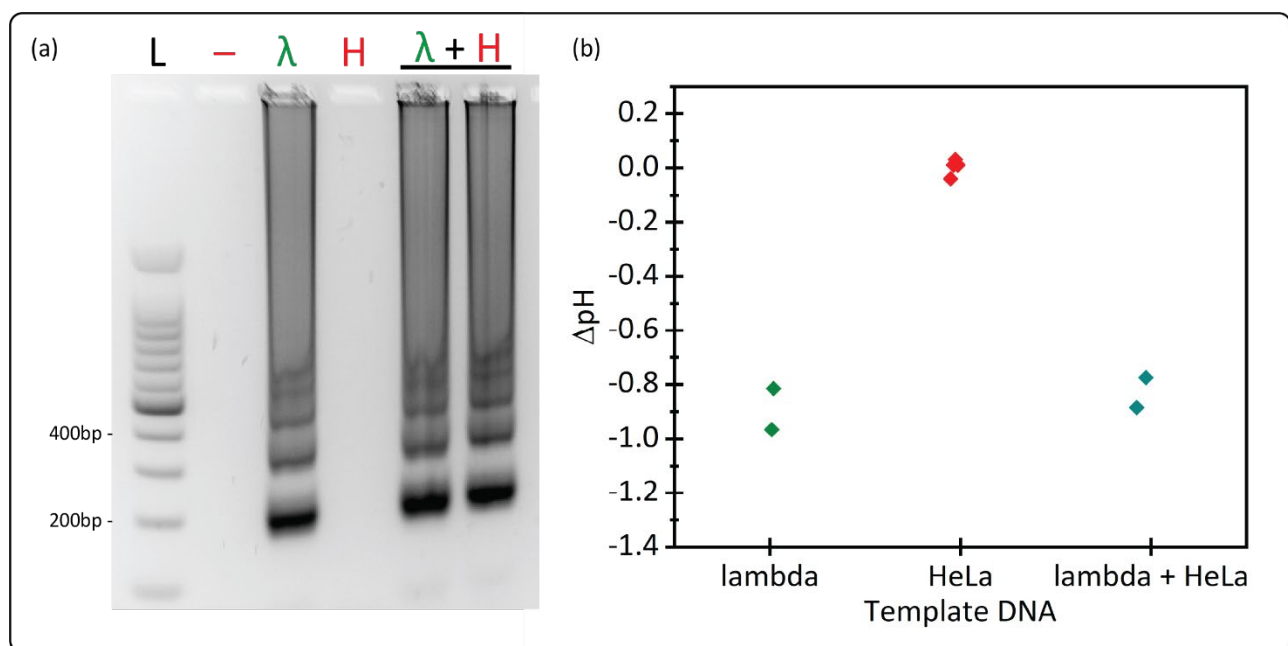


Figure 2.10. Specificity and robustness of LAMP. (a) Representative gel and (b) delta pH measurements after 30 min of incubation with no-template (-), lambda template 10 pg (λ), HeLa genomic template 10 pg (H) and both lambda and HeLa template 10 pg each ($\lambda + H$).

2.3.2.2 Duration of amplification

For 2×10^3 copies of starting lambda DNA concentration, no visible amplification was noticed before 10 minutes of incubation and maximum pH signal was achieved around 30 minutes, signifying the reaction has plateaued. We observed no superior pH shift after 60 minutes of amplification or with different DNA concentrations. To better understand the pH dynamics of our LAMP assay and define the operating range for the reaction, we carried out time-point measurement of pH between 14 to 22 minutes of LAMP. As shown in Figure 2.11 the change in pH is negatively correlated with the incubation time. A linear correlation of pH with time is observed as the pH was measured in the log-linear region of the amplification curve. Amplification was observed at 14 minutes but a measurable pH drop occurred only at 16 minutes.

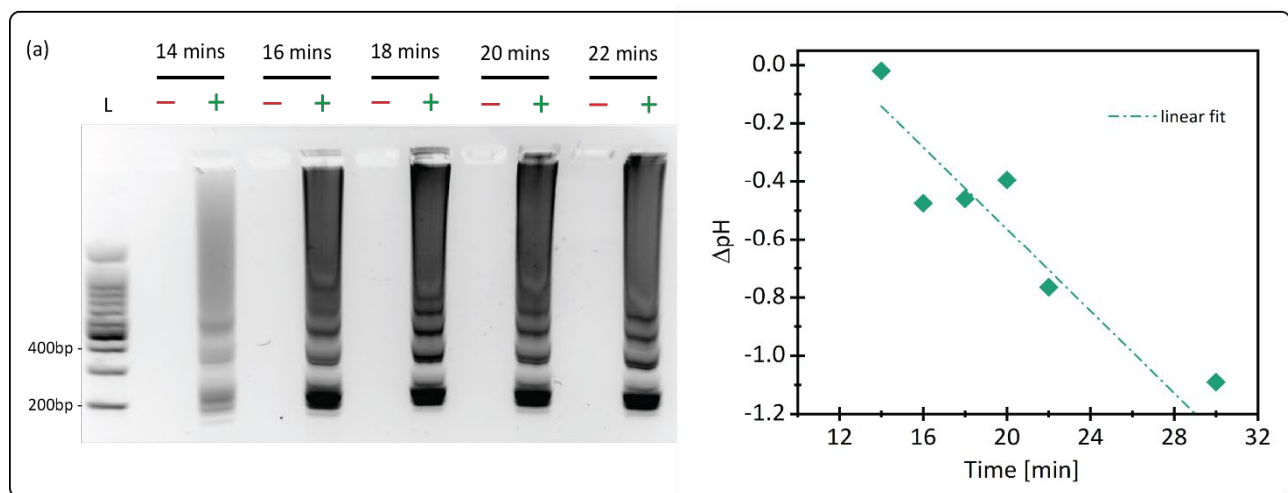


Figure 2.11. pH-based LAMP with different incubation time. (a) Gel and (b) delta pH measurements after amplification of 2000 copies of lambda DNA template, with an incubation time ranging from 14 to 22 minutes. The orange square at 30 minutes (b) is the mean value of three replicates from other experiments, as a reference. A linear model was fitted to the values ($R^2 = 0.70$).

2.3.2.3 Sensitivity and quantitative detection

To characterize the sensitivity of our assay, a 6 step 10-fold serial dilution of the lambda DNA template was made from 2×10^5 copies until below the single-copy limit. The mixture was incubated for 30 minutes, following the standard protocol. Over the four replicates, LAMP was able to amplify down to 20 copies. Low copy number (20 and 200) showed higher rates of amplification failure due to sub-sampling error when adding the template DNA. However, amplification was consistently observed from 2000 copies of DNA. Irrespective of the initial number of template copies, the delta pH of all the positive aliquots reached the average value of $\text{pH} = -1.18 \pm 0.05$. This means reaction has already plateaued. The LAMP reaction is thus very sensitive, able to detect down to 20 copies of template in 25 μL of reaction buffer.

Finally, a 10X serial dilution of the lambda DNA template was performed, but amplified for 18 minutes to be in the linear range of the pH readout. This experiment was conducted three times (biological replicates), with two different replicates (technical replicates) each time, originating from the same reaction mix but separate template loading. For the 6 measurements, the delta pH obtained is proportional to the logarithm of the template copies number. A linear model can be fitted to each curve (mean $R^2 = 0.83$), but the slopes and intercepts are different. The two technical replicates curves, represented with the same color in the Figure 2.12, were more similar than the biological replicates. This is attributed to variability due to pipetting and can be rectified with aliquoting the master mix.

LAMP consistently amplifies 80 copies/ μL of lambda template, which suggest that it would be able to reliably detect single copy template in microchambers of few nanoliters and so be suitable for digitization applications. The dynamics at a low scale may be different and need to be characterized, but sensitivity is expected to be enhanced with reduced reaction volume.

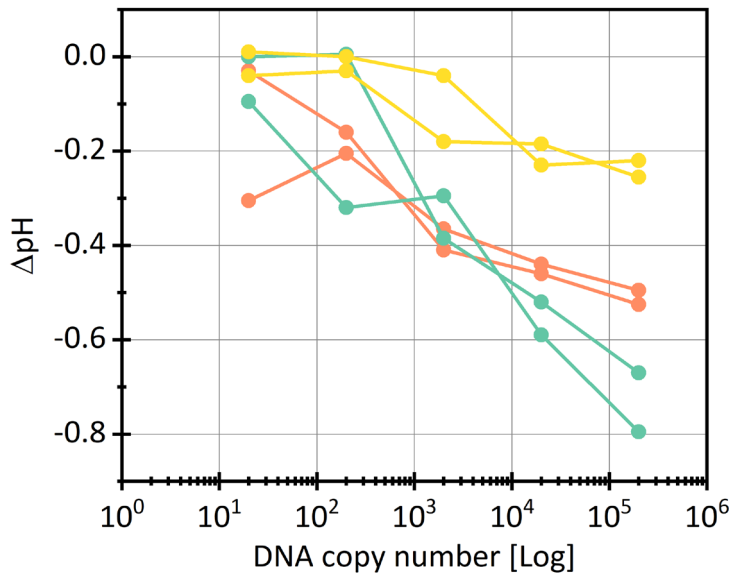


Figure 2.12. Standard curve for pH-based LAMP. delta pH measurements after performing LAMP for 22 minutes with different lambda template concentrations. The two technical replicates from one experiment are displayed in the same color.

2.3.3 LAMP at low temperatures

Being isothermal and not requiring PCR level temperatures for amplification of DNA already makes LAMP an attractive choice for POC applications. However, applicability of LAMP in these settings can be greatly improved if LAMP can be performed at even lower temperatures. Apart from reduction in device complexity, power consumption and reduced evaporation, pH-based electronic readout by ISFET benefits directly from lower amplification temperatures. Field effect devices like ISFETs suffer from carrier mobility degradations at elevated temperatures thus negatively affecting the signal-to-noise ratio. Therefore, lower amplification temperature can enhance the sensitivity of ISFET-based DNA amplification detection.

Temperature influences two key steps in a DNA amplification assay. Firstly, the activity of polymerase follows a bell curve dependence with temperature. Lower temperatures limit catalytic activity of the polymerase while higher temperatures lead to denaturation of the polymerase structure. The optimal temperature for *Bst* 2.0 polymerase is 65°C with its activity falling to 30-50% at 50°C and at 72°C. Secondly, double stranded helical structure of DNA is more stable at lower temperatures, thereby making primer access to the target sequence harder. Furthermore, the usual melting temperature of LAMP primers is around 60°C. Therefore, at temperature below that they are prone to non-specific bindings as their access to complementary sequence is restricted leading to spurious amplifications. Therefore, performing LAMP at low temperatures is not obvious due to reduced amplification efficiency of the polymerase and difficulty of primers to anneal to the target. In the following section, we explore different strategies to address these challenges.

2.3.3.1 Optimizing polymerase activity

Magnesium (Mg^{2+}) is essential for polymerase activity and negatively affects it if the concentration of Mg^{2+} ions is too low. However, high concentration of salt or Mg^{2+} ions also stabilize the double stranded structure of DNA thereby limiting amplification yield. Similarly, excessive Mg^{2+} can also stabilize non-specific annealing of primers to target DNA leading to reduced specificity [45]. Different concentrations of $MgSO_4$ within the reaction buffer, ranging from 0 mM to 10 mM, were tested in challenging amplification conditions. The first experiment happened at 65°C at the lower limit of detection of LAMP (2000 copies, 18 min). The second experiment was performed at low temperature (50°C, $2 \cdot 10^5$ copies, 60 min). It resulted that 6 mM allowed a better amplification in these two conditions, and a better delta pH (Figure 2.13). All the following experiments were performed with this optimal concentration of 6 mM of $MgSO_4$.

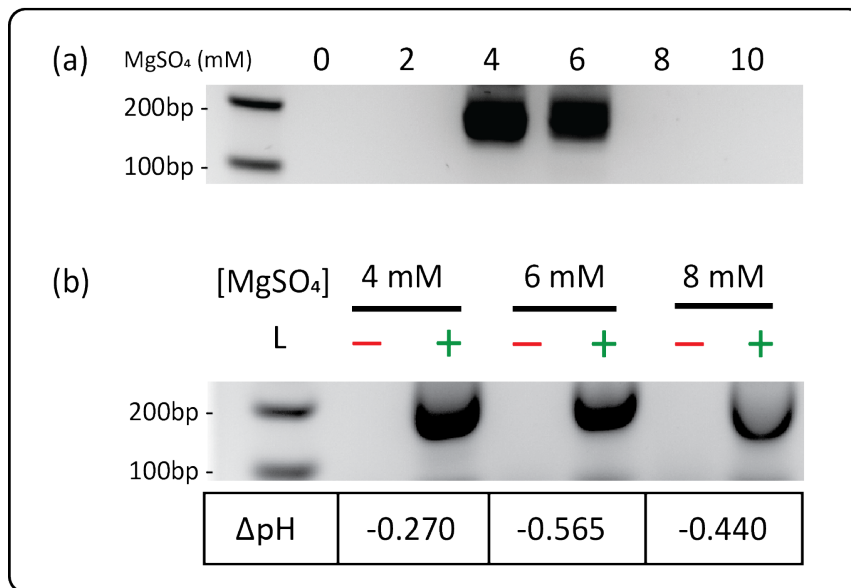


Figure 2.13. Optimization of Mg^{2+} for low temperature LAMP. (a) LAMP performed at 65°C for 18 minutes with 2000 copies of lambda template. (b) LAMP performed at 50°C for 60 minutes with $2 \cdot 10^5$ copies of template, and the delta pH associated.

Increasing the incubation time does not modify the enzyme activity but can allow its visualization, as reduced activity is the equivalent of a lower concentration or decreased incorporation rate. A higher template concentration will also increase the likelihood that the primers reach their target. Using $2 \cdot 10^5$ lambda template copies, LAMP was able to detect and amplify the target gene in less than 60 minutes at 45°C in approximately 50% of the replicate experiments ($n = 10$). It was able to amplify down to 40°C, but inconsistently. Figure 2.14a presents the delta pH obtained at 45°C, compared to the values obtained at 65°C with the same amount of template DNA, but conditions not optimized for low temperature operation (8 mM of $MgSO_4$, 30 min). Expectedly, the pH difference at 45°C ($\Delta pH = -0.395$) is reduced compared to the one at 65°C ($\Delta pH = -1.28$). However, the signal is large enough, such that it should be possible to perform LAMP amplification at 45°C for the detection of target genes albeit with a higher amount of template and longer incubation time.

Increasing polymerase amount did not positively affect efficiency of LAMP at low temperatures (Figure 2.14b). Therefore, the value from the standard protocol (8U) was thus kept for the following experiments.

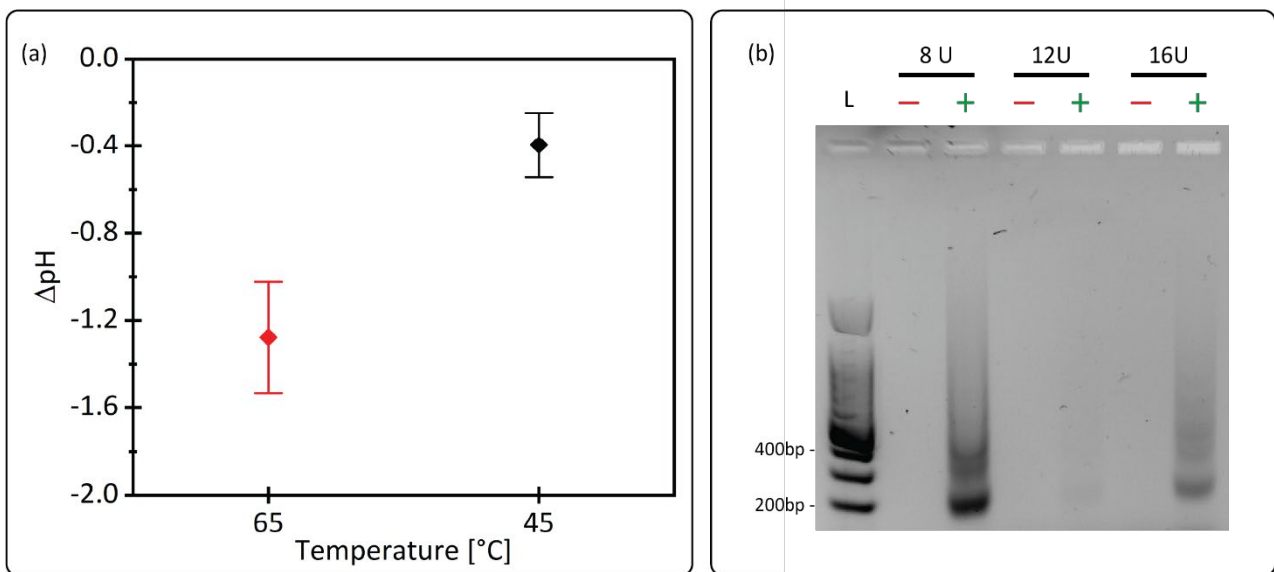


Figure 2.14. Optimized LAMP at low-temperature. (a) Amplification was performed at 45°C for 60 minutes, with 6 mM MgSO_4 . They are compared to data from LAMP performed at 65°C for 30 minutes with 8 mM MgSO_4 following the standard protocol. (b) Titration of *Bst* 2.0 polymerase for LAMP at low temperature. LAMP was performed with different concentrations of the polymerase at 45°C for 60 minutes with $2 \cdot 10^5$ copies of the template.

2.3.3.2 Destabilizing the double stranded DNA

Cai et al [46] used various agents that destabilize the double-stranded structure of DNA to decrease the LAMP's operating temperature. A phosphorothioate (PS) oligonucleotide is a backbone variant of DNA, where the phosphodiester linkage is replaced by a phosphorothioate linkage as shown in Figure 2.15. This feature protects the oligonucleotide from nucleases, and decreases the melting temperature of duplexes between regular DNA and PS-modified oligonucleotides [44]. It has been exploited to develop a new amplification method where PS modifications incorporated in the template promote self-folding of terminal loop structures [45]. Changing the inter nucleotide bond in the F1c part of the FIP primer (and the B1 part of the BIP primer) disrupts the homozygous DNA duplex and favors the hairpin formation. Cai et al. were able to push the LAMP operational temperature from 60°C to 40°C.

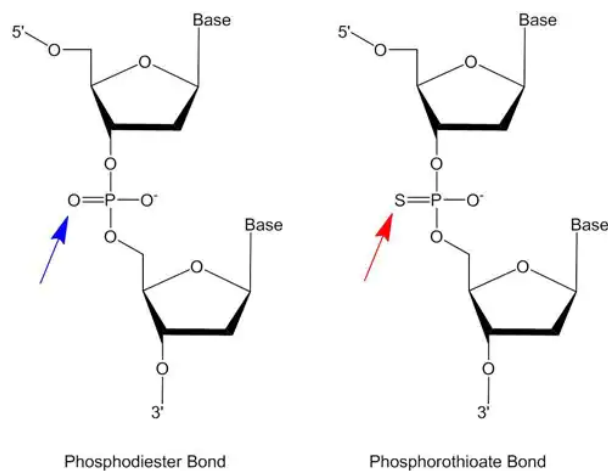


Figure 2.15 Phosphorothioated oligonucleotide. A phosphodiester bond has been replaced by a phosphorothioate bond. Illustration from Merck©

Primer	Sequence
FIP	5'-C*A*G*C*C*A*G*C*C*G*C*A*G*C*A*C*G*T*T*C*GCTCATAGGAGATATGGTAGAGCCGC-3'
BIP	5'-G*A*G*A*G*A*A*T*T*T*G*T*A*C*C*A*C*C*T*C*C*C*A*C*C*G*GGCACATAGCAGTCTAGGGACAGT-3'

Table 2.3. LAMP primer sequences with phosphorothioate modifications. Each "*" represents a phosphorothioate bond between two bases. The rest of the primers were not modified.

The reaction with PS-primers (called PS-LAMP) was performed following the standard protocol and concentrations presented in the methods, and following the protocol and concentrations of the destabilizing agents from the paper. As seen in the Figure 2.16 the amplification was reduced in PS-LAMP compared to regular LAMP. This observation was also reflected in the pH signal.

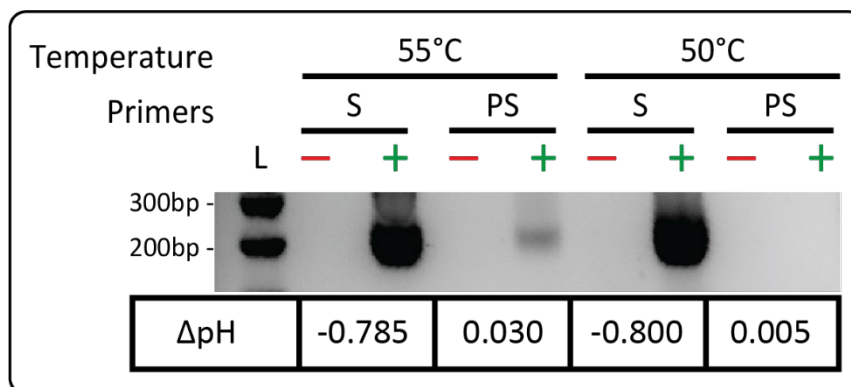


Figure 2.16. LAMP with phosphorothioate-modified primers. Standard LAMP (S) and PS-LAMP (PS) were performed in the same conditions at 55°C and 50°C, with 2.10^5 copies of template DNA for 60 minutes. Corresponding delta pH are displayed below

Other studies using PS-modified primers but with only one modified linkage at the 3' end found similar results. Andreola et al. [47] showed that the yield of the HIV-1 virus reverse transcriptase, an enzyme performing dNTPs incorporation similar to the polymerase, is decreased when using PS-modified primers. At elevated concentrations (30-50 nM), it even inhibits its activity. Di Giusto et al. [48] showed that the PS modification reduced extension rate by 5%. These drastic effects happened with the modification of only one internucleotide bond of the primers, whereas our PS-modified primers contains 20 of them. Also, the modification make the phosphorus a chiral center, leading to existence of two diastereomers (Sp and Rp) for each of this interlinkage [49]. Difference in affinity for nucleotide incorporation by polymerase can also lead to reduction in amplification efficiency. It is known that only Sp-diastereomer dNTPs are a good substrate for the polymerase. Similarly, it could be that steric clashes in the PS-modified primers that can reduce the incorporation rate. In the end, the temperature of LAMP could not be lowered thanks to the PS-modifications primers, at least not without substantially increasing the incubation time.

Apart from use of phosphorothioate primers Cai et al. [16], employed other destabilizing agents to further decrease the temperature and improve performance. Among them, single-strand DNA-binding proteins (SSB) which have already been shown to enhance PCR amplification efficiency [50]. SSBs are commonly used in low temperature isothermal amplification methods, most notably in RPA. Upon primer annealing to the complementary sequence on the target DNA, SSB proteins help stabilize them by binding to the displaced DNA strand, while the polymerase starts elongating [51]. It can also prevent unspecific binding and amplification.

Neither the *E. coli* (ab123224) SSB nor the Extreme Thermostable (ET-SSB), more adapted to incubation above 37°C, succeeded in improving the performances of LAMP at low temperature. Different concentrations were tested, but the more SSB was added, the fewer amplification products and pH differences with

the NTC were obtained, as seen in Figure 2.17a,b. The aliquots with a high concentration of ET-SSB did not amplify after 60 minutes, but they all did after 120 minutes. The reaction is slowed, but not inhibited. Contrary to what was expected, SSB negatively affected the efficiency of LAMP at low temperatures, even when it was associated with PS-modified primers. Cai et al. perform a pre-denaturation step at 95°C to favor primers annealing to the template. With an aim to develop single-step close tube assay, this optional step was not included in our protocol. This can explain why SSB had no positive impact on our reaction, they only stabilize primers when the two strands of DNA are already melted. Furthermore, they can attach to the single-strand primers, preventing them to bind the template, which slows the amplification.

Urea is a chaotropic agent, that can destabilize the DNA structure [52]. It has also been demonstrated to unfold the proteins, in a similar way to heating at a temperature above the melting temperature. Thus, it also affects the polymerase and can influence its activity. Urea was used by Cai et al. [46] and is expected to help circumvent the incubation at 65°C. Different amount of urea were added in the reaction mix (from 0 to 36 μmol per 20 μL aliquots). However, the more urea in the reaction, the fewer amplification products and delta pH were produced, as can be seen Figure 2.17c, d. Urea affects negatively LAMP at low temperature.

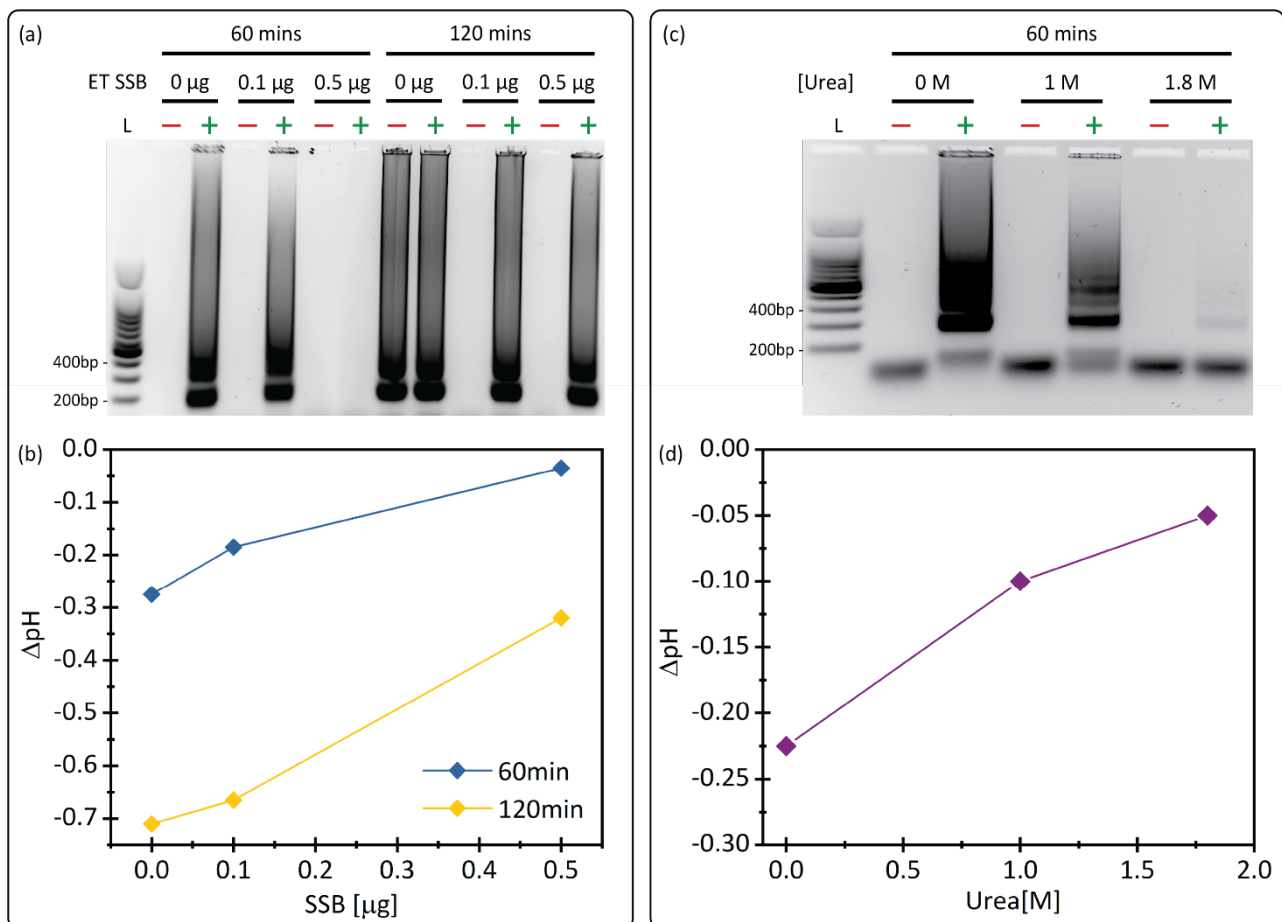


Figure 2.17. Effect of ET-SSB and urea on LAMP. Different concentrations of ET-SSB were added to the LAMP reaction mix. (a) The gel displays amplification product after incubation at 45°C for 60 and 120 minutes, with $2 \cdot 10^5$ copies of template DNA. The NTC with no SSB for 120 min was contaminated, so the delta was calculated from the mean of the others NT. Different concentrations of urea were added to the LAMP reaction mix. Gel (c) and delta pH measured (d) after incubation at 45°C for 60 minutes, with $2 \cdot 10^5$ copies of template DNA.

2.3.3.3 Alternate strategies

The *Bst* 2.0 polymerase is optimized to work at 65°C. This is why its activity is reduced at low temperatures. *Bacillus subtilis* DNA polymerase I (*Bsu*) was explored as a replacement for *Bst* 2.0 as it has a low working temperature of 37°C and possesses properties similar to *Bst* 2.0 such as strand displacement DNA synthesis and lack of 5'-3' exonuclease activity. Its activity was compared to *Bst* 2.0. LAMP was performed at 45°C and 40°C. Only *Bst* 2.0 was able to amplify the target and display a change in pH. This implies probably that even at low temperatures, the *Bst* 2.0 polymerase is more suited to LAMP because its intrinsic performances (strand-displacing and incorporation rate) are superior to those of *Bsu*.

As explained before, the pre-denaturation step consisting in incubating the reaction mix and template at 95°C for 5 minutes before adding the polymerase did not change the result when performing LAMP at 65°C. However, at 45°C, as oligonucleotides have restricted access to the complementary template sequence, this pre-denaturation step becomes significant as it facilitates the annealing of primer to the target. However, to avoid using high-temperature steps in a low-temperature amplification process, the process was adapted to short a pre-incubation step at 60°C for 2.5 or 5 minutes. It is performed while the *Bst* 2.0 polymerase is already in the aliquot, which removes the risk of contamination from reopening the tubes after template addition.

This incubation step had a significant effect on the amplification at low temperatures, as can be observed in Figure 2.18. It improved the reliability of the reaction at low temperature. Over the four replicate experiments, the pre-incubated aliquots always displayed amplification products, unlike the aliquots that only stayed at 45°C. It increased the efficiency of the LAMP, and the absolute delta pH measured. Though still lower than when LAMP is performed at 60°C for 60 minutes, ΔpH of -0.32 is sufficient to be distinguished by an ISFET.

Different tests were performed to understand the mechanisms behind the enhancement in signal due to pre-incubation step. Both the step at 60°C and the incubation at 45°C for 55 minutes are essential to get amplification products. When the reaction was stopped after pre-incubation, no signal was obtained (Figure 2.18a), implying it is the subsequent incubation that leads to majority of the DNA amplification. The short incubation step at 60°C can also be performed at the start or at the end of long incubation at 45°C. Both the cases showed a drop in pH; however, the change in pH is less when incubation step is performed at the end (Figure 2.18b). A short 60°C incubation at the start helps in generation of sufficient amount of dumbbell like structures from template DNA (Figure 2.18c). These dumbbell-like DNA later acts as sites for cyclic amplification. These dumbbell-like DNA are formed with reduced efficiency when no incubation at 60°C is performed at the start, resulting in overall less amplification (Figure 2.18c) and consequently low ΔpH signal (Figure 2.18.d).

LAMP at 45°C may not be at RPA's level, but a 20°C reduction in operating temperature does allow for simplified microfluidic designs for ultra-low volumes. Performing LAMP at 65°C in nanoliter or smaller sized volume necessitates further application of strategies to minimize evaporation thereby increasing device complexity and cost.

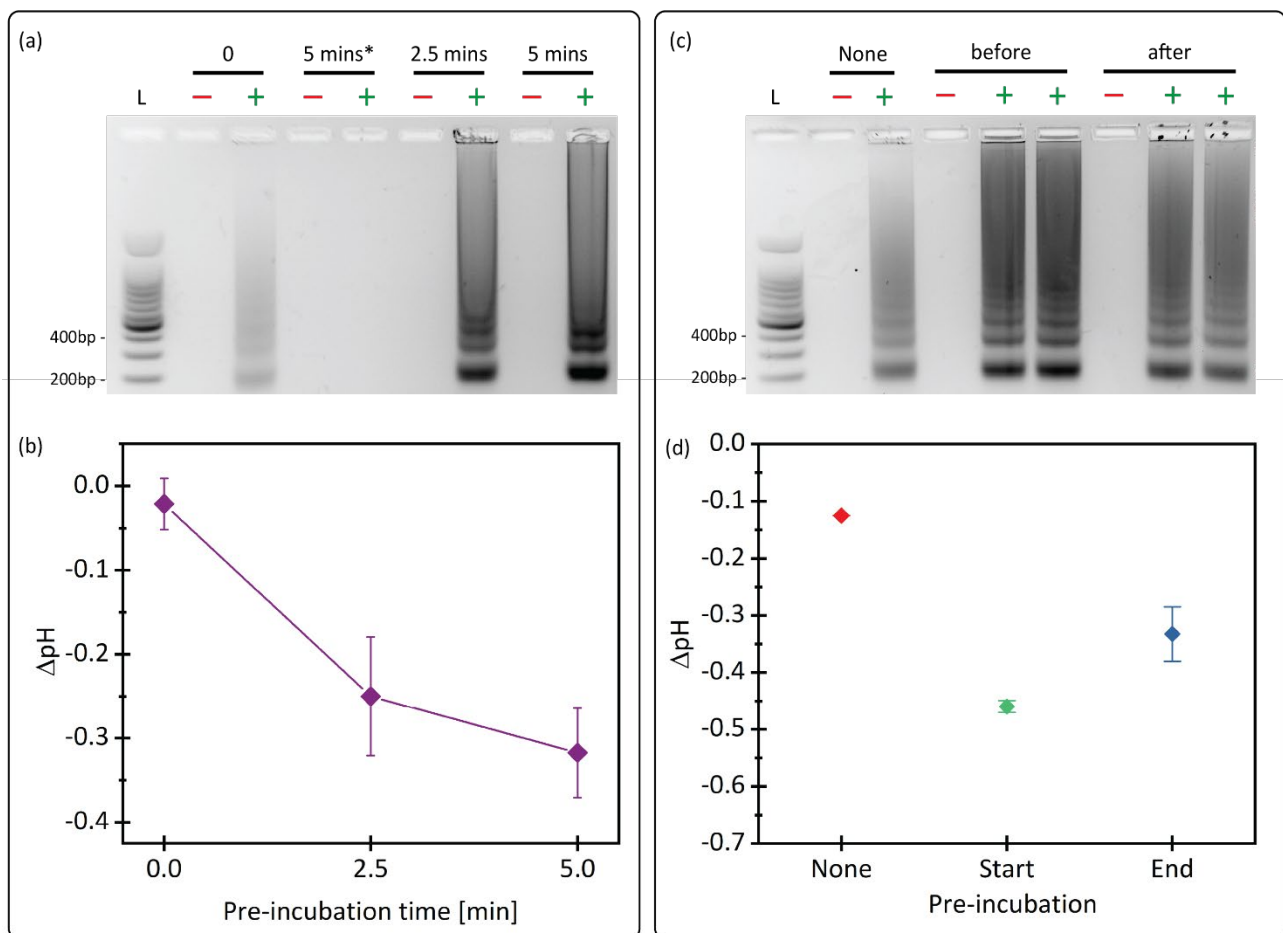


Figure 2.18. Low-temperature LAMP with pre-incubation at 60°C. (a) Gel after amplification of $2 \cdot 10^5$ copies of the template. Aliquots were heated at 60°C for different durations (from 0 to 5 minutes), before incubation at 45°C for a total of 60 minutes of reaction. The exception was for the 5mins* aliquot, which was stopped directly after the 5 minutes at 60°C. (b) ΔpH obtained when pre-incubating at 60°C for 2.5 minutes ($n = 2$), 5 minutes ($n = 4$) or 0 minutes as control ($n = 4$). (c) Gel and (d) ΔpH for LAMP pre-incubated at 60°C during low-temperature LAMP. One NTC is contaminated, so the delta pH was calculated from the mean of the other NTCs. A heating step at 60°C for 5 minutes was performed before or after incubation at 45°C for 55 minutes. “None” is a control, where aliquots were incubated for 60 minutes at 45°C. LAMP was performed with $2 \cdot 10^5$ copies of template.

2.3.4 Summary

LAMP is an isothermal amplification method that displays a change in pH during elongation when the main pH-buffering constituent (tris-HCl) is removed. Similar to RPA even in minimally buffered conditions LAMP buffers retain significant pH buffering capacity. However, due to very high amplification yield, LAMP is able to overcome this buffering capacity and exhibit a noticeable pH shift. At its optimal working temperature (65°C) and in a condition close to a real application (30 minutes of incubation with $2 \cdot 10^5$ copies of lambda template), a mean delta pH of $\Delta\text{pH} = -1.28$ is obtained. The reaction is fast; it is possible to reduce incubation time down to 16 minutes. The delta pH measurement is directly correlated with the initial quantity of the template when operated within the dynamic range of the sensor (low incubation time). After calibration and linear fit, pH readout of LAMP could be used to assess the initial concentration of DNA in the sample. It is sensitive down to 20 copies of the lambda target gene. However, this high sensitivity combined to the huge yield of LAMP makes it prone to carry-over contaminations.

Though recommended temperature for LAMP is 65°C, various strategies were investigated to reduce the LAMP assay's temperature. After optimization of the parameters, especially salt concentration, LAMP

showed successful amplification at 45°C, with a reduced delta pH (mean $\Delta\text{pH} = -0.395$). However, the incubation time had to be increased to one hour, and the detection was inconsistent: only half of the aliquots could amplify. Based on work from Cai et al.[46], we tried adding destabilizing reagents (phosphorothioate primers, single-strand binding proteins, urea) to reduce the melting temperature of DNA, and thus the incubation temperature. The results were not satisfactory and the agents negatively affected the reaction. Replacing the thermostable *Bst* 2.0 polymerase by *Bsu* operating at low temperature showed no positive effect on the amplification and pH readout. Further optimization and verification impact of these modifications in minimally buffered conditions should be performed to understand the differences in the results. Further tailoring of the reaction buffer and operating conditions need to be carried out to adapt these agents into pH-based LAMP assays. A pre-incubation step at 60°C for a few minutes helped to get a reliable amplification at 45°C, with a consistent pH readout. Therefore, in conclusion, until the LAMP assay can be fundamentally adapted to operate at low temperatures, a short pre-incubation at 60°C offers the least complicated way to adapt LAMP for low-temperature pH-based readout.

2.4 Conclusion

In conclusion, we investigated two most popular DNA amplification methods and investigated their applicability for a pH-based readout at low temperatures. Though RPA can operate in near room temperature settings, due to its inherent biochemistry, RPA was found to be not a suitable candidate for pH-based readout of DNA amplification. LAMP on the other hand gave reliable and consistent pH-based readout of amplification. Therefore, going forth LAMP will be the assay of choice for all the future applications.

Chapter 3 Hybrid microfluidic packaging with integrated reference electrode

The work presented in this chapter is partially adapted from the article published in *Micromachines* 2022.

Authors: Saurabh Tomar, Charlotte Lasne, Sylvain Barraud, Thomas Ernst and Carlotta Guiducci.

Contributions: Saurabh Tomar contributed to conceptualization, methodology, validation, investigation, visualization, writing and editing.

Reference: Tomar, S.; Lasne, C.; Barraud, S.; Ernst, T.; Guiducci, C. Integration of Ultra-Low Volume Pneumatic Microfluidics with a Three-Dimensional Electrode Network for On-Chip Biochemical Sensing. *Micromachines* 2021, *12*, 762.

3.1 Introduction

Arrayed biosensors, consisting of multiple sensors on a single platform are of great interest as they allow simultaneous characterization or monitoring of biochemical phenomena at increased resolution and sensitivity. Their ability to multiplex, robustness, increased redundancy and real-time monitoring with higher spatiotemporal resolution offer unparalleled flexibility to perform bioanalysis at different biological levels (eg., DNA, cells, tissue or organ). Buoyed by the advancements in manufacturing technology, biosensor arrays - especially the electrochemical arrays are eliciting greatly renewed interest. Electrochemical arrays of microelectrodes and field effect sensors have benefited immensely from breakthroughs in new materials and microfabrication technology, leading to increased miniaturization and digitization.

Field effect sensors like ISFETs and microelectrodes have been scaled down to nanometer dimensions [53][54] and scaled up in density to hundreds to millions of sensors per chip [55][56][20]. These sensor arrays have been used in a wide variety of applications ranging from NA sequencing [20], small molecules [57], proteins [58], viruses [59], cells [54] and tissues [60]. As evident, much research effort has been spent on the sensor part of biosensing; however, the microfluidic part has comparatively lagged behind. State-of-the-art biosensing solutions for small analytes (less than a few hundred micrometers) still utilize big electrolyte pools with macroscopic reference electrodes for biosensing [53][61][62][55]. Multiplexing in such solutions is limited and generally achieved via capture probes or surface immobilization, which are complex to design and requires post-fabrication processing of the sensor chip.

Combining partitioning microfluidics with electrochemical arrays can eliminate the need for surface functionalization and benefit from increased sensitivity in microfluidic volumes. Reaction multiplexing can be dramatically increased as a large number of reactions can be carried out in parallel. ISFET-based sensor array benefits the most from such microfluidic packaging. However, parcellation-based multiplexing requires that each reaction parcel have access to an in-chamber reference electrode (RE). On-chip miniaturized reference electrodes have addressed these limitations [61]. On-chip miniaturized REs have a relatively larger footprint as compared to an ISFET sensor, which negatively affects the density of ISFETs on the chip. Moreover, fabrication of on-chip RE post-CMOS fabrication can negatively affect the sensor behavior. As post-CMOS processing is a nonstandard process, it may introduce variabilities in the sensing layer, which can affect chip-to-chip response.

To truly achieve the potential of CMOS technology for biosensing implies to be able to simultaneously carry out hundreds or thousands of biosensing reactions in mutually and electrolytically isolated, micro-sized biochemical incubation chambers, each of which is monitored in real-time by one or more ISFET sensors. Such an approach requires parcellization strategies in microfluidics that can integrate a miniaturized reference electrode and all the while avoiding any post-CMOS processing.

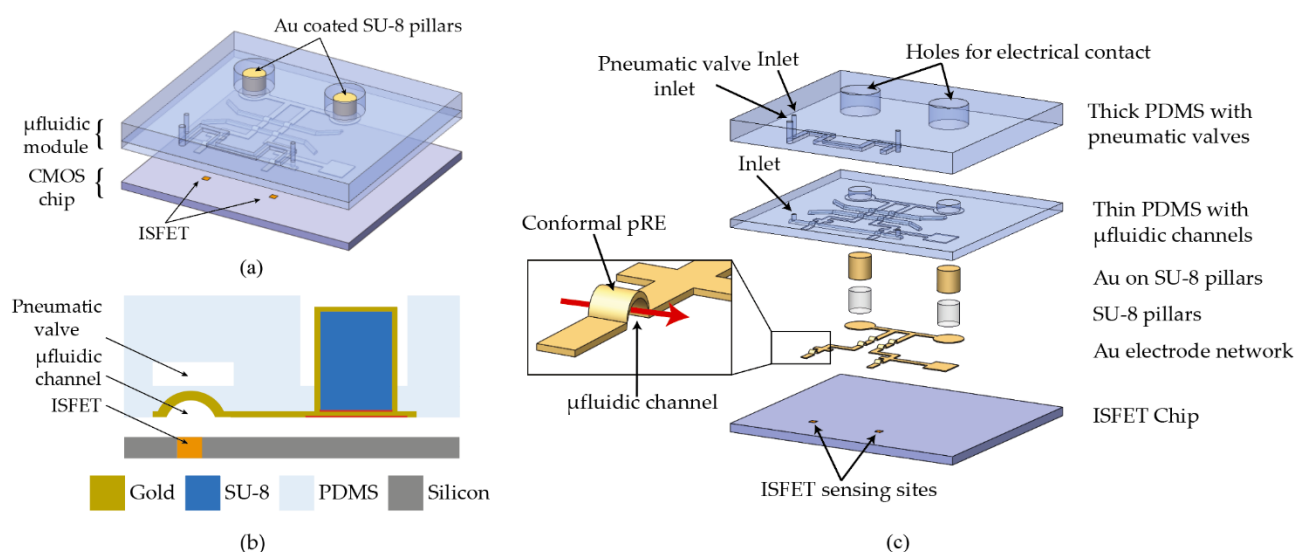


Figure 3.1 Schematic of hybrid microfluidic packaging. (a) 3D schematic of the microfluidic module on a CMOS chip consisting of two nanoliter-sized chambers that are created upon actuation of a pneumatic valve. (b) Cross-sectional schematic of the module showing the metal-coated “Through-PDMS-Vias”. (c) Exploded view of the microfluidic module showing the comprising layers. The inset shows conformal pseudo-RE with the liquid flow (red arrow) in the microchannel.

Here, we propose a microfluidic design that successfully addresses all the above issues. We developed a non-planar miniaturized pseudo reference electrode (pseudo-RE) that conformally coats the inside of the PDMS microfluidic channel. The design concept is presented in Figure 3.1. The pseudo-RE network is integrated into PDMS and is electrically accessible by “through-PDMS-vias” (TPV). TPV are made of gold-coated, very high SU-8 pillars that go through the PDMS matrix. The presented strategy allows reversible integration of a miniaturized reference electrode close to the ISFET sensing surface. Reaction mixture parcellization into nanoliter (nL) size volumes is achieved by the integration of pneumatic valves. These electrolytically isolated parcels over ISFETs are biased by an “in-chamber” pseudo-RE, thereby enabling multi-reaction sensing on a single chip. The need for post-CMOS processing chips is eliminated by the combination of conformal pseudo-RE in microfluidics and TPV [63].

Such a strategy for achieving high throughput and multiplexing differs from the open well configuration of Ion Torrent sequencing. Ion Torrent system utilizes what we can call as “temporal parcellation” for achieving increased throughput. Whenever a nucleotide base is incorporated into the bead-immobilized DNA libraries, there is a sudden increase in the local H^+ concentration. This temporally increase in the local H^+ concentration, which lasts only for couple of seconds is read by the ISFET sensor before these H^+ ions diffuse into the bulk electrolyte. Such “temporal parcellation” and detection of reaction by-products works perfectly well for sequencing read applications, where biochemical reaction time to get measurable signal are short. However, for nucleic acid amplification testing, where the amplification reaction durations are in the order of minutes and DNA target copies low, “temporal parcellation” of H^+ will not work as the generated H^+ will keep on diffusing into the bulk electrolyte before producing any measurable change in the H^+ concentrations at the ISFET surface. Therefore, for NA amplification testing, it is necessary to use “spatial parcellation” by physically isolating the reaction chambers by the means of pneumatic valves, phase boundary separation etc.

3.2 Microfluidic module: Fabrication and Characterization

3.2.1 Microfabrication process

The whole process flow was carried out on a 4-inch silicon wafer. After priming the silicon wafer with HMDS (hexamethyldisilazane), a 10 μm of positive tone resist (AZ 10XT) was spin-coated over it. A negative mold for 150 μm wide microfluidic flow channels was patterned by standard photolithography of AZ 10XT resist. Patterned AZ 10XT was then baked at 140 $^{\circ}\text{C}$ (ramping rate of 4 $^{\circ}\text{C}/\text{min}$) for 2 hours to reflow the resist in order to achieve a rounded cross-section (Figure 3.2a, Figure 3.3a) for microfluidic channel mold from an initially rectangular one. The reflow of the resist also leads to an increase in the channel mold height from 10 μm to 12 μm at its highest point. To protect the resist mold from subsequent processing steps, the whole wafer was passivated by bilayer evaporation (Leybold Optics Lab 600H, Bühler Leybold Optics, Alzenau, Germany) of Ti/Pt (10/100 nm). A 500 nm of sacrificial aluminum layer was sputtered (Pfeiffer SPIDER 600, Pfeiffer Vacuum, Asslar, Germany) on top of Platinum (Figure 3.2b, Figure 3.3b). The aluminum layer is later etched away via anodic dissolution to release the final microfluidic module from the silicon wafer.

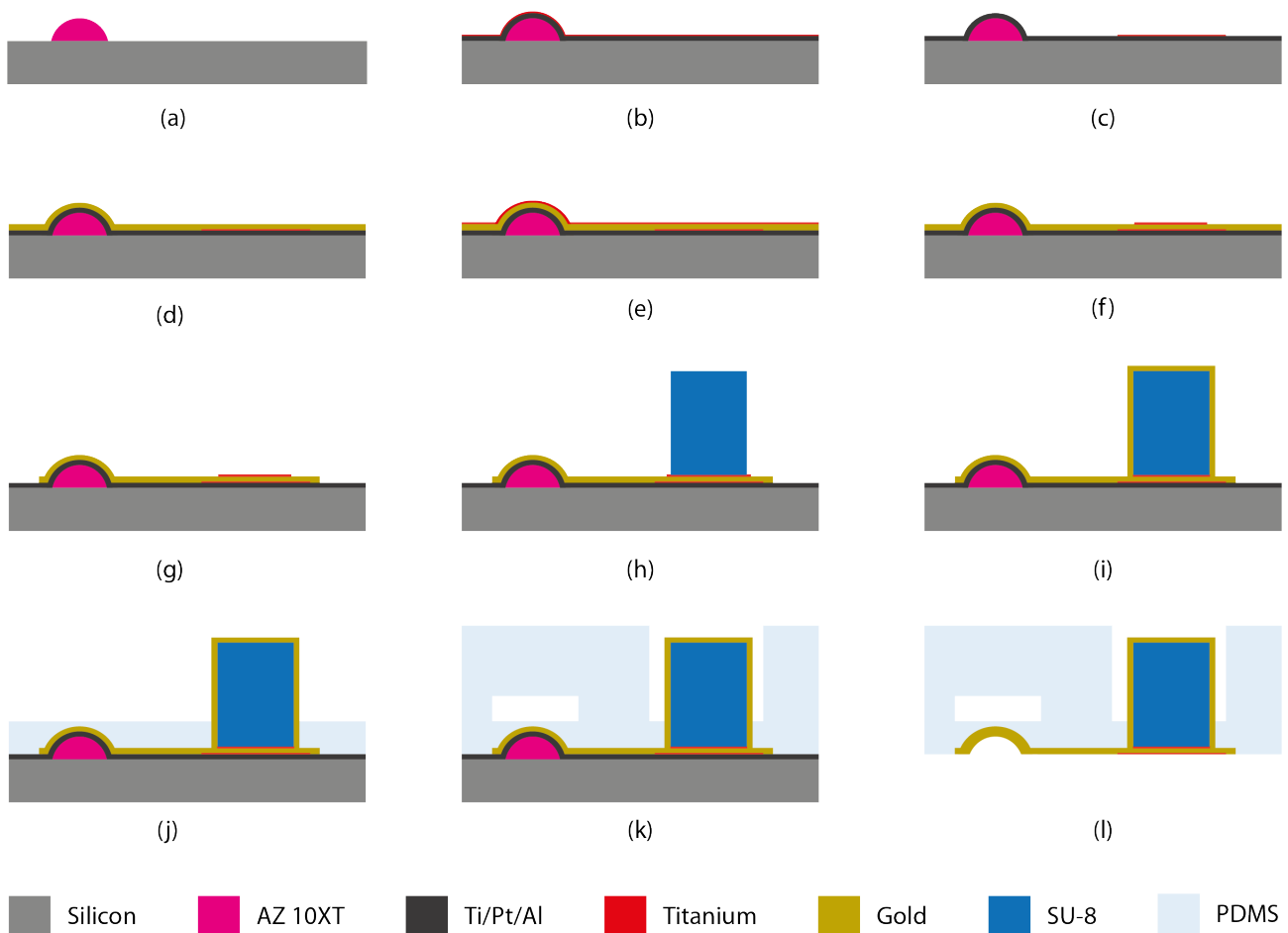


Figure 3.2. Wafer level process steps for fabrication of the microfluidic module featuring pseudo-RE and TPV.

A 20 nm adhesion layer of Titanium (Ti(1)) was evaporated on top of aluminum. The evaporated Titanium was then spin-coated with 5 μm AZ ECI 3027 positive tone resist. The resist was UV exposed on a mask

aligner (KarlSüss MA6/BA6) with a dose of 415 mJ/cm^2 . The resist was developed in AZ Developer MIC (Microchemicals GmbH, Ulm, Germany). Titanium (Ti) was etched by ion beam etching (Veeco Nexus IBE 350, Veeco, Plainview, NY, USA) to define Ti regions, which promote adhesion for gold (Figure 3.2c). After stripping the resist in oxygen plasma (Tepla GiGAbatch, PVA TePla AG, Wetztenberg, Germany), a 200 nm of gold layer (Au(1)) was sputtered (Alliance-Concept DP650, Annecy, France) to cover the entire wafer (Figure 3.2d). Subsequently, a second 20 nm adhesion layer of titanium (Ti(2)) was evaporated on top of gold (Figure 3.2e). Just like the former titanium layer, the second layer (Ti(2)) was patterned via photolithography and etched by ion beam etching (IBE) to serve as an adhesion layer between gold and SU-8 resist (Figure 3.2f). Etching away the second titanium layer in the previous steps exposes the gold layer underneath. After stripping the AZ ECI resist, a $20 \mu\text{m}$ of AZ 10XT is spin-coated over the gold layer. The resist was exposed in a mask aligner with a dose of 880 mJ/cm^2 and developed to define a gold electrode network. Subsequently, the gold electrode network was patterned by etching the gold via IBE (Figure 3.2g). After etching, the resist was stripped via treatment in oxygen plasma.

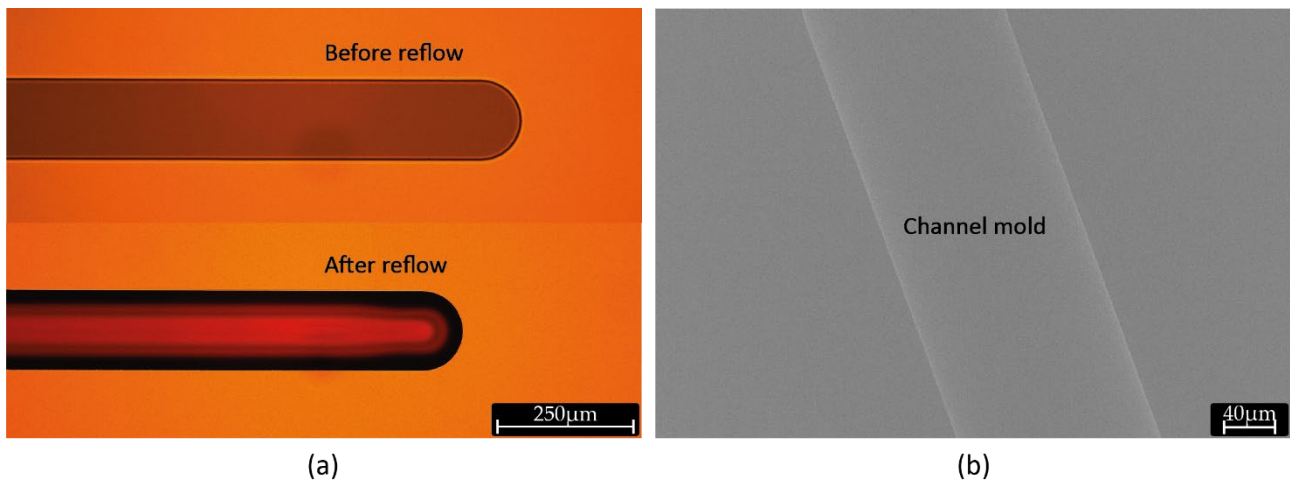


Figure 3.3. Fabrication of microchannel mold. (a) Optical micrograph of negative mold for microfluidic channel before and after reflow of AZ 10XT resist. (b) SEM image of negative mold after sputtering of aluminum.

3.2.2 Metal-coated multi-layer SU-8 pillars

After gold electrode patterning, an $8 \mu\text{m}$ layer of AZ 10XT photoresist was spin-coated on the wafer. The resist was then patterned by photolithography such that the whole wafer, except for the regions where SU-8 will remain after exposure, maintains the positive photoresist layer (Figure 3.4i). A short descum process (30 s, 200 W) in oxygen plasma was performed to remove any residual photoresist in developed regions.

The 1 mm SU-8 pillars were fabricated by spin-coating multiple layers of SU-8. Before SU-8 coating, the wafers were dehydrated by baking at $90 \text{ }^\circ\text{C}$ for 15 min. A $300 \mu\text{m}$ of the first SU-8 (SU-8 100, Kayakli Advance Materials, Westborough, MA, USA) layer was spin-coated on the wafer. The wafer was soft baked on a hotplate at $65 \text{ }^\circ\text{C}$ for 20 min and then at $95 \text{ }^\circ\text{C}$ for 90 min. The SU-8 layer was exposed on the mask aligner to define 2 mm wide circular pillars (two per microfluidic module), which will later serve as freestanding structures to bias the pseudo-RE. UV exposure was done in proximity contact with $15 \mu\text{m}$ of exposure gap between the mask and SU-8 layer. The exposure dose of 900 mJ/cm^2 was delivered in four steps, each of 11.3 s long with 30 s of wait time between each exposure step (Figure 3.4i–iii). Then, the second layer of SU-8 was spin-coated over the first SU-8 layer, with the same parameters as for the first layer. The second layer was soft-baked on a hotplate at $65 \text{ }^\circ\text{C}$ for 45 min and then at $95 \text{ }^\circ\text{C}$ for 90 min. The second SU-8 layer

was exposed with the same mask and parameters as for the first layer (Figure 3.4iv–vi). Finally, the third SU-8 layer was spin-coated on top of second the SU-8 layer, with the same parameters as for the layers before. The third SU-8 layer was soft-baked at 65 °C for 75 min and then at 95 °C for 150 min. The layer was then exposed with the same parameters as for layers before (Figure 3.4viii–ix). Finally, a post-exposure bake (PEB) for the SU-8 multi-layer structure was performed at 65 °C for 30 min and then at 95 °C for 60 min (Figure 3.4x).

All three layers were developed simultaneously (Table 3.1). The wafer was developed face down in a beaker containing PGMEA (Sigma-Aldrich) for 46 min. Throughout the course of development, PGMEA was agitated by gently shaking the beaker in a circular motion. After development, the PGMEA was cleaned by IPA rinse and blow-dried under nitrogen. The average height of the SU-8 pillars measured after development was 1012 μm (Figure 3.4xi).

The SU-8 pillars were then metalized by sputtering a layer of 200 nm gold (Au(2)) through a stencil mask (Figure 3.2i). The 2 mm wide SU-8 pillars were sputtered through 2.7 mm wide circular openings in the stencil mask. The stencil mask was fabricated from a 4-inch silicon wafer by etching 200 μm deep holes via deep reactive ion etching (Alcatel AMS 200 SE). Thereafter, the wafer backside was grinded down to open the etched holes and also thin down the stencil 150 μm. This gold coating ensures an electrical contact between the top of the pillar and the patterned gold electrode lines on the silicon wafer.

SU-8 Layer	Spin Coat	Soft bake	Exposure	PEB	Development
First Layer	5 s ramp up to 500 rpm	3200 s hold at 30°C	Type: Proximity Exposure gap: 15 μm Duration:4x11.3 s, 30 s wait Intensity: 20 mJ/cm ²	Occurs during soft bake of second layer	No development
	10 s hold at 500 rpm	700 s ramp up to 65°C			
	3.3 s ramp up to 1000 rpm	1800 s hold at 65°C			
	28 s hold at 1000 rpm	700 s ramp up to 95°C			
	1 s at 14000 rpm	5400 s hold at 95°C			
	5 s hold at 1000 rpm	Cool down to RT			
Second Layer	5 s ramp up to 500 rpm	3200 s hold at 30°C	Type: Proximity Exposure gap: 15 μm Duration:4x11.3 s, 30 s wait Intensity: 20 mJ/cm ²	Occurs during soft bake of third Layer	No development
	10 s hold at 500 rpm	2100 s ramp up to 65°C			
	3.3 s ramp up to 1000 rpm	2700 s hold at 65°C			
	28 s hold at 1000 rpm	1800 s ramp up to 95°C			
	1 s at 14000 rpm	5400 s hold at 95°C			
	5 s hold at 1000 rpm	Cool down to RT			
Third Layer	5 s ramp up to 500 rpm	3200 s hold at 30°C	Type: Proximity Exposure gap: 15 μm Duration:4x11.3 s, 30 s wait Intensity: 20 mJ/cm ²	10 s hold at 30°C	46 minutes in PGMEA
	10 s hold at 500 rpm	2100 s ramp up to 65°C		1800 s ramp up to 65°C	
	3.3 s ramp up to 1000 rpm	2700 s hold at 65°C		1800 s hold at 65°C	
	28 s hold at 1000 rpm	1800 s ramp up to 95°C		1800 s ramp up to 95°C	
	1 s at 14000 rpm	5400 s hold at 95°C		3600 s hold at 95°C	
	5 s hold at 1000 rpm	Cool down to RT	Cool down to RT		

Table 3.1. Parameters for 1 mm high SU-8 pillars via three-layer coating and exposure and a single development

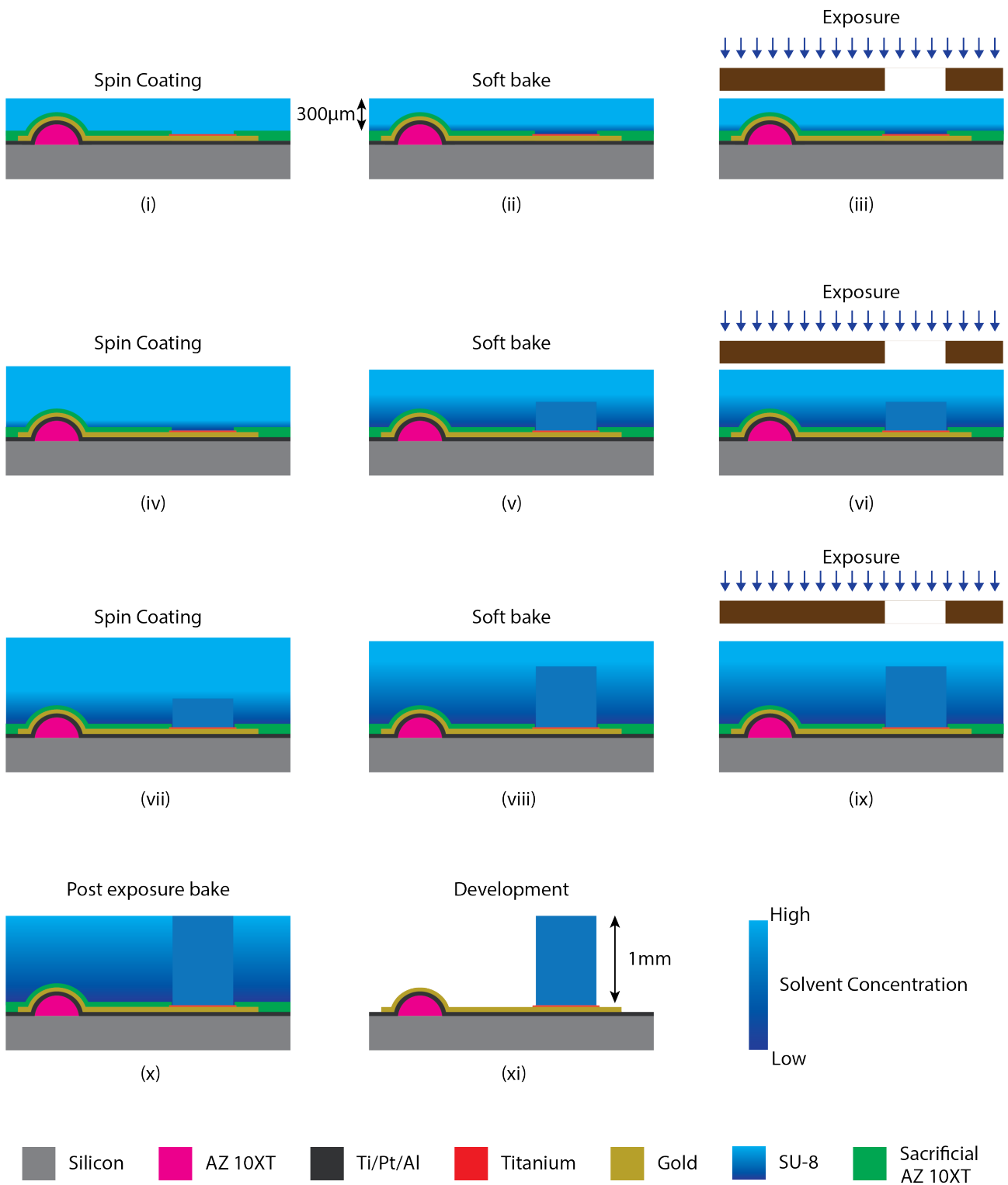


Figure 3.4. Process flow steps for multi-layer SU-8 lithography

The quality of the electrical contacts of the 3D pillars with the wafer was probed by measuring the electrical resistance between the top of the two SU-8 pillars (Figure 3.5a,b). We estimated an average pillar-to-pillar resistance of $3.51\ \Omega$ over nine different electrode pairs. Moreover, we positively assess the presence of ohmic contact between the 3D pillars in 100% of the fabricated structures (36 3D pillars on two wafers).

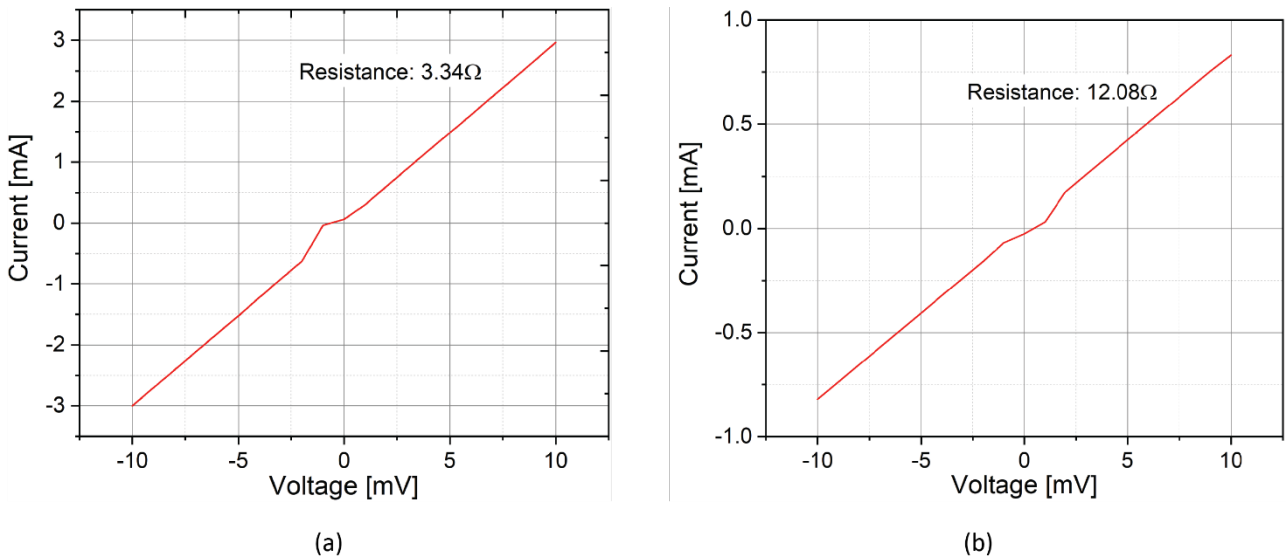


Figure 3.5. Typical two-point resistance measurement between one pair of SU-8 pillars (5mm apart) (a) before anodic release from the wafer and (b) after anodic release from the wafer. The increase in resistance upon release is due to the loss of the sacrificial aluminum layer, which provided an additional conductive path apart from gold.

3.2.3 Through-PDMS-Vias

The wafer now consists of a patterned gold electrode line with 1 mm high gold-coated SU-8 pillars. To promote adhesion between gold and PDMS, the wafer was silanized with 3-Mercaptopropyl trimethoxysilane (MPTMS). The wafer was dipped in 60 mM MPTMS-ethanol mixture for two hours. Afterwards, the wafer was rinsed in pure ethanol and blow-dried with nitrogen. Before spin coating the wafer with PDMS, the top of the pillars was protected with UV curable tape (Adwill E-6152, Lintec Advanced technologies GmbH, Munich, Germany). The wafer was then exposed to UV light to cure the tape. This reduces the tapes adhesion to the pillar top to minimize shear stress on the pillar during tape removal later. A thin layer of PDMS and curing agent mixture (20:1) was spin coated at 900 rpm over the wafer (Figure 3.2j). A thick PDMS and curing agent mixture (5:1) was drop casted over a silicon wafer containing negative mold of the pneumatic control valves. Prior to drop casting, the mold wafer was treated with trimethylchlorosilane (TMCS) to facilitate PDMS demolding upon curing. After 15 min of relaxation on a flat surface and degassing under vacuum, both PDMS layers were partially cured at $80\ ^\circ\text{C}$ for 20 min. Thick PDMS was demolded from the silicon wafer, inlet hole for control valve and 3 mm access holes for SU-8 pillars were punched into it. After dicing, the thick PDMS and the thin spin-coated PDMS were manually aligned and fully cured at $80\ ^\circ\text{C}$ for 1.5 h (Figure 3.2k). The curing was done under pressure to remove air bubbles formed during the alignment and bonding of the two PDMS layers.

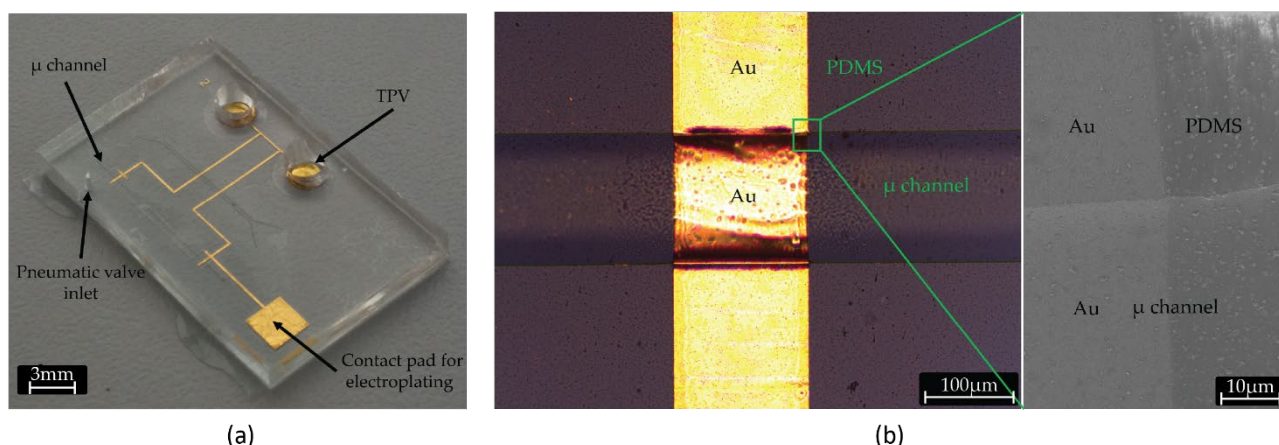


Figure 3.6. Microfluidic module and conformal pseudo-RE. (a) Microfluidic module after sacrificial release, featuring the pseudo-RE network and TPVs; (b) Optical (left) and corresponding SEM (right) image of the microchannel showing conformally coated gold pseudo-RE lines in the microchannel.

These metal-coated SU-8 pillars now function as “through-PDMS-vias” (TPV) for electrical contact to outside world. Lastly, the 500 nm aluminum layer was anodically etched to release the microfluidic module from the wafer (Figure 3.2i). The wafer was dipped in a 2 M sodium chloride (NaCl) solution to act as an anode. Another platinum-coated wafer in the NaCl solution functioned as a cathode. The anodic dissolution was carried out at a constant voltage of 0.7 V until (typically 4–5 h) all microfluidic modules have been released. Upon release, modules were rinsed with DI water and microfluidic inlets/outlets were punched. The microfluidic channel of the module is aligned with the position of ISFETs on the CMOS chip (Figure 3.1b) and bonded reversibly by one hour of thermal bonding at 80 °C or irreversibly by oxygen plasma treatment.

3.2.4 CMOS Chip and silicon nanowire ISFETs

To characterize the pseudo-RE, we employed an n-type, FDSOI silicon nanowire ISFET (length: 2.35 µm and width: 80 nm) with 3 nm thermally grown SiO₂ as sensing oxide. The ISFETs are 50 nm high and sit on top of a 400 nm thick SiO₂ insulating bulk oxide layer. The ISFETs are located on a 2 cm × 2 cm CMOS chip. The entire surface of chip, with exception of contact pads and a silicon nanowire, is passivated by a multilayer of silicon nitride (50 nm), tetraethyl orthosilicate (300 nm) and phosphosilicate glass (200 nm).

The stability of our pseudo-RE was evaluated by measuring its open circuit potential (OCP) with respect to a commercial flow through Ag/AgCl electrode (16-702, Microelectrodes, Inc., Bedford, New Hampshire, USA) over time in a 3 M KCl solution (Figure 3.7a). The observed mean OCP drift of 2 mV/hour is similar to other reported gold-based miniaturized reference electrodes [24]. Due to the macroscopic size of the standard Ag/AgCl reference electrode, OCP characterization of our gold pseudo-RE is performed in electrolyte volumes that are much larger (> 50 µL) than the volumes (~1.5 nL) when using them on a CMOS chip. Therefore, the observed OCP behavior may not reflect the true behavior of the pseudo-RE in no-flow ultra-low volume conditions as generally, microelectrodes, suffer from poor stability when used in large chambers or flow conditions [64]. Though difficult to verify, due to ultra-low volume conditions, we expect the OCP behavior of our gold pseudo-RE to be superior to that observed in Figure 3.7a.

The microfluidic module is coupled to a CMOS chip (Figure 3.7b), exposing silicon nanowires to the microfluidic channel. After injection of KCl electrolyte, the nanowire ISFET was gated via an isolated volume of few nanoliters, achieved by closing the ends of 1 mm long section of the microchannel by the actuation of pneumatic valves. Figure 3.7c shows silicon nanowire ISFET’s drain current (I_D) characteristics under varying

bias (V_{ref}) from the pseudo-RE, exhibiting a typical transistor behavior. The ISFET demonstrates an excellent static response (I_D drift = ~ 1 nA/hour) when under a constant electrode bias applied through the pseudo-RE (Figure 3.7d). With our design, we could benefit from the high surface-to-volume ratio of pseudo-RE in small-volume chambers, resulting in a low (~ 1 nA/h) drain current drift.

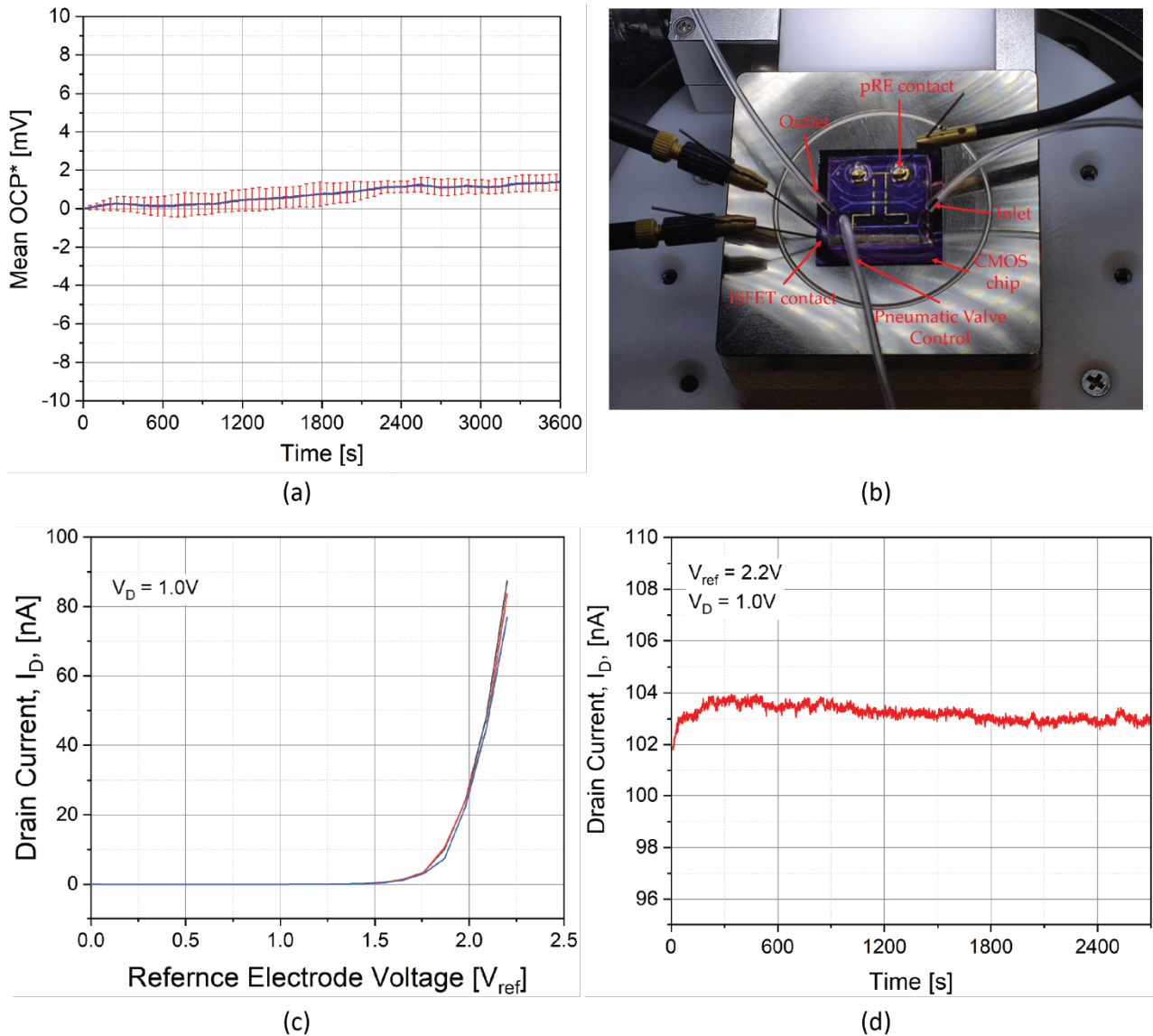


Figure 3.7. Electrical characterization of the pseudo-RE and ISFET. (a) Mean OCP (*offset to zero at $t = 0$) drift of pseudo-RE for three measurements in 3M KCl over a period of an hour. (b) Characterization setup showing fluidic conduit, pneumatic valves, and pseudo-RE contact (c) I_D - V_{ref} characteristics (three repetitions) of electrolytically gated Silicon nanowire ISFET in presence of 3 M KCl. (d) ISFET static response over time in 3 M KCl solution. Estimated drain current drift: ~ 1 nA/h

3.3 Discussion of choices related to the process

3.3.1 Negative Microchannel Mold

A rounded geometry of the channel's cross-section is required for the functioning of the pneumatic valve and, in particular, to allow complete sealing when under pressure from pneumatic valves [65]. A reflow resist (AZ 10XT) was chosen as structural material for the negative mold. A width of $150 \mu\text{m}$ is the largest

possible channel width whilst maintaining the round cross section. At larger widths, the channel mold's cross section develops a "cat's ear" shape upon reflow, which will lead to leaky pneumatic valves [63].

Designing a negative mold that can withstand the subsequent processing steps has been a major challenge throughout the process development. Platinum coating over the mold serves the dual purpose of mold passivation and later acts as an electrical contact layer during the anodic dissolution of aluminum. Sputtering is the preferred method of depositing the Ti/Pt/Al/Ti stack. However, evaporation can also be used, provided the mold does not have features that can cause the shadowing effect. The shadowing effect can lead to unprotected mold regions that become susceptible to later processing steps.

While designing the negative mold, care should be taken to avoid sharp corners in the mold pattern. During the IBE, the sharp concave regions of the mold are disproportionately etched more than the flatter regions of the wafer (Figure 3.8a). This over etch is due to reflection of Argon ions by one of the non-planar face of the corners which, subsequently strike the other side of the corner wall leading to increase localized etching. These localized etching are strong enough to etch thorough the sacrificial aluminum and protective titanium and platinum layers, thereby exposing the mold resist to subsequent processing steps which are detrimental to structural integrity of the negative mold. This can be easily corrected by filleting any sharp corners or kinks in the design (Figure 3.8b).

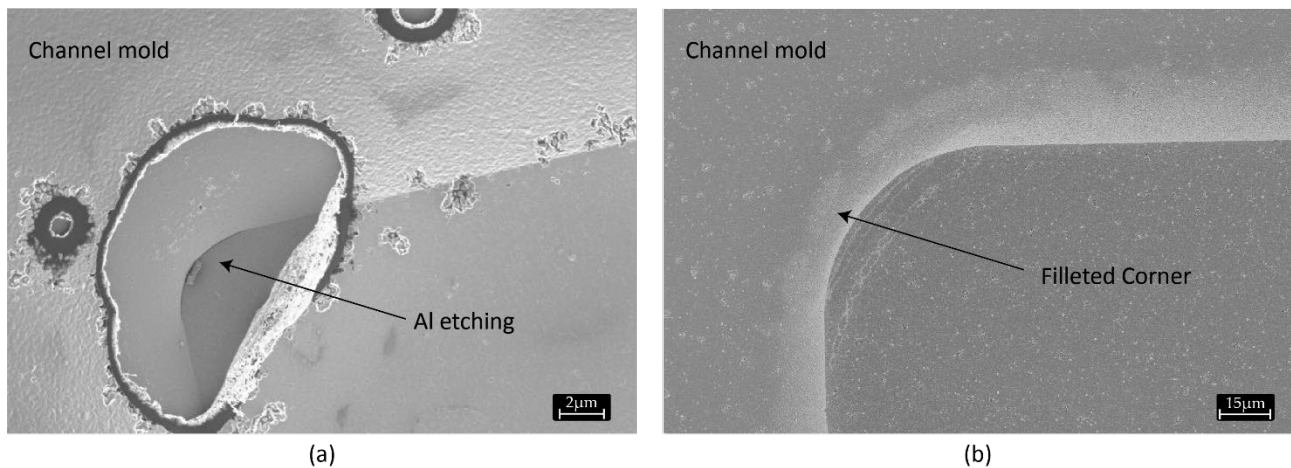


Figure 3.8. SEM micrograph after IBE of gold. (a) A negative mold of microchannels showing pronounced localized etching in the concave corners. (b) Elimination of localized etching by filleting the concave corners of the microchannel molds.

3.3.2 Gold electrode lines

We had to define specific process parameters for the fabrication of the gold electrode lines in order to ensure the conformity of the metal layers over the 12 µm high topology of the mold. Proper definition of gold electrode lines on top of the negative mold was achieved by spin coating a resist with thickness higher than the highest feature on the wafer (Figure 3.9a). Development of positive resist in photolithography steps after depositing sacrificial aluminum layer was carried out using AZ developer MIC, which unlike TMAH (TetraMethylAmmoniumHydroxide) and KOH-based developers does not etch aluminum. Although the aluminum layer is covered by titanium (Figure 3.2b), thin layers tend to have pinhole defects that can allow the developer to attack aluminum underneath (Figure 3.9b).

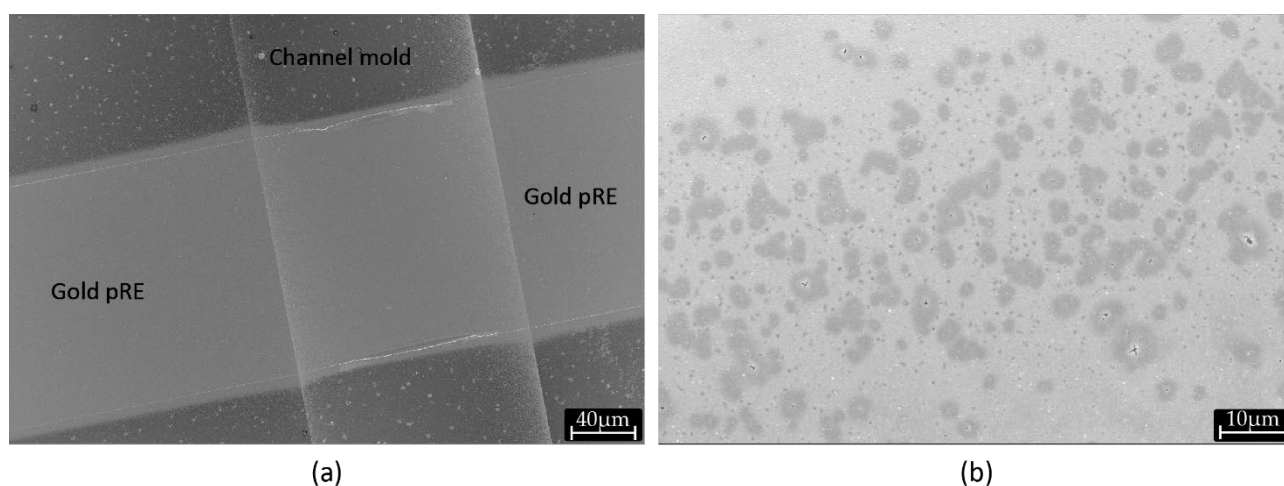


Figure 3.9. SEM images of pseudo-RE and protective titanium layer. (a) SEM micrograph of gold pseudo-RE conformally covering the negative channel mold. (b) SEM micrograph after development with KOH-based developer, showing dark regions of etched aluminum under the pinholes in the titanium layer

SU-8 pillars of the foreseen height of 1 mm experience strong shear forces, which can lead to pillars detaching from the wafer. Therefore, a sandwich of titanium adhesion layers is used in regions prone to shear stress in order to enhance the adhesion of gold to aluminum and SU-8 to gold (Figure 3.2c, f). Elsewhere, titanium is etched away by IBE.

After each IBE step, in order to strip the photoresist completely, it is extremely important to perform a short oxygen plasma (~30 s) etching before complete stripping of the resist in Remover 1165. High-energy Argon ion bombardment during IBE chemically modifies the top surface of the resist, which makes the resist difficult to strip via wet etch. A short oxygen plasma etch of the photoresist's top layer greatly enhances its removal during subsequent wet stripping.

3.3.3 Metal-coated SU-8 pillars

The 1 mm thickness of SU-8 was achieved by multiple SU-8 coatings and exposure steps, followed by a single development step at the end. Although the thickness of the first SU-8 layer upon spin coating is 300 μm, successive coatings of two additional SU-8 layers lead to the final thickness of ~1000 μm instead of 900 μm. This implies that the second and third coatings are of larger thickness than the first SU-8 layer due to different substrates they are coated on. PEB was performed only on the last coating, since PEB for the exposed layer automatically occurs during soft bake for the next layer. In order to reduce stress build up in the exposed layer during polymerization, slower ramp up and longer hold time at 65 °C were used during soft bake of later coatings of SU-8. Multi-layer coating of SU-8 is a non-standard method and therefore the specifications for listed in the Table 3.1 are to be used as point of reference. The baking parameters can vary depending upon the age of SU-8 and substrate type. At such high thickness, it is important to bake SU-8 on highly level hotplate. Else, SU-8 will flow and will lead to non-uniform thickness across the wafer and may even flow off the wafer edge.

Baking on hotplate results in non-uniform concentration of solvent in the SU-8 layers, with a highly solvent depleted region closer to the wafer surface. In our case, featuring thick layers and requiring multiple baking steps, it may lead to solvent concentrations in the first SU-8 layer to fall below the recommended processing levels and formation of a thin layer of cross-linked SU-8 above the wafer surface. This thermally cross-linked SU-8 layer cannot be removed during development (Figure 3.10a, b). Multi-meter measure-

measurements show $M\Omega$ level surface resistance, indicating the presence of thin insulating SU-8 layer. The issue of solvent concentration gradient is usually mitigated by skipping the high temperature ($95\text{ }^\circ\text{C}$) step and by performing a long soft bake solely at low temperatures (for instance $65\text{ }^\circ\text{C}$). However, in the case of thick resists, this can extend the soft baking time up to days [66]. Alternatively, we overcame this issue by employing a positive resist (AZ 10XT) as a sacrificial layer, coated prior to SU-8 coating and patterned to remain on the regions where SU-8 was sought to be removed (Figure 3.4i). AZ 10XT resists only begin to crosslink at $140\text{ }^\circ\text{C}$ and therefore is stable at SU-8 soft bake temperatures. This layer is easily removed during the development of SU-8 (Figure 3.10c, d) as PGMEA functions as both SU-8 developer and as AZ 10XT solvent. Conventionally, a clean organic-free substrate is recommended to enhance SU-8 adhesion. On the contrary, by deliberately “dirtying” the substrate by coating AZ 10 XT, we prevent the adhesion of overbaked/cross-linked SU-8 to the substrate.

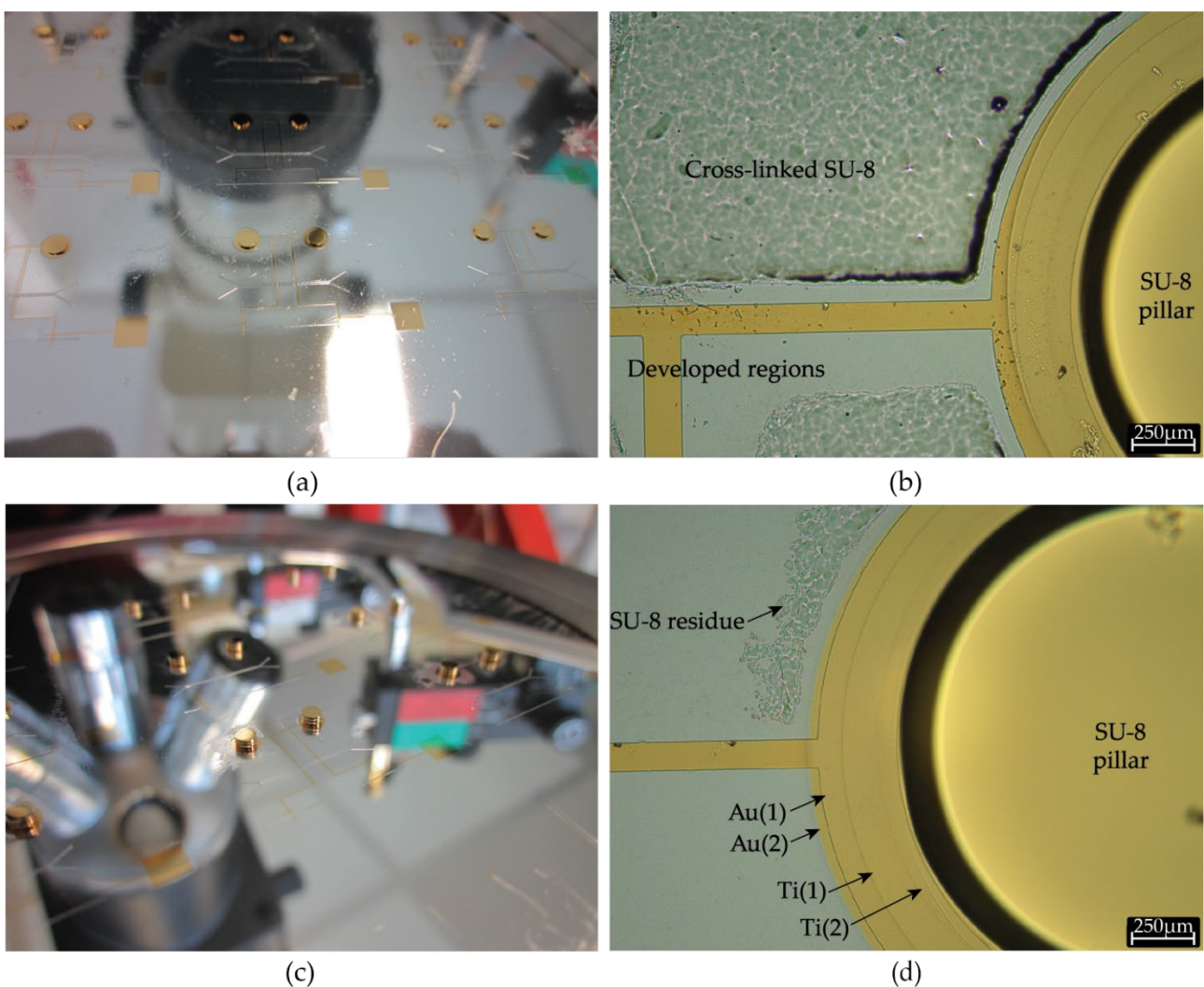


Figure 3.10. Processing of SU-8 pillars. (a) Silicon wafer after metallization of $300\text{ }\mu\text{m}$ SU-8 pillars. No sacrificial resist layer was used prior to SU-8 lithography leading to a thin glossy coating of cross-linked SU-8. (b) Optical micrograph of the wafer in Figure 3.10a, showing unexposed yet cross-linked SU-8 regions resisting overnight development in PGMEA (c) Silicon wafer after metallization of 1 mm SU-8 pillars (resulting from stacking of three SU-8 layers). AZ 10XT was used as sacrificial layer, resulting in vastly cleaner surface after development. (d) Optical micrograph of the wafer in Figure 3.10c, showing the region around the SU-8 pillar. Metallic stack consisting of a sandwich (Ti(1)/Au(1)/Ti(2)/Au(2)) of titanium adhesion and gold electrode layers is also visible.

Although development time is highly dependent on operating conditions, use of positive photoresist layer led to almost 50% reduction in development time for $300\text{ }\mu\text{m}$ SU-8 layer. In the current work as resolution

of SU-8 features was of less concern, hard baking of positive resist was not performed prior to SU-8 coating. However, upon SU-8 coating solvent from SU-8 will mix with the positive resist, which may result in the lateral flow of the positive resist into SU-8 exposure regions, leading to loss of resolution. To mitigate it, a hard-baked thin positive resist layer is highly recommended prior to SU-8 coating. Similar use of positive photoresists has been reported previously in the sacrificial release process [67] and liftoff of SU-8 structures [68][69]. We employed 8 μm of AZ 10 XT resist to ensure adequate step coverage over the microchannel mold; however, thinner layers can be used on substrates with flatter topography.

Metal sputtering of the 1 mm high SU-8 freestanding pillars was successfully achieved via stencil lithography. A stencil mask was thinned down to 150 μm by backside grinding to minimize the shadow effect of mask sidewalls during gold sputtering. Further thinning was spared to prevent fragility and mask breakage. Conformal coating during sputtering is critical to achieving ohmic electrical contact between the top of the pillar and the planar circular-base interconnection at the bottom.

3.3.4 Integration of pseudo-RE in PDMS microfluidics

Upon metallization of freestanding SU-8 pillars, a pseudo-RE network consisting of planar gold lines and metal-coated SU-8 pillars was integrated in PDMS microfluidics. This tri-dimensional structure has to be transferred to the PDMS microfluidic module that is mold casted over it in order for the microchannel to expose the pseudo-RE on their top internal surface. The transfer is achieved by depositing a self-assembled monolayer of MPTMS in liquid phase on gold surface. The thiol ($-\text{SH}$) end of the silane selectively binds to gold whereas the methoxy ($-\text{OCH}_3$) end binds to the PDMS, thereby selectively enhancing adhesion of gold to PDMS [70]. Upon sacrificial etch of aluminum layer, the gold pseudo-RE line are conformally transferred onto PDMS microfluidic module. The complete removal of unexposed SU-8 during the earlier development step is a critical requirement at this stage to avoid the residual SU-8 (Figure 3.10a) to interfere with MPTMS binding on gold. Incomplete removal of SU-8 would result in patchy transfer of gold electrode lines to PDMS and thereby breaking continuity of electrode lines [71]. Moreover, we noticed that upon sacrificial release, this thin residual SU-8 layer transfers to PDMS and greatly reduces the bonding capability of PDMS to CMOS chip.

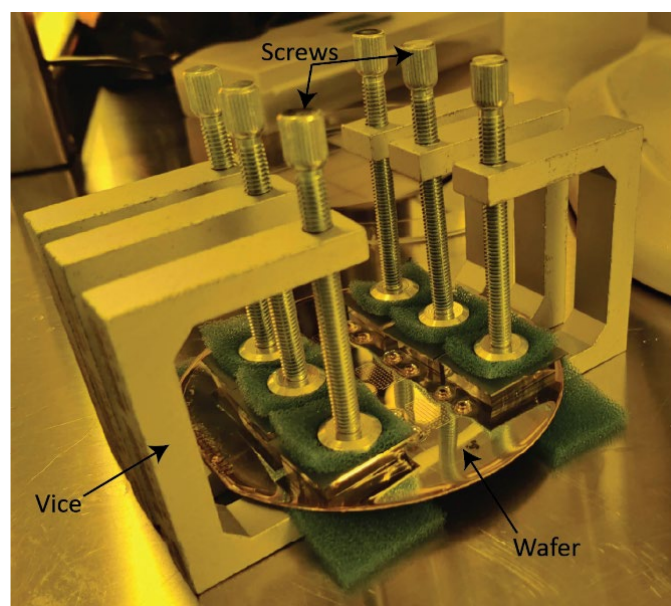


Figure 3.11. Ad-hoc setup screw vices to bond PDMS layers under pressure.

After spin coating, the PDMS adheres to the sidewall of TPV and forms a concave meniscus around its base. This leads to formation of region around the pillar where thickness of PDMS is higher than that on rest of the wafer. Non-uniform thickness of PDMS results in formation of air bubbles around the TPV. This trapped air can be released by performing the curing under pressure (Figure 3.11). Partially cured PDMS plastically deforms under pressure, substantially reducing the bubble formation around the SU-8 pillars.

3.4 Evaporation in low volume

PDMS is an excellent material of choice for microfluidic applications due to its ease of fabrication, wide range of optical transparency, inexpensiveness and biocompatibility. PDMS has high free volume, which provides it with excellent flexibility leading to the realization of microfluidic valves and pumps. PDMS's high free volume also makes it permeable to gases and liquids. While this gas permeability is advantageous to achieve high-density microfluidic structures by dead-end loading, it is mostly undesirable in microfluidic devices as it leads to loss of reagent via vapor loss. The speed of vapor loss in PDMS increases with an increase in temperature. As the majority of biochemical reactions occur at temperatures higher than room temperature, the vapor loss issue becomes more critical.

3.4.1 Vapor barrier

The simplest solution to the problem is to use large reaction volumes where relative volume loss during the reaction is too low to be of consequence. However, such large volumes are comparable to conventional methods, thus one loses the benefit of miniaturization. To resolve the problem in microfluidic settings various strategies have been proposed. A common way is to modify the surface properties of PDMS by coating the PDMS surface with various polymers [72][73] that suppress the diffusion of small molecules into the PDMS matrix. The most popular approach consists of chemically coating the inner surface of the flow channel by flushing the microchannels. In our case, since the gold electrode lies exposed on the inner surface of the flow channel, chemical modifications of the inner surface may negatively affect the reference electrode behavior. Therefore, instead of coating the flow channel, a vapor impermeable layer can be placed just above the microfluidic channel network Figure 3.12a. The impermeable layer prevents diffusion of water vapor into the bulk PDMS and creates a region of vapor saturated PDMS which prevents further evaporation of water from the flow channels.

We explored the use of Parylene C [74] and Novec 1720 [73] as vapor barrier layers in our design. However, integration of these layers in PDMS proved particularly challenging, as these coating made irreversible bonding to PDMS extremely difficult. Heyries et al. employed a mixture of three silanes to functionalize the polymerized Parylene C and promote bonding to PDMS. However, in our experiments, the silane mixture did not offer us any marked improvement over using only oxygen plasma to bond polymerized Parylene C to PDMS. The adhesion due to oxygen plasma treatment is primarily due to increased surface roughness of Parylene C, which forms mechanically interlocking microstructures with PDMS. Since the adhesion is mechanical in nature and not chemical, the bond strength is not high. This significantly reduced the maximum working pressure of the microfluidic chip and the reliability.

Zhu et al. employed an electronic grade coating (NOVEC 1720) to integrate a vapor barrier layer in PDMS microfluidic module. However, in our experiments, instead of forming uniform thin layer coating on the cured PDMS, as described in their process flow, NOVEC 1720 instead formed small islands on the PDMS surface. Moreover, unlike their claim, no chemical bond was achieved with PDMS even after curing at rec-

commended temperature. Therefore, these efforts were dropped in the favor of hydration channels, which are described in the following section.

3.4.2 Hydration channels

Another way to minimize vapor loss from the flow channels is via the use of hydration channels (Figure 3.12b). Hydration channels are microchannels that are filled with liquid that has the same vapor pressure as that of the flow channels. These channels prevent liquid loss from flow channel by saturating the PDMS region above the flow channel with liquid of similar vapor pressure. These channels can be easily integrated in the pneumatic valve mold. Unlike vapor barrier layers, PDMS surface is not chemically modified therefore the PDMS chip containing pneumatic-hydration network can be irreversibly bonded to the thin PDMS containing the flow channels. At elevated temperatures, the hydration channels will lose liquid though their top surface at the normal rate for PDMS. Therefore, to avoid formation of bubbles, the hydration network should remain pressurized throughout the experiment. The hydration network pressure depends on the temperature. Higher the temperature, greater will the rate of liquid loss and therefore larger hydration pressure will be required to keep the channels filled. For our experiments carried out at 65 °C, hydration pressure of 450 mbar was found to be ideal.

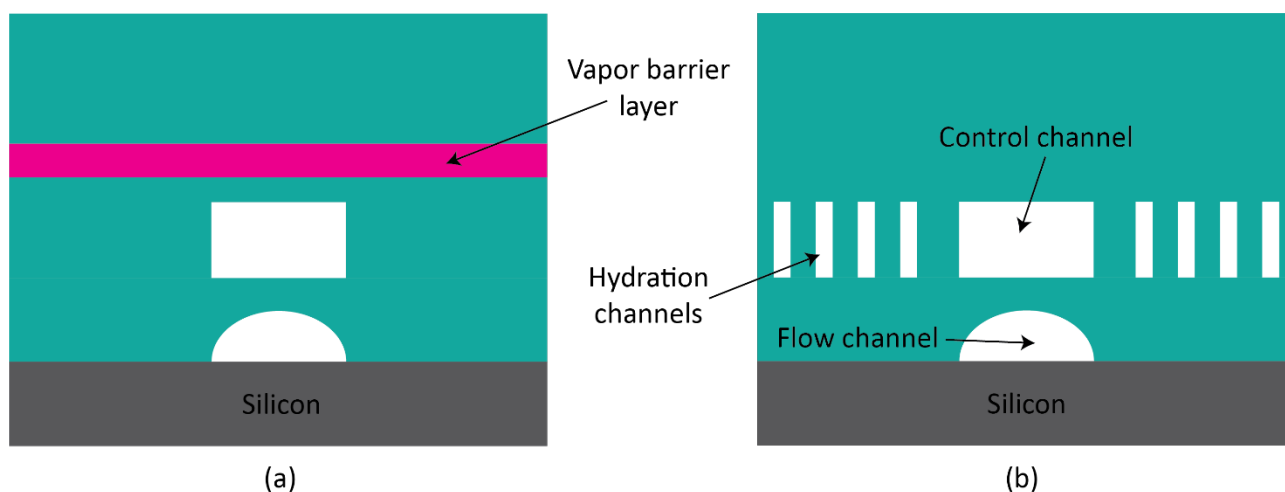


Figure 3.12. Various schemes for minimizing evaporation in PDMS microfluidics. (a) Impermeable polymer layers integrated just above the fluidic network saturate the thin PDMS below it after minimal liquid loss from the microchannels. The transparent polymer layer provides unobstructed viewing of the flow channels. (b) Hydration channels saturate the region below them with the liquid thereby preventing any liquid loss from flow channels. Filled hydration channels are generally transparent but can lead to optical artifacts in the imaging.

3.5 Conclusion

In this chapter, we introduced a new process for pseudo reference electrode (RE) integration in microfluidics based on the combination of a novel SU-8 photolithography process to achieve thick pillar-like vias and a silane-mediated conformal transfer of metal electrodes into PDMS microfluidics. The 3D conformal design of pseudo-RE when combined with parcellation microfluidics, allows very small analyte volumes to be isolated and characterized by ISFET. The pseudo-RE design here presented is scalable to a large number of reaction parcels, each of which can be independently monitored by ISFET or any other solid-state sensor. The density of reaction parcels is only limited by photolithography of the mold to form the microfluidic module. The presented pseudo-RE design can be easily converted to Ag/AgCl reference electrode system by electrodeposition of silver and its subsequent chlorination [75]. We present preliminary attempts at that in

the section 6.2. We believe that our design can solve the issue of short lifetime of miniaturized Ag/AgCl electrodes resulting from degradation of AgCl in aqueous solutions [76]. Few hundred nanometers of AgCl layer can easily be consumed in constant-flow conditions or big electrolyte volumes. Conversely, due to the ultra-low volume of the electrolyte in our design, the concentration of Cl^- ions in the electrolyte will reach equilibrium with minimal loss of AgCl layer.

Our approach is most suitable for label-free, semiconductor-based molecular diagnostic applications that require sample digitization. For example, digital molecular assays for early detection of sepsis-causing pathogens [77][78] have been shown to have significantly reduced time to detection when compared to blood culture based identification, leading to reduced mortality rates. Similar digital assays have been used in absolute quantification of nucleic acids [6], digital-ELISA [79], tumor-DNA analysis [80] etc. Hassibi et al. have demonstrated multiplexed detection of nucleic acid amplification and sequence analysis on CMOS chip consisting of 32×32 array of photodiodes using fluorescence detection [81]. However, requirement of external optical excitation source, utilization of post-CMOS processing to integrate optical filter layers and capture probes for detection of DNA increases the complexity of the biosensor device. Leveraging scaling advantage of CMOS technology and electrochemical sensing of molecular assays, optical readout in these applications can be replaced by label-free electronic readout via ISFETs, leading to increased readout speeds and reduced device footprint. Use of segregated volumes for amplification reaction and pH-based amplification assays can obviate the need for post-CMOS processing and design of complex capture probes.

Chapter 4 Label-free detection of DNA amplification in small volumes.

4.1 Introduction

Nucleic acid testing (NAT) is a powerful method of great significance to healthcare and basic research. NAT is widely employed in clinical diagnosis, environmental monitoring and biological analysis. Its importance only got accentuated with the outbreak of the COVID-19 pandemic, leading to a sharp increase in demand for fast and high-throughput analysis of nucleic acids from a large number of samples. This explosive growth in demand for NAT laid bare the shortcomings of the automated solutions developed for pre-COVID-19 times, leading to a renewed emphasis on developing simpler, rapid and cheaper solutions. Even though the COVID-19 pandemic has been described as a once-in-a-lifetime event, the continued emergence of newer SARS-CoV-2 variants indicates that the demand for increased NAT will not subside. Moreover, NAT is increasingly used for microbial detection as a faster alternative to conventional culture-based assays. Recently CRISPR-Cas-based methods for the detection of pathogens have burst onto the scene, offering outstanding sensitivities and specificities [82]. Therefore, there is an increased research effort and motivation towards the development of newer methods and solving numerous issues in the applications of NAT.

The classical method of performing NAT, which involves amplifying the target nucleic acid sequence, relies on labeling the product of nucleic acid amplification with optical labels and tags. Depending upon the type of method, these tags need to be specifically engineered, leading to increasingly complex assays. Though optical readout offers the highest sensitivity, the benefits of simplicity, robustness and lower costs have motivated the development of numerous label-free DNA detection techniques. Of these, field-effect detection of DNA has attracted massive attention due to well-established CMOS technologies that can be directly leveraged for sensor miniaturization and integration. Detection of hydrogen ions resulting from the amplification of NA is one of the most popular methods of label-free readout. The production of hydrogen ions during the incorporation of nucleotides is the most fundamental step in the amplification of nucleic acid. Therefore, it allows for a more generalized label-free method of readout that is common among all NA amplification methods.

Over the past decade, NAT methods have benefited greatly from sustained research in microfluidics. The effort has been driven by the several benefits offered by microfluidic devices over their conventional macroscale counterparts, such as lower cost due to low reagent use, portability, laminar flow, rapid heat transfer and low thermal inertia. This has led to the emergence of various microfluidic systems with microchambers and microchannels. Digital quantification assays like digital PCR have especially leveraged the scalability of microfluidics to offer lower limits of detection, better precision and robust detection of rare target sequences. Being able to carry out multiple reactions in parallel has allowed the development of solutions beyond the current hospital-based centralized molecular diagnostic paradigm [83]. Such microfluidic ap-

proaches can leverage the high parallelism offered by CMOS technology to develop the next generation of molecular diagnostics solutions.

Apart from the advantages conferred due to reduced size in microfluidics, pH-based sensing in very low volumes can offer unique advantages over its optical counterparts. Since pH is a property of size, the discrimination signal, i.e. the change in hydrogen ion concentration due to amplification, will occur faster in smaller volumes. Coupled with the unprecedented charge sensitivity of nanowire ISFET (NW-ISFET), a faster time to detection can be achieved. In fact, NW-ISFETs have been shown to be sensitive to changes in surface charge density of as low as 350 electrons per micrometer square [12], which essentially corresponds to a few NA copy cycles.

Though it is obvious to have nanometer-sized ISFET sensors and NA amplification in nanolitre-sized microfluidic parcels in isolation, performing readout of NA amplification in such ultra-small volumes via ISFETs is not trivial. The requirement of the miniaturized reference electrode in the nanolitre-sized amplification chamber makes the endeavor non-obvious. Therefore, the goal of this thesis is to demonstrate pH-based detection of amplification in nanolitre-sized microchambers and its readout via ISFET and investigate its advantages over its optical counterpart.

4.2 QUASR LAMP

The optical readout is the gold standard for the detection of DNA amplification. Optical methods for the readout of DNA amplifications have been researched and characterized exceptionally well since the inception of nucleic acid testing. They are routinely used for nucleic acid-based diagnostics to deliver healthcare solutions, as they have become the gold standard for nucleic acid-based testing. Any alternate readout strategy for DNA amplification detection must be verified against the reference optical methods.

Optical readout of amplification via LAMP can be carried out in several ways. The most basic is to run the amplified product on gel and observe the banding pattern. Colorimetric readout of amplification can be achieved with the addition of indicators like hydroxynaphthol blue [84] or pH-sensitive dyes [21]. An increase in turbidity of the LAMP mixture over time can also be used as a readout of amplification [39]. Fluorescence-based readout of amplification can be carried out via the use of either intercalating dyes (like SYBR Green, SYTO, etc.) [85], manganese-quenched calcein [86], or fluorophore (like Cy3, Cy5, etc.) labeled probes [87]. Each method has specific advantages and disadvantages, making one method preferable over the other in specific settings. Amplified product in nanolitre volume is too little to be extracted and run on the gel. Though small volumes are not an issue for microfluidic capillary electrophoresis, the technique is not scalable to high-throughput settings. The readout signal from methods like turbidity measurements and colorimetric readout via color change is too subtle to be detected in tiny volumes. Fluorescence-based methods have been widely used to detect DNA amplification in small volumes [88][73][72] as they offer a very high sensitivity due to their superior signal-to-noise ratio (SNR) at those scales.

Though simpler to use for fluorescence readout, intercalating dyes tend to inhibit the amplification of DNA and can negatively affect the SNR for our pH-based LAMP. Tube-based LAMP with SYBR Green and Quant-iT dyes showed a marked reduction in ΔpH ($\Delta\text{pH} = -0.35$ instead of $\Delta\text{pH} = -1.28$ for no dye) even at low concentrations (0.01X). SYTO-82 and SYTO-9 dyes have been reported to be non-inhibitory in LAMP and offer a higher SNR [85]. Though the use of SYTO-9 (1 μM) showed a marked improvement ($\Delta\text{pH} = -0.97$ instead of $\Delta\text{pH} = -1.28$ for no dye) over SYBR Green and Quant-iT in ΔpH signal, the signal was still degraded. Fluorescence measurement for these dyes needs to be carried out at elevated temperatures for maximum discrim-

ination between positive and control amplifications[87], which can exacerbate the evaporation problem from small reaction chambers in PDMS.

Therefore, fluorophore-labeled oligonucleotide probes offer a non-interfering, sequence-specific mode of amplification readout. Since *Bst* 2.0 polymerase used for LAMP does not have 5'-3' exonuclease activity and the dsDNA structure never melts, the Taqman probes cannot be used in LAMP. For probe-based readout in LAMP, reports describe using fluorescence resonance energy transfer (FRET) [89], strand displacement of a quencher bound to an oligonucleotide probe targeting the loop regions of the amplicon (DARQ) [90], or quenching of unincorporated labeled primers (QUASR) [87]. Techniques like DARQ that rely on strand displacement of an oligonucleotide probe can be inhibitory. Therefore, we decided to use QUASR for optical monitoring of our LAMP assay in tiny volumes.

QUASR is an endpoint detection method that relies on using one of the LAMP's primers (preferably FIP, BIP, LoopF or LoopB) labeled with a fluorophore on its 5' end. A short quencher labeled oligonucleotide that is complementary to the 5' end of the fluorophore-labeled primer is also introduced in the assay. The quencher probe is labeled with a dark quencher at the 3' end. The quencher oligonucleotide, usually 7-13 bp in size, is designed such that the melting temperature (typically <55°C) of quencher oligo annealed to labeled primer is well below the amplification temperature of LAMP (60-65°C). During amplification at 65°C, the quencher probe is fully dissociated from the labeled primer and therefore does not interfere or participate in the amplification process (Figure 4.1a). In the presence of template DNA, labeled primer gets incorporated into the amplicons (Figure 4.1b). When the temperature is brought down at the end of the reaction, the quencher probe anneals to any labeled primer that has not been incorporated. This brings the fluorophore and quencher in close proximity. The incorporated primers remain unquenched, resulting in fluorescent amplicons. In the negative control, none of the labeled primers is incorporated, leading to complete fluorescent quenching upon cooling down. The availability of quencher probes in excess ensures that fluorescence from unamplified sources is wholly quenched.

Primer	Sequence
Cy5-FIP	5'-Cy5-CAGCCAGCCGCGAGCACGTTGCTCATAGGAGATATGGTAGAGCCGC-3'
FIP-IBRQ	5'-GGCTGGCTG-IBRQ-3'

Table 4.1. Labeled oligonucleotide sequences used in QUASR LAMP of bacteriophage lambda DNA.

We labeled the forward inner primer (Cy5-FIP) of lambda DNA with Cy5[®] fluorophore to act as a reporter signal of amplification. Based on the Cy5-FIP, a complementary 9 bp sequence labeled with Iowa Black[®] dark quencher (IBRQ) was generated to act as the quenching probe for Cy5-FIP (Table 4.1). The "Cy5-FIP and FIP-IBRQ" duplex has a melting temperature of 55°C. Concentrations of labeled FIP primers were kept unchanged in the LAMP assay, while FIP-IBRQ was added 1.5X times the concentration of Cy5-FIP to maintain an excess of quencher probes in the assay.

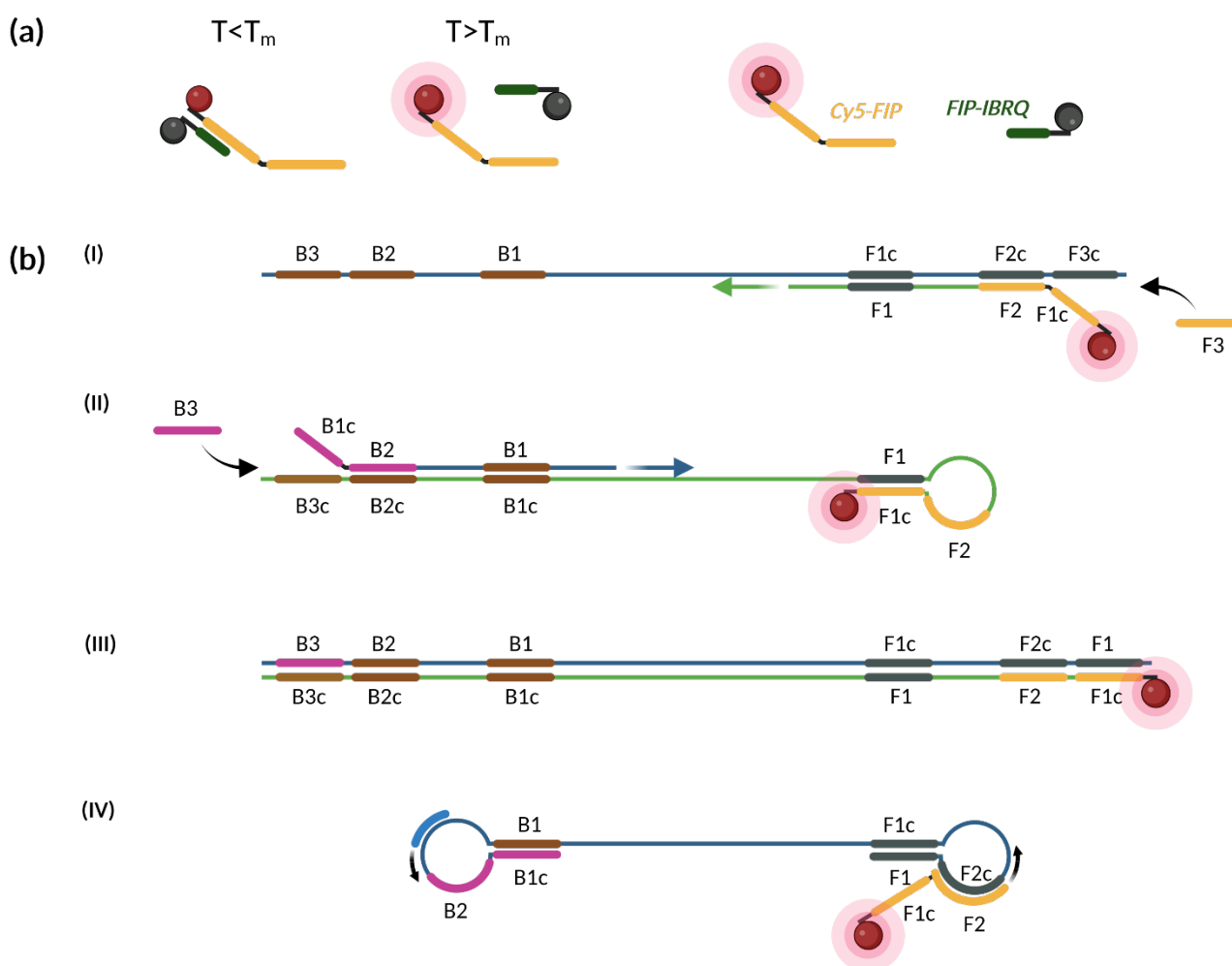


Figure 4.1. Schematic depiction of QUASR LAMP. (a) Schematic showing two states of labeled FIP primer (Cy5-FIP) and quencher probe (FIP-IBRQ) depending upon the melting temperature (T_m) of the duplex. (b) Schematic showing incorporation of Cy5-FIP during amplification of DNA when incubated above T_m .

4.3 Translating LAMP assay from tube to micro-channels

4.3.1 Experimental design and setup

PDMS, primarily due to its ease of fabrication, flexibility, gas permeability and optical transparency, makes an excellent candidate for performing on-chip DNA amplification reactions. Our microreactor chip (Figure 4.2) to perform on-chip LAMP is a two-layer device made via multilayer soft-lithography of PDMS. The bottom layer houses two microchannels (10 μm high and 150 μm wide) for performing LAMP. The bottom layer was fabricated by spin coating a PDMS-curing agent mixture (20:1) at 2000 RPM over the negative channel mold and partially curing it at 80°C for 13 minutes. The top PDMS layer consists of pneumatic valves (35 μm high and 250 μm wide) and hydration channels (35 μm high, 50 μm wide and 85 μm pitch). The top layer was created by drop casting PDMS-curing agent mixture (5:1) over silicon mold and partially curing at 80°C for 11 minutes. After partial curing, the top PDMS was demolded, diced, bonded with the bottom PDMS mold, and fully cured at 80°C for 1.5 hours to generate a monolithic PDMS chip. After final demolding and punching inlet/outlet holes, the PDMS chip was plasma bonded (30 s at 30 W in ~ 500 mbar O_2) to a silicon chip with a 200nm SiO_2 layer.

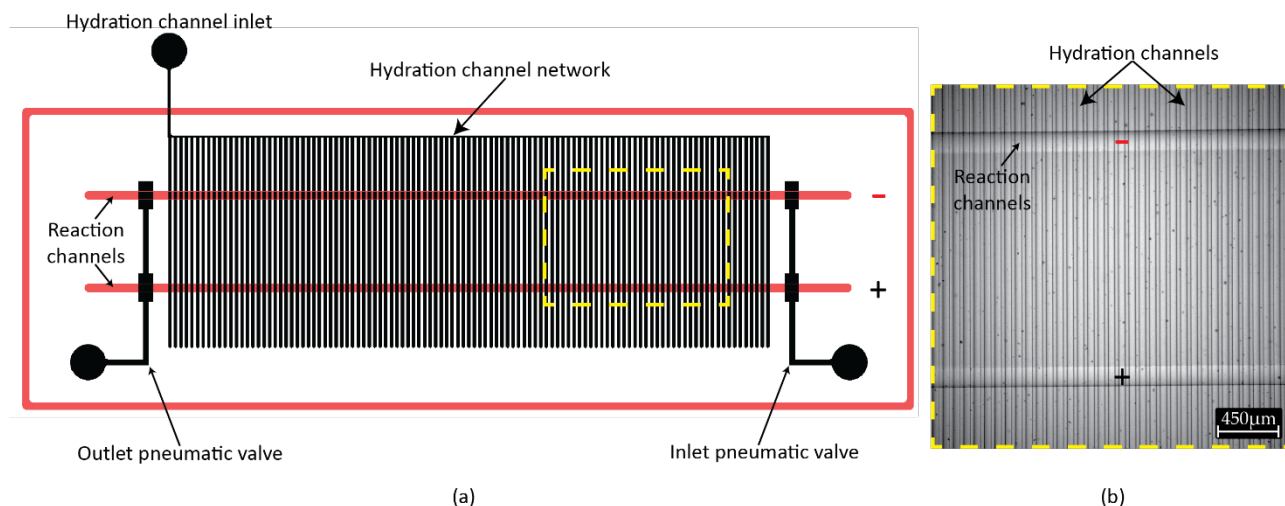


Figure 4.2. Schematic design of the microreactor chip to perform on-chip QUASR LAMP. (a) Negative template control (-) and mixture with target DNA (+) were injected in separate channels and monitored simultaneously. (b) Optical micrograph of the chip region in the yellow outline.

Hydration channels and pneumatic valves were dead-loaded with LAMP reaction buffer. During the amplification reaction, pneumatic valves were actuated under the pressure of 700 mbar while the hydration channels were kept pressurized at 450 mbar. Before injection of the LAMP amplification mixture, the reaction channels were flushed with LAMP buffer to prime and passivate the microchannels. The priming procedure reduces the adsorption of LAMP reactants onto the channel walls. A 2 μL aliquot was taken from a 25 μL QUASR LAMP master mix and injected into the reaction channels. Upon actuation of inlet-outlet pneumatic valves, two 17 nL reaction chambers are created. The chip's temperature was controlled by a thermal chuck and temperature controller (TC102SF, mk2000, Instec. Inc.). The LAMP mixture was incubated on-chip at 65°C. The temperature was ramped at 10°C/min. Fluorescence measurements of the microchannels were taken at regular intervals of 5 minutes.

4.3.2 On-Chip QUASR-LAMP

The biochemistry of nucleic acid amplification is highly sensitive to changes in the chemistry of the reaction. Therefore, assays developed for benchtop systems may not translate equally to different reaction environments. This becomes especially pronounced when analytical assays are scaled down to microchip format. Factors like material properties of the reaction chamber and surface effects due to the high surface-to-volume ratio begin to play an increasingly critical role in miniaturized conditions[91][92]. The reduction in volume from tube to microchannels increases the surface-to-volume ratio for the reaction chamber. Therefore, the chamber walls start playing an increasingly dominant role in the chemistry of the biochemical reaction both chemically and via physical effects of absorption and adsorption. Thus, it is critical to adapt the assay to compensate for these effects when moving from macro to micro conditions.

At 65°C, FIP-IBRQ is not annealed to Cy5-FIP in both negative control (-) and positive control (+) reactions. Therefore, during the amplification reaction, both (-) and (+) reactions emit similar levels of fluorescence that are not specific to the polymerase activity. After the reaction, when the mixture is cooled, the fluorescence in the (-) microchannel goes down while the (+) microchannel maintains residual fluorescence due to the incorporation of fluorophores. Therefore, readout of the amplicons can only be performed when the reaction mixture has been cooled down to room temperature, making QUASR-LAMP an endpoint readout method.

On-chip amplification with the LAMP assay developed in the chapter did not perform as expected. Upon cooling the chip to room temperature at the end of the reaction, the fluorescence in the negative control was not completely quenched. Initially, this was attributed to non-specific amplification. However, similar behavior was observed even when no polymerase was added to the negative control (Figure 4.3a). This signified that not enough quencher probes were annealing back to the Cy5-FIP primer and there was a decrease in the availability of quencher probes at the end of the reaction. A reduction in the total available quencher probes, even in the absence of polymerase activity, was attributed to a decrease in the ionic strength of the reaction buffer. Due to the high surface-to-volume ratio of microchannels (two orders of magnitude more than the tubes), the effective concentration of positive charge species (K^+ and Mg^{2+}) volume is reduced due to absorption on the microchannel walls. Oligonucleotides are negatively charged in an aqueous state. The lack of sufficient positive ions to stabilize the negative charge on oligonucleotides and DNA leads to their electrostatic adsorption on surface walls, making them unable to participate in the amplification reaction. The reaction buffer was modified by increasing the concentration of K^+ and Mg^{2+} ions (100 mM & 10 mM from 50 mM & 6 mM), the quantity of quencher probes to 2X the Cy5-FIP and the inclusion of 0.05 mg/ml of BSA (bovine serum albumin) for surface passivation. The incomplete quenching of Cy5-FIP in negative control was rectified with the use of the modified buffer.

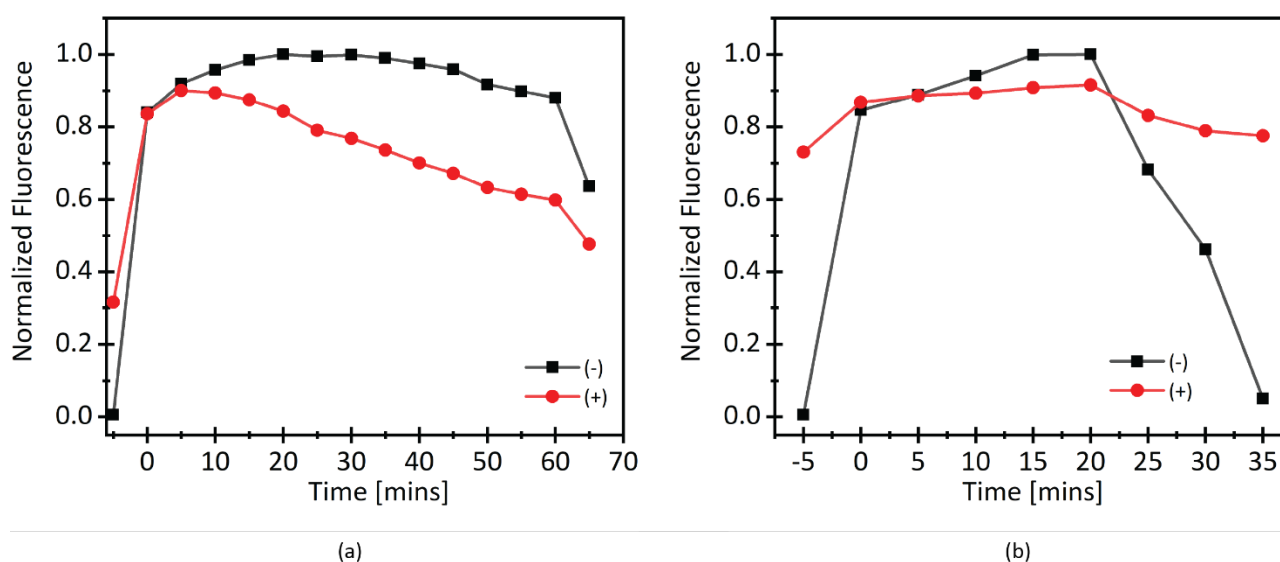


Figure 4.3. Non-ideal artifacts in on-Chip QUASR LAMP. (a) Normalized fluorescence in microchannels during incubation (0-60 mins) at 65°C when using the unmodified reaction buffer. Fluorescence in (-) does not return to the background at the end of incubation ($t = 65$ mins). Fluorescence at the start ($t < 0$ mins) and end of the incubation were measured at 25°C. (b) Normalized fluorescence in microchannels during incubation (0-30 mins) at 65°C with the modified reaction buffer, showing fluorescence in (-) return to the background at the end of incubation ($t = 35$ mins). However, due to non-specific amplification at room temperature, (+) microchannel starts with a residual fluorescence. Fluorescence at the start ($t < 0$ mins) and end of the incubation ($t = 35$ mins) were measured at 25°C.

However, we begin to notice unequal fluorescence levels among (+) and (-) at the start of the reaction. Expectedly, the (-) reactions had near background fluorescence, but the (+) reactions already showed significant fluorescence levels at room temperature (Figure 4.3b). Since the modified reaction buffer was used in both, this was a clear sign of non-specific amplification by the *Bst* 2.0 polymerase. Though *Bst* 2.0 works optimally at 65°C, it still possesses, albeit low levels of activity levels at room temperature. The time between preparation of the master mix and injection into the chip (~15 mins) was sufficient for the polymerase to non-specifically incorporate Cy5-FIP primers. This issue was fixed by substituting *Bst* 2.0 polymerase with *Bst* 2.0 Warmstart® polymerase. *Bst* 2.0 Warmstart® is essentially a *Bst* 2.0 polymerase but with a re-

versibly bound aptamer, which inhibits polymerase activity at temperatures below the annealing temperature of the aptamer (which is 45°C). The post-reaction activity of the polymerase is also inhibited as the aptamer reversibly anneals back to the polymerase at room temperature. The substitution of *Bst* 2.0 with *Bst* 2.0 Warmstart® did not affect the pH-based LAMP assay in standard tubes. Therefore, from now on, all LAMP assays will employ *Bst* 2.0 Warmstart®.

Elimination of room-temperature non-specific amplification and oligonucleotide stabilization still did not result in on-chip amplification. After cooling to room temperature, fluorescence in both (-) and (+) microchannels returned to initial background fluorescence levels (Figure 4.4a). Increasing the initial target DNA concentration did not lead to any change in the endpoint fluorescence. This could only be attributed to sub-optimal polymerase activity in the microchannels. Reduced polymerase activity could be attributed to a combination of surface absorption, interference of BSA and stochastic effects of sub-sampling, leading to fewer polymerase molecules in the microchannels. On-chip amplification was observed after increasing the initial polymerase amount by 15 times (from 8 U to 120 U) in the 25 µL LAMP master mix. However, 240 U of polymerase was the optimal concentration that led to a strong and consistent amplification on-chip (Figure 4.4b).

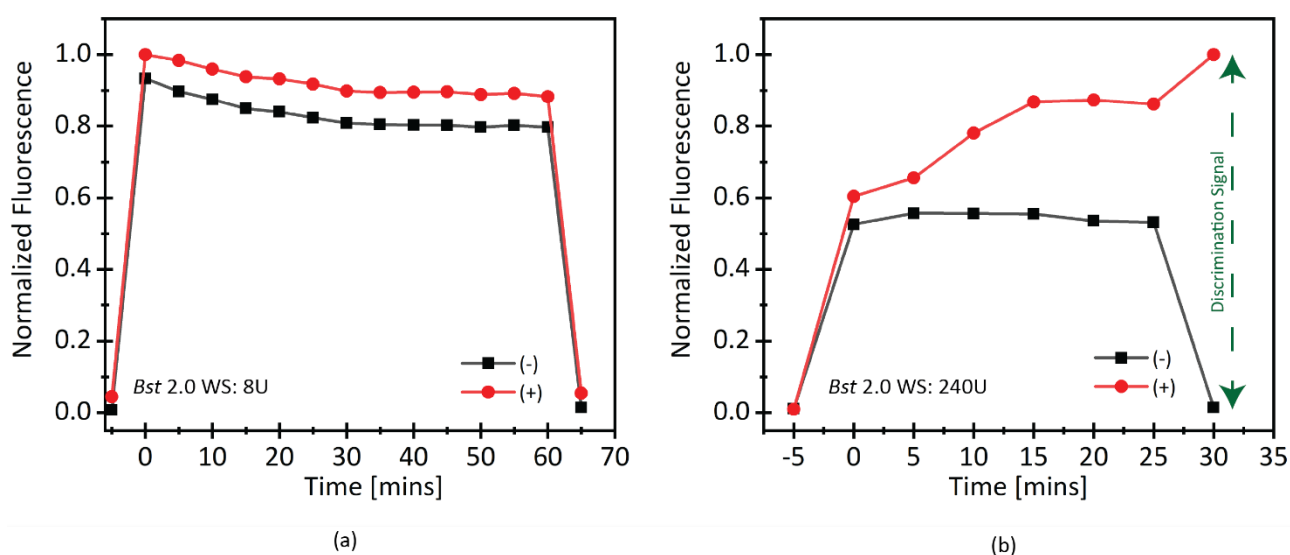


Figure 4.4. On-chip QUASR LAMP. (a) Normalized fluorescence in microchannels during incubation (0-60 mins) at 65°C using *Bst* 2.0 Warmstart® (8 U). Convergence of fluorescence in (-) and (+) microchannels at the end of the incubation show lack of DNA amplification. Fluorescence at the start ($t < 0$ mins) and end of the incubation ($t = 65$ mins) were measured at 25°C. (a) Normalized fluorescence in microchannels during incubation (0-25 mins) at 65°C after increasing the *Bst* 2.0 Warmstart® (240 U) amount. The signal between (-) and (+) was measured at the end of the reaction. Fluorescence at the start ($t < 0$ mins) and end of the incubation ($t = 35$ mins) were measured at 25°C.

After realizing the right conditions to perform QUASR LAMP on-chip, we performed amplifications of serial dilution of lambda DNA on-chip to perform a calibration curve. As QUASR LAMP is an endpoint readout method, time-to-positive analysis of the real-time method is not possible. However, our goal with optical readout is only to verify the functionality of our pH-based LAMP assay in microfluidic channels. Figure 4.5 shows the on-chip calibration curve for serial dilutions of lambda phage DNA. Our dynamic range in which we could amplify DNA on-chip was between 300 ng-0.1 ng. Amplification efficiency was reduced for DNA concentrations above 300 ng as we observed lower fluorescence. The lowest concentration that we could amplify on-chip was 0.1 ng of lambda DNA. Concentrations lower than 0.1 ng of DNA showed no on-chip amplification.

Compared to our tube-based assays where we could reliably amplify up to 0.1 pg level of DNA, the dynamic range of our on-chip amplification setup is lower. Amplification is hindered at DNA concentrations larger than 1 μg due to false priming and steric hindrance of polymerase by DNA. The lower limit on quantification is imposed by statistics. As known in digital PCR, the lower limit of DNA that can be quantified is limited by the total volume of the sample analyzed. Analyzing the subsample and not the whole sample volume imposes a lower limit on the amount of DNA that can be quantified [93][94]. We are analyzing a 17 nL subsample out of the 25 μL master mix volume. This subsampling leads to variations in the fractional concentration of the DNA in the subsample. The standard deviation in the number of targets in the subsample is \sqrt{n} , where n is the expected copy number in the subsample. Therefore, for a low copy number of <1000 (which corresponds to <1 ng DNA in the master mix), we end up with subsamples that have either zero DNA copies or a number too low to be reliably amplified. The high standard deviation observed in the discrimination signal for the technical repeats is probably due to variations in the copy numbers of DNA that are actually in the microchannels. Apart from the aforementioned statistical variation due to subsampling, the variation in copy number could be due to the adsorption of DNA on the walls of the microchannels leading to drastic variations in the actual copy numbers in the 17 nL chamber.

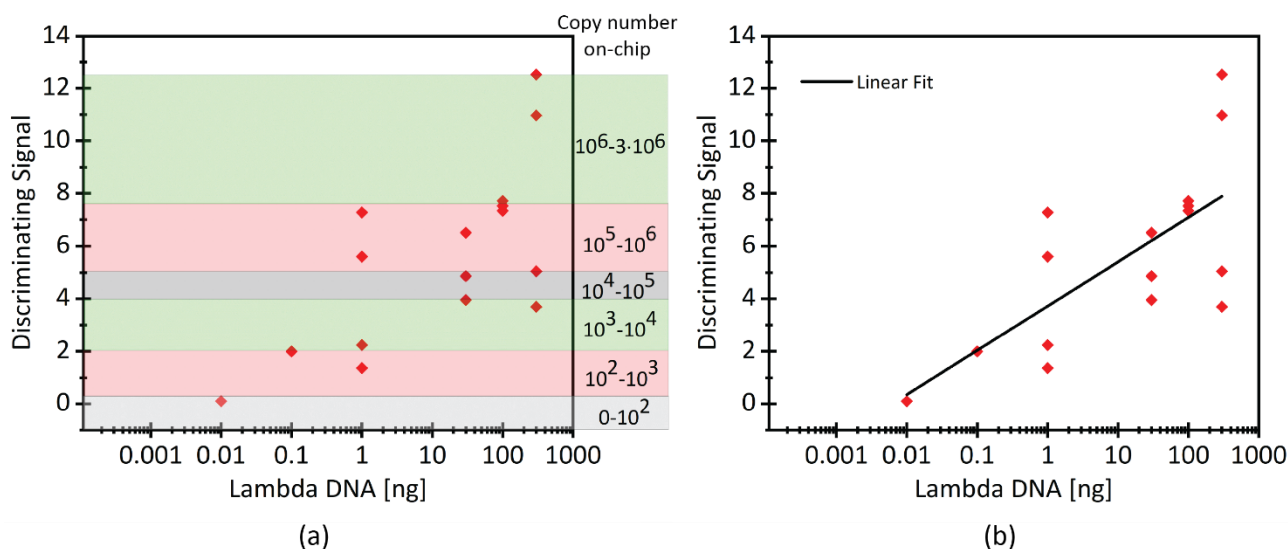


Figure 4.5. Standard Curve for different concentrations of lambda DNA. (a) The horizontal axis shows the amount of DNA (300 ng, 100 ng, 30 ng, 10 ng, 1 ng and 0.1 ng) added to the 25 μL master mix before a 2 μL of sub-volume was injected into each microchannel. Copy number on-chip indicate actual theoretical number of DNA copies in the 17 nL volume. Discrimination signals were taken at the end of 25 mins of incubation. (b) Standard Curve for different concentrations of lambda DNA with linear fit.

An interesting phenomenon was observed when amplifying target concentrations that are near the lower limit of detection for our setup. For a target amount less than 1 ng (Figure 4.5a); instead of uniform fluorescence throughout the microchannel, we observed discreet regions with relatively higher fluorescence than the surrounding regions (Figure 4.6). This is clearly attributed to the low copy number (less than 1000) of DNA in the microchannel. The low number of DNA copies dispersed along the length of a 1.15 cm long microchannel leads to isolated pockets of DNA amplification. The cauliflower-like LAMP amplicons have very high molecular weight, which limits their lateral diffusion leading to discreet regions with localized fluorescence. This is not expected to influence the pH readout of amplification, as aqueous H^+ is a very small molecule with a large diffusion coefficient, leading to uniform H^+ concentration throughout the microchannel. However, such a phenomenon does present opportunities to develop new kinds of devices for NAT. In no-flow conditions, it can be used to achieve “parcellation” of DNA without the need for pneumatic valves or oil-based physical separation. One such iteration of the device would be used to perform digital quantifica-

tion and comprise of just a very long serpentine channel filled with target DNA containing amplification mixture. In no-flow conditions, upon amplification, the dispersed DNA copies will lead to the formation of isolated fluorescent regions. Since lateral diffusion is very slow, automated image acquisition can be used to capture the distribution in the whole channel and quantify the concentration of DNA. However, such an approach is only suitable in a low copy number regime. Serial dilutions can be used to quantify higher DNA concentrations with such an approach.

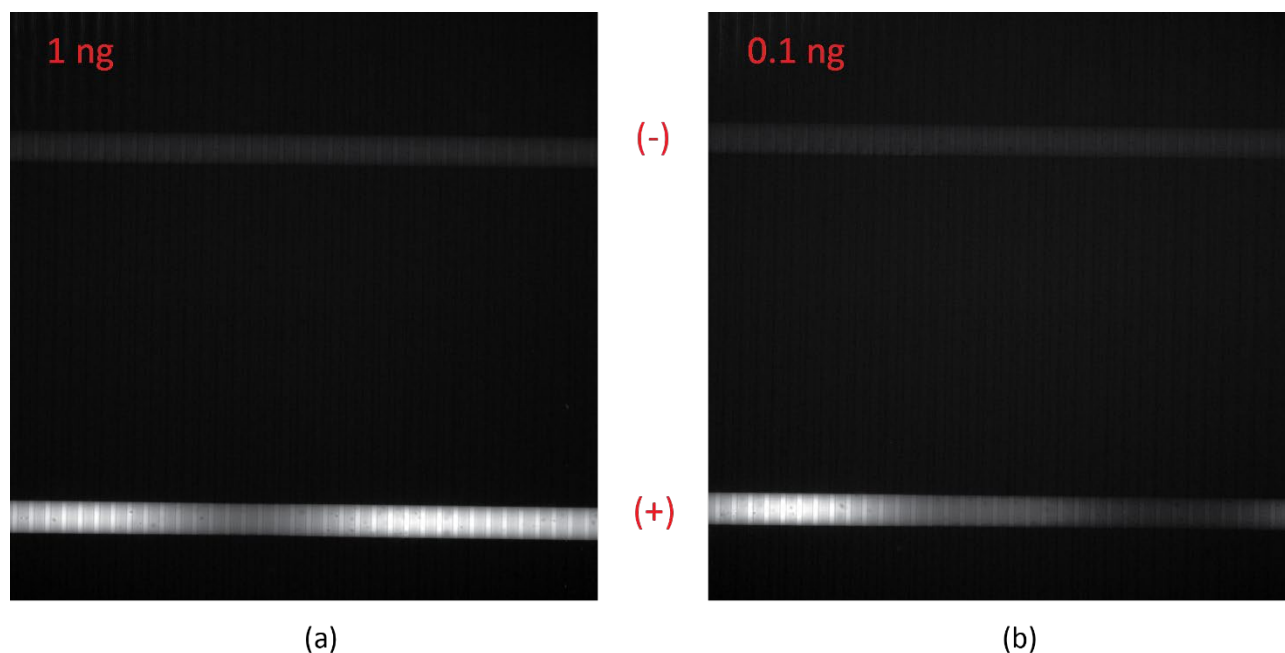


Figure 4.6. DNA amplification in low copy number regime. Fluorescence image of the microchannels at the end of 25 mins incubation for different initial lambda DNA amounts. The initial lambda DNA amount corresponds to the amount of DNA added to the 25 μ L amplification mix before injection into the chip. Corresponding copy numbers in microchannels are (a) \sim 1000 and (b) \sim 100.

4.4 On-chip chemical sensing of amplification

4.4.1 Experimental design and setup

On-chip electronic detection of DNA amplification was carried out via silicon nanowire ISFETs (NW-ISFETs). The $n^+/p/n^+$ fully ISFET devices were based on fully depleted silicon-on-insulator (FDSOI) technology. NW-ISFET devices were fabricated by standard top-down deep ultraviolet photolithography and e-beam lithography followed by reactive ion etching to define the active silicon area. The detailed process flow for the fabrication of the devices has already been described in the previous works of the lab by Accastelli et al. [95]. We employed n-type, FDSOI silicon NW-ISFETs (length: 8 μ m and width: 170 nm) with a 3 nm thermally grown silicon oxide as a sensing layer. The ISFETs are 50 nm thick and sit atop a 400-nm-thick insulating buried oxide layer of SiO₂. The ISFETs are located on a 2 cm x 2 cm CMOS chip (Figure 4.7). Apart from the sensing area and contact pads, the entire chip is passivated with a multilayer of silicon nitride (50 nm), tetraethyl orthosilicate (300 nm) and phosphosilicate glass (200 nm).

To bias the NW-ISFETs for on-chip amplification detection, the CMOS chip was post-processed to fabricate an on-chip miniaturized pseudo reference electrode (pRE). The pREs were fabricated by lift-off of the evaporated gold layer. Before post-processing, the CMOS chip was dipped in acetone for 10 minutes to remove any organic impurities, followed by 5-minute dip in isopropyl alcohol. Finally, the chips were cleaned with deionized water and blow-dried with nitrogen. A LOR 5A and AZ 1515 HS multi-layer was spin-coated at

2000 RPM on the CMOS chip. The liftoff resist was exposed with direct laser writing and developed to define the pRE geometry. A Ti/Au (20 nm/200 nm) bilayer was evaporated on top of the patterned resist. Finally, the pRE was realized by incubating the chip overnight in Remover 1165 to strip the resist. A PDMS microfluidic module, similar to the one used in section 4.3.1, was aligned and plasma bonded to the post-processed CMOS chip. The microfluidic module was designed such that each flow microchannel overlaps a single NW-ISFET for sensing of DNA amplification. This allows for simultaneous monitoring of negative control and positive control reactions using ISFETs. The PDMS module was operated under the same conditions as described in section 4.3.1. DNA amplifications on CMOS chips were carried out in a PM8 probe station enclosed in a faraday cage. Similar to Chapter 3, the electrical characterization was performed by a semiconductor parameter analyzer (SPA). EasyEYPERT group+ was used to control SPA and record data.

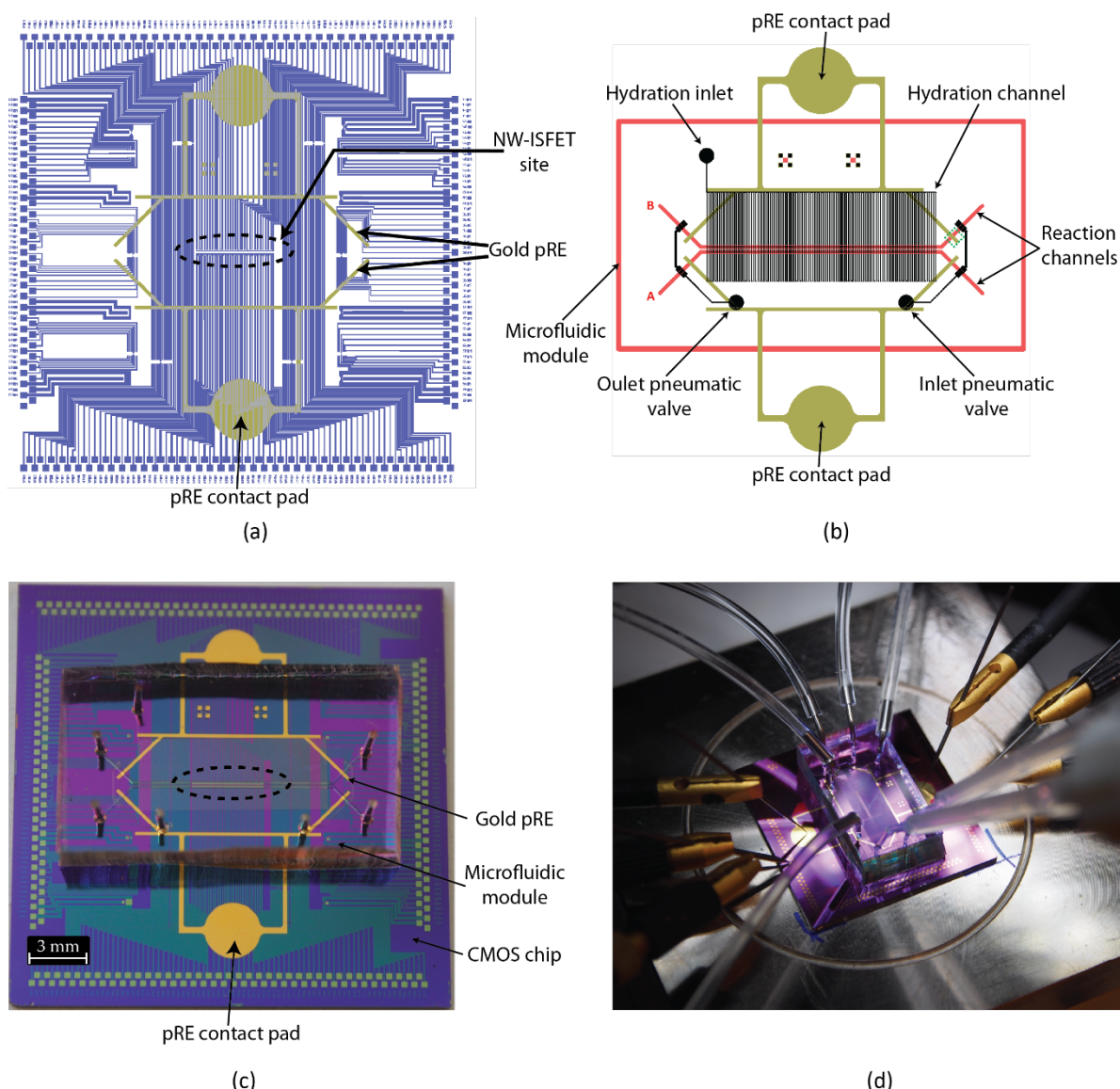


Figure 4.7. Experimental setup for label-free readout of DNA amplification. (a) Schematic of the CMOS chip, showing layout of gold pRE. (b) CAD schematic of the microfluidic module, containing two microchannels A & B and their relative position with respect to gold pRE. (c) Optical image of post-processed CMOS chip with gold pRE and plasma bonded microfluidic module. (d) Characterization setup for performing on-chip DNA amplification.

4.4.2 Electronic readout of DNA amplification on-chip in ultra-low volumes

The CMOS chips used in this work have been characterized extensively for pH sensing in the works of Accasteli [12]. The pH resolution of as low as 0.0024 pH was demonstrated in a multi-wire configuration. However, since the current work diverges significantly due to the very low-volume environment for sensing and the employment of an on-chip pRE instead of an external Ag/AgCl electrode, it is prudent to characterize if the current setup can discriminate changes in pH due to DNA amplification. Figure 4.8 shows the drain current of an n-type NW-ISFET measured in real-time under fixed polarization of the gold pRE. Aliquots of off-chip amplified DNA mixture were sequentially injected into the microchannel and pneumatic valves were actuated to create a 17 nL isolated volume. The measurements were carried out in no-flow conditions. The same aliquots were reinjected again to verify if similar drain current levels are achieved again. This result is significant as it shows that we can detect and differentiate various H^+ concentrations on-chip in 17 nL volumes. The microfluidic design allows for creation of even lower volume sizes; however, a further reduction of volume will lead to emergence of digital regime where statistical variations in DNA copy numbers due to sub-sampling will become unsustainable.

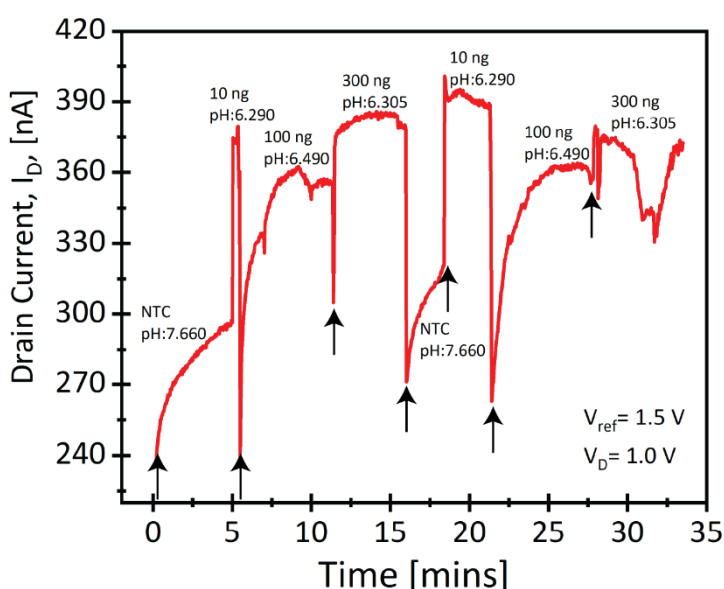


Figure 4.8. On-chip sampling measurement of different post-amplification mixtures. Real-time drain current (I_D) measurement at fixed polarization by gold pRE for injections of off-chip amplified aliquots. Different starting lambda concentrations were amplified off-chip for 22 minutes before sequentially injecting them on-chip. The pH of the aliquots was measured by a macroscopic pH probe. The arrows in the figure indicate the point of injection of different aliquots. I_D instability in the last 300 ng in injection was due to the formation of an air bubble in the channel.

4.4.2.1 Measurement strategy for on-Chip amplification

NW-FETs with widths below 300 nm exhibit enhanced transconductance due to a marked increase in corner effect. Therefore, drain current-based readout of pH offers enhanced sensitivities over readout via threshold voltage (V_T) variations [95]. Readout via V_T variations does not depend on the device dimensions and tends to perform worse at high ionic strength [12]. In order to exploit the full potential of our nanoscale ISFET and the requirement of high ionic strength for on-chip LAMP assay, we will employ drain current-based readout for pH throughout the rest of the thesis.

Apart from the readout method, two different experimental strategies can be adopted for the on-chip amplification of DNA. The obvious strategy is to have the positive sample and negative control simultaneously in different microchannels and perform a readout on both reactions simultaneously. The other method involves performing the negative control reaction first and then injecting the positive control mixture into the same channel for subsequent incubation. The choice of one over the other is influenced by a combination of factors ranging from inter-ISFET variability and behavior of threshold voltage drift in ISFET. Source of variability in among ISFETs are numerous and range from variations during the manufacturing process, leading to different gate oxide thickness, variations in the channel doping or channel height, length or width. Suboptimal layout design can introduce asymmetric series resistance in the source-drain contact lines. Post-CMOS processing is another source that can introduce variabilities in the ISFET response. Since the sensing gate oxide in ISFETs is always exposed, subsequent packaging or processing steps like electrode sputtering, electrochemical deposition and oxygen plasma can induce non-ideal changes in sensing oxide leading to disparity in ISFET sensor response. Therefore, its critical to be aware of and mitigate the effects of these variability sources, to achieve a reliable sensor platform.

In case of low variability in ISFET characteristics and similar V_T drift in identical conditions, the first approach is preferable as it reduces the assay time and increases throughput. The discriminating signal is then obtained by subtracting the negative control-ISFET signal from the positive sample-ISFET signal. However, in case of significant disparity among ISFETs in their characteristics, the aforementioned method becomes untenable. It becomes difficult to discern whether the discriminating signal between the negative and positive reaction is due to the amplification of DNA or due to the different behavior of the ISFETs. In such a situation, monitoring sequential incubation of negative control and positive sample by the same ISFET obviates the impact of inter-ISFET variabilities. The discriminating signal is obtained by offsetting the starting signal of both incubations to the same value and then subtracting the negative signal from the positive. However, care should be taken to eliminate or minimize non-specific amplifications in the negative control incubation step. Otherwise, residual non-specific amplicons can act as template sites during the incubation of the positive reaction. This is typically achieved by heat denaturing the polymerase in negative control or eliminating one of the dNTPs [10]. Since the incubations are done sequentially, the method is relatively longer and more complex.

4.4.2.2 pH-based readout of DNA amplification via ISFET

Before performing any on-chip amplification of any kind, the NW-ISFET surface is conditioned by flushing a heat-inactivated negative control LAMP mixture into the microchannels and incubating it at room temperature for approximately 20 minutes. The conditioning process is important to reduce charge traps induced in the sensing oxide during the plasma bonding procedure, leading to the stabilization of threshold voltage drift and improvement of the subthreshold slope [12].

Figure 4.9 shows the readout of amplification of lambda DNA in 17 nL reaction chambers when negative and positive reaction mixtures are incubated simultaneously on chip. The NW-ISFETs monitoring both reactions exhibit similar current-voltage (I-V) characteristics (Figure 4.9a). Amplification was monitored in real-time by sampling the drain currents of both ISFETs under fixed bias. The discriminating signal (Figure 4.9b) showing amplification was obtained by subtracting the drain current of (-) ISFET from the drain current of the (+) ISFET. The differential measurements between the two ISFET signals eliminates common-mode noise and non-ideal ISFET behavior. We were able to detect the amplification of lambda DNA in less than two minutes. Since the primers used in our LAMP assays are QUASR compatible, on-chip amplification of lambda DNA was verified by fluorescence measurement of incorporated Cy5-FIP (Figure 4.9c).

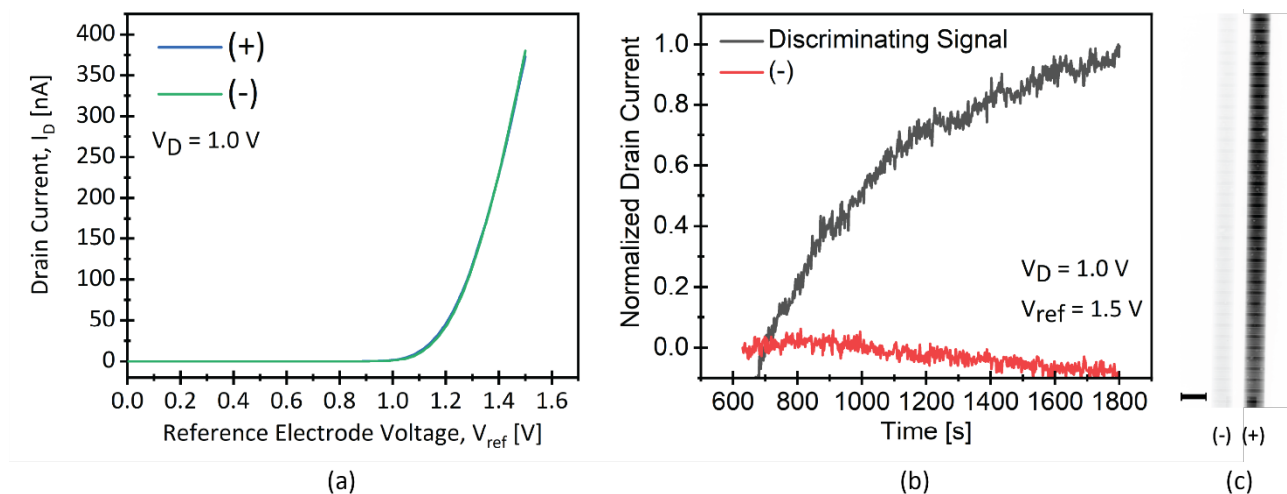


Figure 4.9 On-chip readout of LAMP with low variability among ISFETs. A 17 nL subsample from a 25 μ L master-mix containing 100 ng of lambda DNA was injected on-chip (a) I-V characteristics of two NW-ISFETs ($L = 8000$ nm, $W = 290$ nm) in the presence of amplification mixture. (b) Discriminating signal showing real-time amplification of lambda DNA in 17 nL volume. The negative control reaction contained no template DNA and was heat inactivated to prevent DNA amplification. After differential measurement between the NW-ISFETs, the discriminating signal is normalized by dividing the differential values by the maximum differential value. (-) is normalized to show the baseline. (c) Fluorescent readout of amplification in the microchannel at the end of incubation. The scale bar is 150 μ m.

Next, we performed on-chip amplification and detection via sequential injection and incubation of negative control followed by the target amplification mixture. Figure 4.10a shows the I-V characteristics of two similarly sized NW-ISFETs used to monitor the amplification of lambda DNA in real-time. Due to the different V_T and transconductance, differential measurements will not be able to compensate for all the non-ideal contributions to the signal.

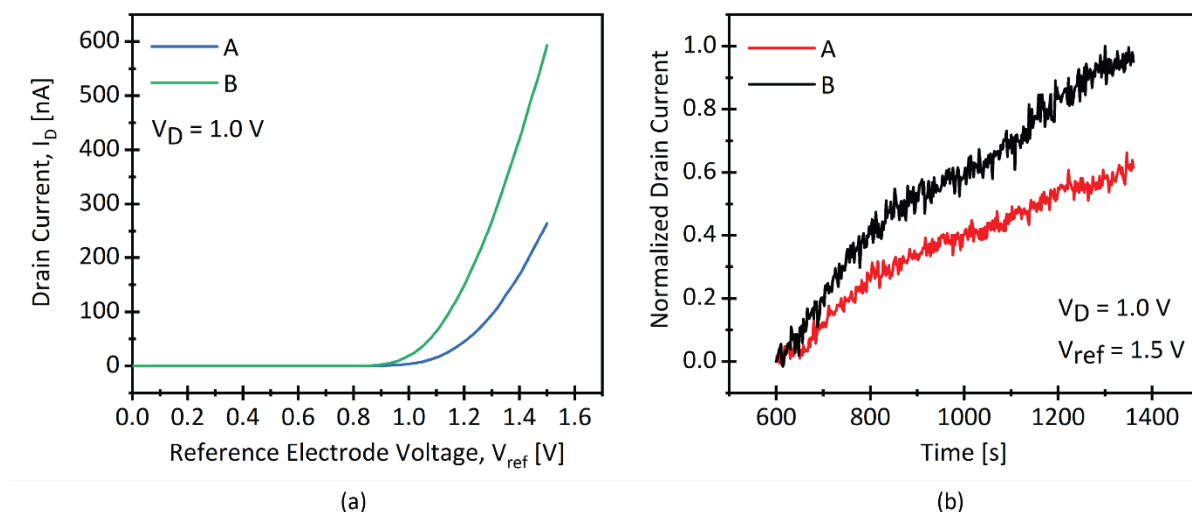


Figure 4.10. On-chip readout of LAMP with high variability among ISFETs. A 17 nL subsample from a 25 μ L master-mix containing 100 ng of lambda DNA was injected on-chip (a) I-V characteristics of two NW-ISFETs ($L = 8000$ nm, $W = 170$ nm) in the presence of amplification mixture. (b) Discriminating signal for two NW-ISFETs in two separate channels A and B, showing real-time amplification of lambda DNA (100 ng) in 17 nL volume. The negative control reaction contained no template DNA and was heat inactivated. The discriminating signal is normalized by dividing the differential values with the maximum differential value for both the NW-ISFETs.

After conditioning the microchannels, negative control mixture was injected in both the channels (A & B) and incubated at 65°C for 30 minutes. After flushing out the negative control mixture, positive control containing lambda DNA template was injected in both the channels. Reaction mixture exchange was carried out at room temperature. After the injection of positive control, the mixture was incubated again at 65°C. The discriminating signal (Figure 4.10b) is obtained by subtracting the negative control's drain current signal from the positive control's drain current signal. Similar to the first measurement strategy, we were able to detect amplification lambda DNA in 2 minutes. Due to the lack of integrated fluorescence measurement in the experimental setup, the optical readout is done by removing the chip and imaging it under a fluorescent microscope. Since the experiment ends with the incubation of positive control, differential fluorescence measurement between negative control and positive control is not possible. Only the presence of amplification can be verified.

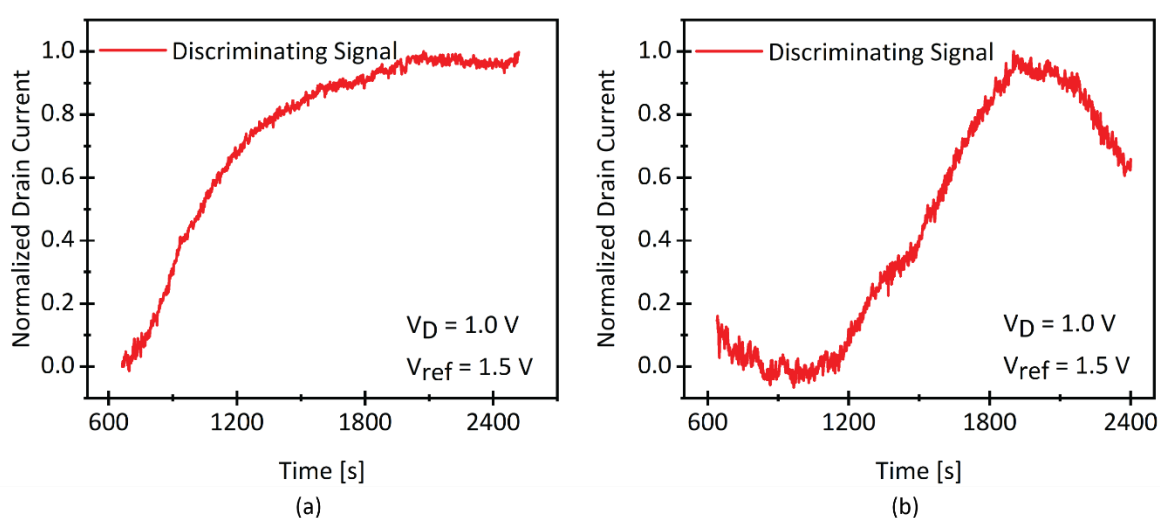


Figure 4.11. Real-time amplification curve of lambda DNA (100 ng) in the presence of HeLa genomic DNA (100 ng). (a) When negative and positive reactions are incubated simultaneously and (b) when negative and positive reactions are incubated sequentially in the same microchannel. The polymerase in the negative controls was not heat-inactivated.

In section 2.3.2.1, we have demonstrated the specificity of the pH-based LAMP assay in the presence of non-specific DNA. However, the assay conditions since then have evolved due to changes in buffer concentration, labelled primers and an increase in polymerase concentration. Therefore, it is prudent to verify the specificity of the LMAP assay for on-chip amplification in reduced volume conditions. We performed on-chip amplification of lambda DNA in the presence of HeLa genomic DNA to assess the impact of the presence of non-specific template DNA in the amplification mixture. On-chip amplifications were carried out in both simultaneous incubation and sequential incubation of negative and positive control mixtures. Unlike the experiments in Figure 4.9 and Figure 4.10, the negative control was not heat-inactivated and contained HeLa genomic DNA as a non-specific template. Figure 4.11a shows the real-time amplification curve when both negative and positive mixtures are incubated simultaneously. We see no significant change in performance when compared to amplification in the absence of non-template-specific DNA (Figure 4.9). We were able to detect the amplification of lambda DNA in less than 3 minutes. However, on-chip amplification was performed via sequential incubation; the time to detection was increased to 10 minutes (Figure 4.11b). Moreover, upon continued incubation (around 20 minutes), we saw a decrease in the discrimination signal due to non-specific amplification in the negative control. The delayed time to detection during the incubation of positive control could be attributed to the leftover non-specific amplicon generated during prior

negative control incubation. This can be mitigated by heat inactivating the negative control to minimize any non-specific amplification.

4.4.2.3 Effect of volume on time-to-positive signal

Label-based optical readout of nucleic acid amplification remains unaffected by volumetric scaling. A fluorophore-labelled DNA will generate the same signal intensity in both nanoliter or microliter-sized volumes. However, readout of NA amplification by sensing the change in concentration of hydrogen ions benefits directly from volumetric scaling, as concentration is a property of size. The concentration of hydrogen ion on the surface of ISFET's sensing oxide depends on the concentration of hydrogen ion in the bulk via the relation $[H^+]_s = [H^+]_B e^{-q\Psi_0/kT}$, where $[H^+]_s$ is the concentration of hydrogen ions at the surface of ISFET's sensing oxide, $[H^+]_B$ is the concentration of hydrogen ions in the bulk electrolyte, Ψ_0 is the surface potential across the sensing oxide, k is the Boltzman constant, q is the elementary charge and T is the operating thermodynamic temperature.

This implies that a quicker change in the bulk concentration will lead to quicker change in the surface charge density at ISFET's sensing oxide leading to faster readout of NA amplification. In NA amplification assay, "time-to-positive signal" or "time-to-detection" refers to the amount of time it takes for a target DNA mixture to differentiate from the negative control mixture. Time-to-detection in DNA amplification assay depends on numerous factors, such as starting template DNA concentration, amount of polymerase, design of primers, source of extracted DNA, incubation temperature etc. When these variables are kept constant, as shown in the Figure 4.12, for pH-based NA amplification assays, time-to-detection is achieved significantly quicker in nanoliter-sized volumes as compared to microliter-sized volume. LAMP of lambda phage DNA in 25 μ L takes at least 12 minutes to differentiate from its negative control, whereas same assay when performed in 17 nL volume differentiates from its negative control by 2 minutes. These NW-ISFETs have been shown to resolve changes in surface charge of as low as 350 electrons per micrometer square, which effectively amounts to a single DNA template amplifying 3 or 4 times [95]. Therefore, analysis of noise and its removal from the ISFET signal can further improve the time-to-detection, forgoing the need to exponentially amplify DNA.

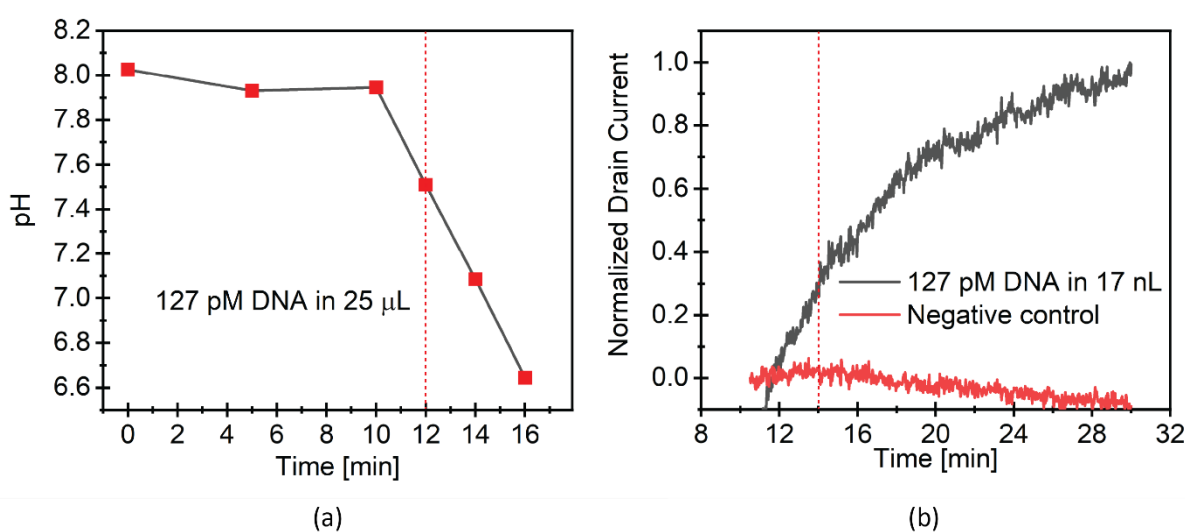


Figure 4.12. Effect of volume on pH-based readout of LAMP. (a) Evolution of pH with time in LAMP of 100 ng bacteriophage Lambda DNA, in 25 μ L reaction tubes. The reaction aliquots were prepared from same master-mix and were heat inactivated at various time points prior to pH measurement via a commercial pH meter. (b) ISFET signal from on-chip LAMP in 17 nL reaction chambers. A 17 nL subsample from a 25 μ L master-mix containing 100 ng of lambda DNA was used as positive template control. The red dotted line indicates the time where positive control differentiates from negative control.

4.4.3 Conclusion

In this chapter, we show label-free readout of LAMP in nanoliter-sized volumes by sensing changes in the reaction pH via NW-ISFETs. We discovered that the translation of tube-based LAMP assay to microfluidic channels is not obvious due to the increased surface-to-volume ratio in nanoliter-sized volumes. Adsorption of reaction species on the microchannel surface changes their effective concentration on-chip. Therefore, the concentrations of LAMP species were increased to compensate for adsorption-based losses. Due to the small volume size in our setup (17 nL) the dynamic range for DNA quantification was reduced. The pH sensitivity of the NW-ISFETs was verified by injecting post-LAMP mixtures on chip. For on-chip amplification and detection we devised two methods depending upon the relative variability among the two NW-ISFETs employed for positive and negative control reactions. If the NW-ISFETs demonstrate similar characteristics, real-time signal was captured by simultaneous incubation of positive and negative reaction. In case of large dissimilarities in the NW-ISFET response, sequential incubation of first negative control followed by the positive control was carried. Using both these methods, we were able to detect amplification of DNA in 17 nL volume. We show that we can also specifically detect the amplification of DNA in the presence of non-specific human genomic DNA. Finally, we demonstrate that pH-based amplification assay offer quicker readout in nanoliter volumes as compared to microliter volumes.

Chapter 5 Conclusions and prospective

5.1 Main Achievements

In this section, we summarize the main achievement of the thesis

5.1.1 pH-based readout of isothermal nucleic acid amplification

We analyzed two isothermal amplification recipes to develop near-room temperature amplification assays that can be read out via sensing changes in pH. Our investigation of recombinase polymerase amplification revealed that removing the dedicated pH buffers from the amplification assay is insufficient to adapt the amplification assay for pH-based readout. Moreover, the unique chemistry of RPA grants it the intrinsic ability to buffer changes in the pH brought about by the amplification of DNA, making it intrinsically unsuited for pH-based readout. The work reveals considerations and strategies for developing pH-based amplification assays from methods whose biochemistry involves ancillary proteins that hydrolyze nucleotides. We further investigated the pH-based LAMP assay and reliably reduced its operating temperature from 65°C to 45°C while maintaining a pH-based readout of the assay. A lower temperature of pH-based LAMP assay is important for better signal-to-noise ratio for ISFET-based point-of-care devices and reduced evaporation from small volume assays.

5.1.2 Design of scalable microfluidic module with integrated reference electrode

We proposed and fabricated a PDMS-based microfluidic module design that eliminates the need to post-process CMOS chips to fabricate on-chip reference electrodes. The design can be adapted to any layout and scaled up in numbers to monitor hundreds of reaction chambers by ISFETs simultaneously. The microfluidic module can be bonded to the CMOS chip both reversibly and irreversibly. The novel module design has a gold reference electrode that is conformally integrated into the microchannels or microchambers, allowing biasing of very low volumes and high-density layouts. Using this design, we could bias a 1.5 nL volume and monitor it via ISFET.

5.1.3 Fabrication of “through-PDMS-via” using 1 mm high SU-8 structures

We developed a process flow to fabricate very high (1 mm) conductive SU-8 structures. Issues with very high thickness SU-8 processing are long time durations for baking, resist development and poor surface cleanliness post-development. By coating and patterning a thin positive photoresist layer in the unexposed regions of SU-8, we can selectively depress SU-8 adhesion to the substrate. This deliberate dirtying of the substrate leads to reduced baking time due to quicker ramps and faster development time. These structures allow a “through-silicon-via” like contact in a PDMS matrix, leading to the realization of the microfluidic module that requires no post-processing of CMOS chips.

5.1.4 pH-based DNA amplification readout in nanoliter volume via semiconductor devices

We demonstrate DNA amplification and its readout via nanowire ISFET in nanoliter volumes. Traditionally nanoscale ISFET devices have been used to readout DNA amplification in microliter-sized volumes. Readout of DNA amplification in very small volume benefits from the enhanced sensitivity of nanowire ISFETs leading to a faster readout of amplification. We can detect the amplification of DNA in as low as 2 minutes. The readout of DNA amplification by ISFETs in small chambers is hindered by the requirement of an in-chamber reference electrode, limiting the parallelism and scalability of ISFET-based nucleic acid testing solutions. Our design demonstrates the concept of NAT in ultra-low volumes, with the capability to scale in numbers with CMOS technology, leading to parallel CMOS-based NAT solutions.

5.2 Prospective Outlook

In this section, we outline possible future investigations and project directions that can be undertaken. Some of them are being undertaken currently, and the preliminary results are presented below.

5.2.1 Technology

We foresee many technological improvements that can leverage the work presented in the thesis.

Microfluidic Module: The yield of the PDMS microfluidic module illustrated in Chapter 3 needs to be improved. The current design suffers from the collapse of hydration channels when the thick PDMS layer is bonded to the thin PDMS layer under pressure. The pressure exerted by the screw vice to eliminate the bubbles around TPV is so high that it leads to the collapse of the hydration channel, leading to regions that cannot be filled with hydration liquid. This makes DNA amplification at elevated temperatures unreliable. A new setup that exerts localized pressure in the TPV region of the PDMS module can help mitigate the issue of the collapse of hydration channels.

Integration of Ag/AgCl electrode in microfluidic module: In the appendix, we illustrate our attempts to realize Ag/AgCl electrode in our microfluidic module. However, the process lacks scalability as it can only be performed on a single microfluidic module at a time. Methods that can integrate the silver layer during the fabrication of the gold pRE can greatly enhance the application potential of the presented microfluidic module design. Due to low noise and surface potential drift, integrating Ag/AgCl electrode in the module will allow even more sensitive detection of DNA amplification.

Arrayed device for parallel detection of amplification: Small volume size (17 nL) of our setup limits the lower end of the dynamic range for DNA quantification. The total analyzed volume can be increased by increasing the number of microfluidic chambers. It also requires adequately designed CMOS sensing chips that have a large number of arrayed NW-ISFET devices. An iteration of a similar design that we are currently working on is shown in Figure 5.1. In collaboration with CEA-LETI, we designed and fabricated a 22 mm X 22 mm sized CMOS chip that consists of an array of 100 ISFET sensing sites with two differently sized multi-wire NW-ISFETs. However, due to the use of just one metal layer for routing, the chip lacks integrated row and column registers for automated inquiry of the ISFET. Therefore, the CMOS chip is packaged as chip-on-board (COB) and can be interrogated via readout circuitry mounted on a printed circuit board. We also fabricated a microfluidic module for the parcellization of the DNA amplification mixture over the 100 ISFET sensing sites. However, due to lingering issues with the integration of hydration channels, we were not able to demonstrate a readout of DNA amplification with this setup. The future work will involve the complete

realization of the setup and demonstrate parallel readout of up to 100 DNA amplification reactions with the multi-wire ISFETs.

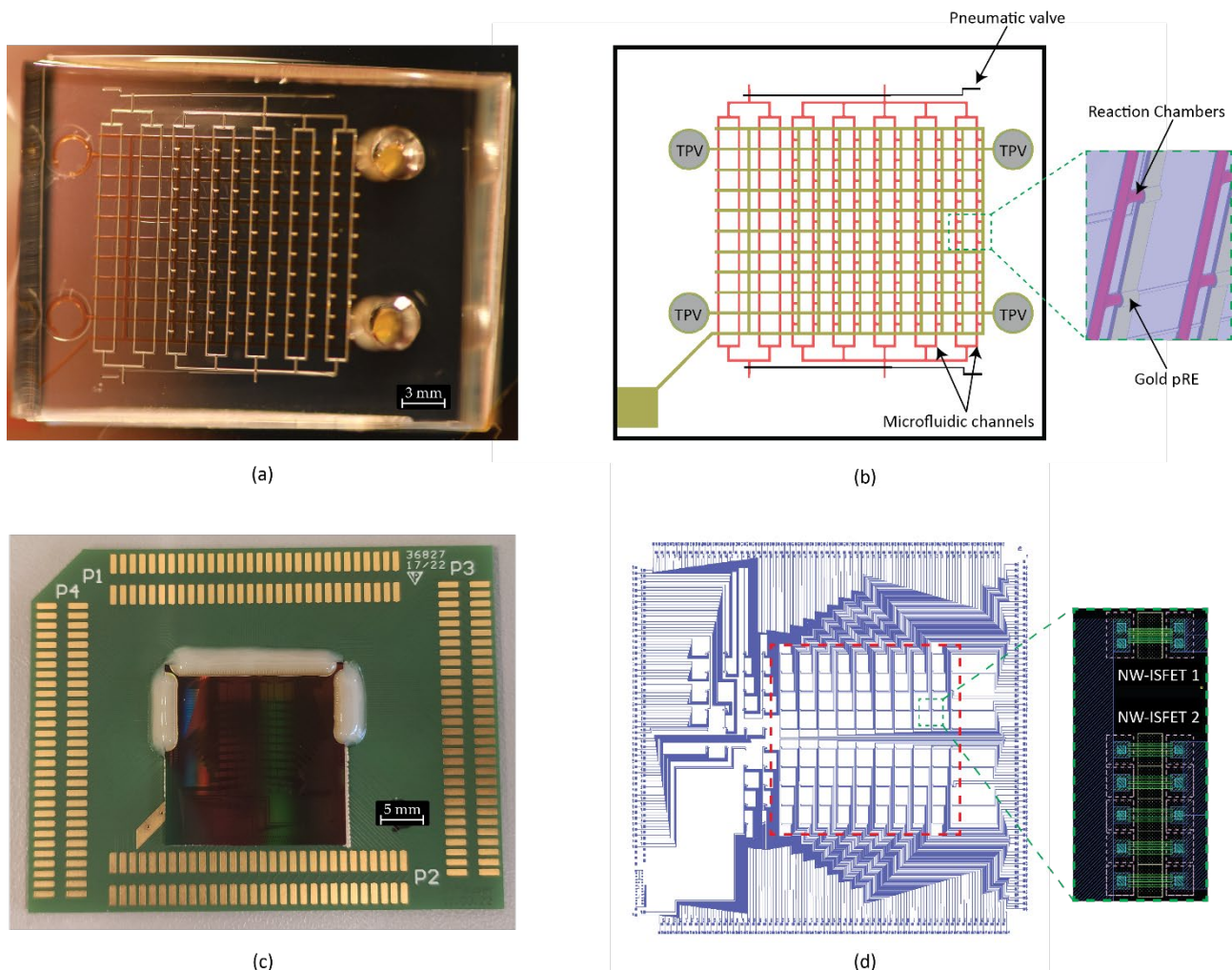


Figure 5.1. Future iterations of the fluidic module for multiplex readout. (a) Microfluidic module for oil-based parcellization of 100 partitions arranged in 10 X 10 array. The shown design lacks hydration channels. (b) Schematic showing the layout of the microfluidic module and placement of gold pRE (green square). (c) COB of NW-ISFET chip consisting of an array of 100 NW-ISFET sites. (d) The layout of the NW-ISFET chip shows 10 X 10 array (red square) of 100 sensing sites. The inset shows the two different-sized multi-wire ISFETs that are located at each sensing site. NW-ISFET 1 (6 nanowires, $W = 80 \text{ nm}$, $L = 1.5 \mu\text{m}$) and NW-ISFET 2 (5x3 nanowires, $W = 150 \text{ nm}$, $L = 1.5 \mu\text{m}$).

5.2.2 Rapid antibiotic susceptibility testing

An important area where NW-ISFETs can find applications is antibiotic susceptibility testing (AST). AST is a method that specifies effective antibiotic dosage and empirical therapy for the treatment of bacterial infections. With the rapid emergence of antibiotic resistance bacteria, primarily due to incorrect and over-prescription of antibiotics, AST is becoming increasingly relevant for managing the resistance and its burden. However, existing methods to perform AST are culture-based and take more than 48 hours to deliver actionable minimum inhibitory concentration (MIC) of the antibiotic. Resistance to β -lactam antibiotics is one of the fastest emerging and most common types of resistance among pathogens. β -lactam antibiotics represent up to 65% of the antibiotic market and are the most successfully used drugs to treat bacterial infections[96]. Pathogens develop resistance to β -lactam antibiotics mainly due to the production of β -lactamase enzymes, which inactivates the antibiotics by hydrolyzing the β -Lactam ring in the molecule.

Hydrolysis of the β -lactam ring generates an aqueous hydrogen ion, which leads to a decrease in the pH of the bacterial suspension. Hydrolysis-based AST assays using a pH or colorimetric readout already exist but require a minimum overnight culture after identifying the pathogen[97]. Then a small portion of that colony is suspended in water or a buffered medium and its pH is monitored in the presence of a suitable antibiotic. Figure 5.2 shows the evolution of the pH for suspensions of carbapenem-resistant *Klebsiella pneumoniae* in the presence of a carbapenem antibiotic (Imipenem). At very high bacterial concentrations, the readout via the change in pH is rapid. However, such bacterial concentrations are achieved after long cultures, thereby prolonging the time to result. At lower concentrations, the rate of pH change due to antibiotic hydrolysis decreases significantly.

Rapid AST requires detecting the presence of resistance directly from the patient sample where the bacterial load is low. The extremely low resolution of multi-wire ISFETs can detect small changes in pH produced by low bacterial copy numbers. Parallelizing the patient sample into small volumes and monitoring them via ISFETs in the presence of various concentrations of antibiotics can reduce the time to AST to a few minutes. Besides monitoring the enzymatic activity of β -lactamase, the parcellization strategy can also carry out growth-based AST. In certain growth mediums, the pH of the medium falls due to the growth and metabolic activity of the bacteria[98]. When cultured in tiny volumes, the resulting change in pH can be monitored by extremely sensitive NW-ISFETs. Growth-based assays, though not as quick as the enzymatic assay, will still give faster readout due to the low volume of the culture chamber.

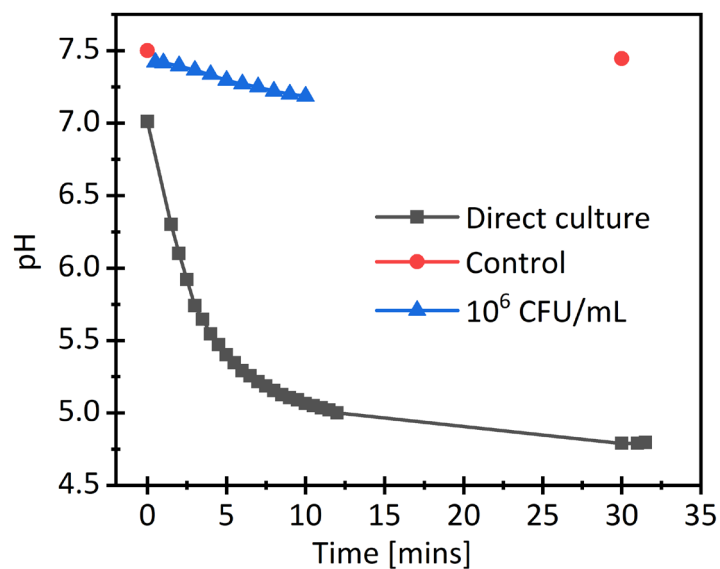


Figure 5.2. Antibiotic hydrolysis by resistant bacteria. Change in pH of various concentrations of *Klebsiella pneumoniae* (K.pn.) suspensions in the presence of Imipenem (100 μ M) antibiotics. The “Direct culture” consist of a colony of resistant positive K.pn. (ATCC BAA-1705) picked from a culture plate and diluted in 500 μ L of water. The “Control” consist of a colony of resistant negative K.pn (ATCC BAA-1706) picked from the culture plate diluted in 500 μ L of water.

5.2.3 Towards ISFET-based digital quantification system

The unprecedented parallelism offered by CMOS technology makes an obvious case for ISFET devices to be used for the digital quantification of nucleic acids. Ion Torrent’s next-generation sequencing has already demonstrated readout of nucleotide incorporation via sensing H^+ from up to 600 million wells [99], offering the possibility of a number of parallelism that are up to two orders of magnitude larger than the current

state-of-the-art droplet dPCR [100]. However, the realization of the ISFET-based digital quantification system is complicated by the need for a miniaturized reference electrode in each reaction well. In this thesis, we have attempted to address that problem. However, the requirement of large numbers of single-volume partitions for precise quantification can be ameliorated by employing multi-volume digital assays [94]. Instead of using single sized partitions as in conventional digital assays, multi-volume digital assays use partitions with different volume sizes. Multi-volume digital assays can reduce the requirement on the number of partitions by an order of magnitude while maintaining a similar dynamic range [101]. This frees up the on-chip real estate and relaxes constraints on the size of the reference electrode, making ISFET-based digital assays more feasible.

Chapter 6 Appendices

6.1 Composition of isothermal amplification reaction buffers

	RPA Buffer	Acetate Buffer	Chloride Buffer
TRIS [pH = 8.0]	50 mM		
Potassium acetate	100 mM	100 mM	
Potassium chloride			100 mM
PEG-20000	5 %(w/v)	5 %(w/v)	5 %(w/v)
DTT	2 mM	2 mM	2 mM

Figure 6.1. Composition of different reaction buffers utilized for RPA.

	Custom E-mix (1x)	E-mix_ATP (1x)
ATP	3 mM	20 mM
Creatine phosphate	50 mM	

Figure 6.2. Composition of different energy sources for recombinase activity in RPA

	RPA Buffer*	Acetate Buffer	Chloride Buffer
TRIS [pH = 8.0]	50 mM		
Potassium acetate	100 mM	100 mM	
Potassium chloride			100 mM
PEG-20000	5 %(w/v)	5 %(w/v)	5 %(w/v)
DTT	2 mM	2 mM	2 mM
Magnesium acetate	14 mM	14 mM	
Magnesium chloride			14 mM

	RCA Buffer (1X)
Potassium chloride	66 mM
Betaine	400 mM
Triton-x 100	0.1 %(v/v)
BSA	1 mg/ml
dNTPs	2 mM
Magnesium chloride	10 mM

Figure 6.3. Composition of reaction buffers that are titrated with HCl to measure their buffering power.

6.2 Fabrication of Ag/AgCl electrode in microfluidic module

Electroplating of silver and subsequent chlorination was used to fabricate a conformal Ag/AgCl reference electrode in the microfluidic module. Already fabricated Gold pRE forms the template for the electrochemical deposition and chlorination of silver allowing for the realization of conformal Ag/AgCl in the microfluidic channel.

Figure 6.4a shows the custom PMMA holder designed to carry the microfluidic module with gold pRE, for fabrication of Ag/AgCl electrode. A thin gold layer on a flexible substrate like PDMS is very delicate and prone to develop cracks under strain. To prevent localized strain on the thin gold layer, a wide area of contact was realized by sticking copper tape to the PMMA holder. For the electrodeposition of silver, the electrolyte consisted of 0.2 M Silver Nitrate, 30% (v/v) Methanol, 0.05 M Nitric acid and 0.015 M Tartaric acid [102]. A pure silver wire cleaned in nitric acid (1 min in 0.1 M HNO₃) was used as the anode while the gold pRE on the PDMS module acts as the cathode. Silver was electrodeposited under a constant current of 160 μ A over the 0.0947 cm² of gold pRE area (Current density = 1.6894 mA/cm²). The time duration of electrodeposition was modulated to achieve various thicknesses of silver (12 μ m in 30 min, 6 μ m in 15 min and 4 μ m in 8 min). The same PMMA module was used to perform chlorination of the deposited silver. A platinum wire was used as a cathode, the electrodeposited silver acted as an anode and 0.1 M KCl was used as an electrolyte for chlorination. Under a constant current of 160 μ A, 1 μ m of silver was chlorinated to achieve an Ag/AgCl structure. After chlorination, the module was incubated overnight in a 3 M KCl solution saturated with AgCl.

The stability of the obtained Ag/AgCl electrode was measured by measuring its open circuit potential (OCP) against a commercial flow through Ag/AgCl electrode. The microfluidic module was bonded to a silicon substrate through its intrinsic adhesion. A 3 M KCl electrolyte was injected into the microchannel to obtain a fluidic contact with the flow-thru reference electrode. A TPV was used to connect the fabricated Ag/AgCl electrode to the potentiostat for OCP measurement. We observe that though the average trend in OPC is stable over time, there are numerous fluctuations (Figure 6.4d). We attribute this to incomplete chlorination of the silver layer. As seen in Figure 6.4e, 1 μ m of chlorination is not enough to completely chlorinate the top layer of silver. The fluctuation in OCP could be due to native silver reacting with the chloride ions in the electrolyte. In future iterations, OCP can be improved by chlorinating a larger fraction of deposited silver.

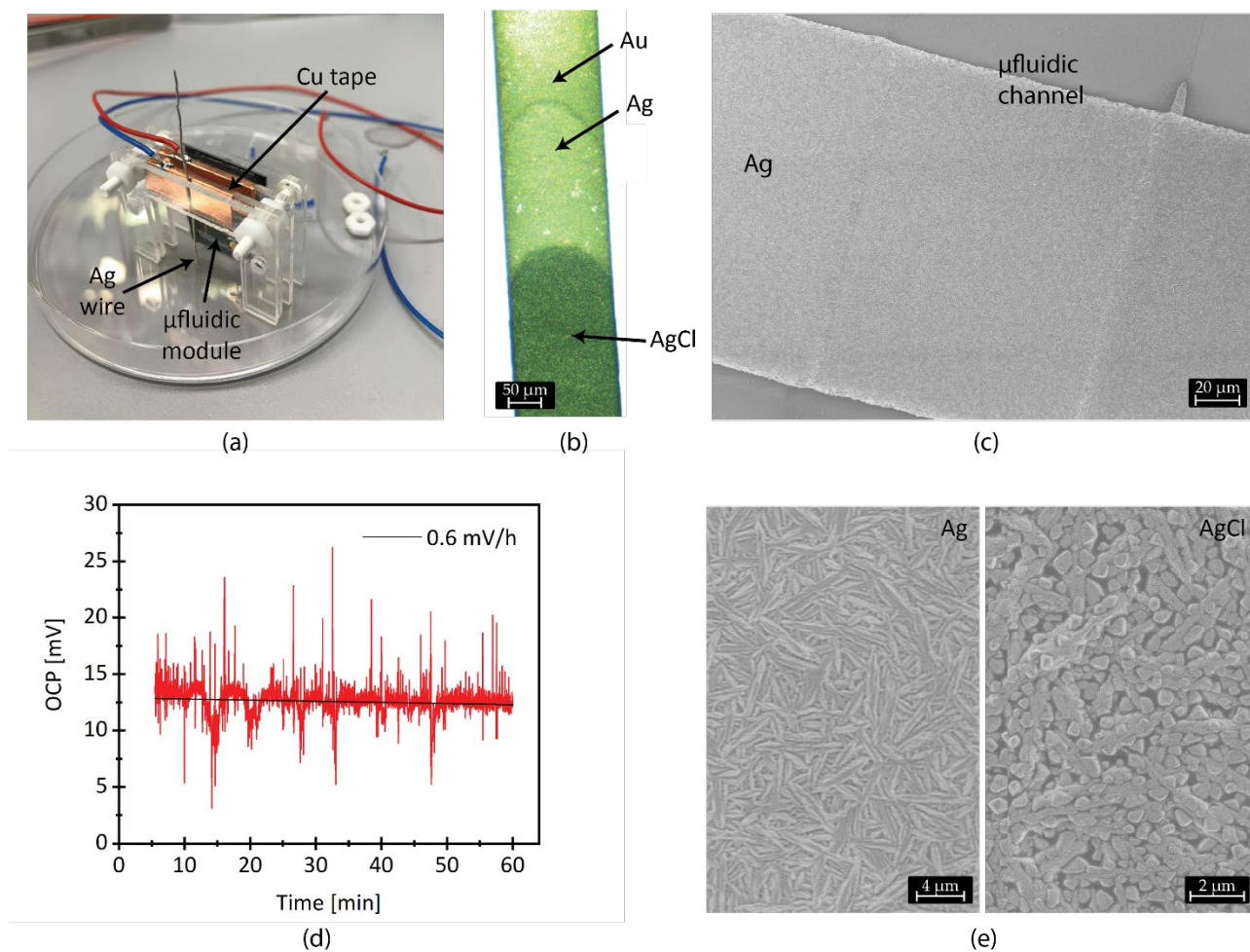


Figure 6.4. Fabrication of Ag/AgCl electrode in microfluidic module. (a) A custom holder made from laser-cut PMMA. Teflon screws provide enough pressure to maintain reliable contact. (b) Optical micrograph of gold pRE on PDMS showing regions with electroplated silver and subsequently chlorinated to AgCl. (c) A SEM micrograph of microchannel showing conformal electrode with electrodeposited silver. (d) OCP characterization of the Ag/AgCl electrode in microchannel. (e) SEM micrograph of electrodeposited silver and post-chlorination silver, showing incomplete chlorination of long silver grains into “spherical” AgCl.

References

1. Roth, W.K. History and Future of Nucleic Acid Amplification Technology Blood Donor Testing. *Transfus. Med. Hemotherapy* **2019**, *46*, 67, doi:10.1159/000496749.
2. Higuchi, R.; Dollinger, G.; Walsh, P.S.; Griffith, R. Specific Dna Sequences. *Nat. Biotechnol.* **1992**, *10*, 413–417.
3. Hennig, H.; Luhm, J.; Hartwig, D.; Klüter, H.; Kirchner, H. A novel RT-PCR for reliable and rapid HCV RNA screening of blood donations. *Transfusion* **2001**, *41*, 1100–1106, doi:10.1046/J.1537-2995.2001.41091100.X.
4. Quan, P.L.; Sauzade, M.; Brouzes, E. DPCR: A technology review. *Sensors (Switzerland)* **2018**, *18*, doi:10.3390/s18041271.
5. Sykes, P.J.; Neoh, S.H.; Brisco, M.J.; Hughes, E.; Condon, J.; Morley, A.A. Quantitation of targets for PCR by use of limiting dilution. *Biotechniques* **1992**, *13*, 444–449.
6. Vogelstein, B.; Kinzler, K.W. Digital PCR. *Proc. Natl. Acad. Sci. U. S. A.* **1999**, *96*, 9236–41, doi:10.1073/pnas.96.16.9236.
7. Sanger, F.; Coulson, A.R. A rapid method for determining sequences in DNA by primed synthesis with DNA polymerase. *J. Mol. Biol.* **1975**, *94*, 441–448, doi:10.1016/0022-2836(75)90213-2.
8. Goodwin, S.; McPherson, J.D.; McCombie, W.R. Coming of age: Ten years of next-generation sequencing technologies. *Nat. Rev. Genet.* **2016**, *17*, 333–351, doi:10.1038/nrg.2016.49.
9. Robison, K. Semiconductors charge into sequencing. *Nat. Biotechnol.* **2011**, *29*, 805–807, doi:10.1038/nbt.1965.
10. Toumazou, C.; Shepherd, L.M.; Reed, S.C.; Chen, G.I.; Patel, A.; Garner, D.M.; Wang, C.-J.A.; Ou, C.-P.; Amin-Desai, K.; Athanasiou, P.; et al. Simultaneous DNA amplification and detection using a pH-sensing semiconductor system. *Nat. Methods* **2013**, *10*, 641–646, doi:10.1038/nmeth.2520.
11. Hu, C.; Kalsi, S.; Zeimpekis, I.; Sun, K.; Ashburn, P.; Turner, C.; Sutton, J.M.; Morgan, H. Ultra-fast electronic detection of antimicrobial resistance genes using isothermal amplification and Thin Film Transistor sensors. *Biosens. Bioelectron.* **2017**, *96*, 281–287, doi:10.1016/j.bios.2017.05.016.
12. Accastelli, E. Tri-gate silicon nanowire transistors for ultra-low pH resolution and improved scalability PAR. **2015**, 6468.
13. Purushothaman, S.; Toumazou, C.; Ou, C.P. Protons and single nucleotide polymorphism detection: A simple use for the Ion Sensitive Field Effect Transistor. *Sensors Actuators, B Chem.* **2006**, *114*, 964–968, doi:10.1016/j.snb.2005.06.069.
14. Credo, G.M.; Su, X.; Wu, K.; Elibol, O.H.; Liu, D.J.; Reddy, B.; Tsai, T.-W.; Dorvel, B.R.; Daniels, J.S.; Bashir, R.; et al. Label-free electrical detection of pyrophosphate generated from DNA polymerase reactions on field-effect devices. *Analyst* **2012**, *137*, 1351, doi:10.1039/c2an15930a.
15. Gibson, N.J.; Newton, C.R.; Little, S. A Colorimetric Assay for Phosphate to Measure Amplicon Accumulation in Polymerase Chain Reaction. *Anal. Biochem.* **1997**, *254*, 18–22, doi:10.1006/ABIO.1997.2324.
16. He, L.; Musick, M.D.; Nicewarner, S.R.; Salinas, F.G.; Benkovic, S.J.; Natan, M.J.; Keating, C.D. Colloidal Au-enhanced surface plasmon resonance for ultrasensitive detection of DNA hybridization. *J. Am. Chem. Soc.* **2000**, *122*, 9071–9077, doi:10.1021/JA001215B/SUPPL_FILE/JA001215B_S.PDF.
17. Hansen, K.M.; Ji, H.F.; Wu, G.; Datar, R.; Cote, R.; Majumdar, A.; Thundat, T. Cantilever-based optical deflection assay for discrimination of DNA single-nucleotide mismatches. *Anal. Chem.* **2001**, *73*, 1567–1571, doi:10.1021/AC0012748/ASSET/IMAGES/LARGE/AC0012748F00005.JPEG.
18. Steel, A.B.; Herne, T.M.; Tarlov, M.J. Electrochemical quantitation of DNA immobilized on gold. *Anal. Chem.* **1998**, *70*, 4670–4677, doi:10.1021/AC980037Q/ASSET/IMAGES/LARGE/AC980037QF00007.JPEG.

19. Wang, J.; Kawde, A.N.; Musameh, M. Carbon-nanotube-modified glassy carbon electrodes for amplified label-free electrochemical detection of DNA hybridization. *Analyst* **2003**, *128*, 912–916, doi:10.1039/B303282E.
20. Rothberg, J.M.; Hinz, W.; Rearick, T.M.; Schultz, J.; Mileski, W.; Davey, M.; Leamon, J.H.; Johnson, K.; Milgrew, M.J.; Edwards, M.; et al. An integrated semiconductor device enabling non-optical genome sequencing. *Nature* **2011**, *475*, 348–352, doi:10.1038/nature10242.
21. Tanner, N.A.; Zhang, Y.; Evans, T.C. Visual detection of isothermal nucleic acid amplification using pH-sensitive dyes. *Biotechniques* **2015**, *58*, 59–68, doi:10.2144/000114253.
22. Hamidi, S.V.; Perreault, J. Simple rolling circle amplification colorimetric assay based on pH for target DNA detection. *Talanta* **2019**, *201*, 419–425, doi:10.1016/j.talanta.2019.04.003.
23. Tenaglia, E.; Imaizumi, Y.; Miyahara, Y.; Guiducci, C. Isothermal multiple displacement amplification of DNA templates in minimally buffered conditions using phi29 polymerase. *Chem. Commun.* **2018**, *54*, 2158–2161, doi:10.1039/c7cc09609g.
24. Duarte-Guevara, C.; Swaminathan, V. V.; Burgess, M.; Reddy, B.; Salm, E.; Liu, Y.S.; Rodriguez-Lopez, J.; Bashir, R. On-chip metal/polypyrrole quasi-reference electrodes for robust ISFET operation. *Analyst* **2015**, *140*, 3630–3641, doi:10.1039/c5an00085h.
25. Kalofonou, M.; Toumazou, C. Semiconductor technology for early detection of DNA methylation for cancer: From concept to practice. *Sensors Actuators, B Chem.* **2013**, *178*, 572–580, doi:10.1016/j.snb.2012.12.054.
26. Salm, E.; Zhong, Y.; Reddy Jr, B.; Duarte-Guevara, C.; Swaminathan, V.; Liu, Y.-S.S.; Bashir, R.; Reddy, B.; Duarte-Guevara, C.; Swaminathan, V.; et al. Electrical detection of nucleic acid amplification using an on-chip quasi-reference electrode and a PVC REFET. *Anal. Chem.* **2014**, *86*, 6968–6975, doi:10.1021/ac500897t.
27. Li, J.; Macdonald, J.; Von Stetten, F. Review: a comprehensive summary of a decade development of the recombinase polymerase amplification. *Analyst* **2019**, *144*, 31–67, doi:10.1039/c8an01621f.
28. Crone, M.A.; Priestman, M.; Ciechonska, M.; Jensen, K.; Sharp, D.J.; Anand, A.; Randell, P.; Storch, M.; Freemont, P.S. A role for Biofoundries in rapid development and validation of automated SARS-CoV-2 clinical diagnostics. *Nat. Commun.* **2020**, *11*, 1–11, doi:10.1038/s41467-020-18130-3.
29. Xia, S.; Chen, X. Single-copy sensitive, field-deployable, and simultaneous dual-gene detection of SARS-CoV-2 RNA via modified RT-RPA. *Cell Discov.* **2020**, *6*, 4–7, doi:10.1038/s41421-020-0175-x.
30. Piepenburg, O.; Williams, C.H.; Stemple, D.L.; Armes, N.A. DNA Detection Using Recombination Proteins. *PLoS Biol.* **2006**, *4*, e204, doi:10.1371/journal.pbio.0040204.
31. YONESAKI, T.; RYO, Y.; MINAGAWA, T.; TAKAHASHI, H. Purification and some of the functions of the products of bacteriophage T4 recombination genes, *Uvs X* and *Uvs Y*. *Eur. J. Biochem.* **1985**, *148*, 127–134, doi:10.1111/j.1432-1033.1985.tb08816.x.
32. Kiani, F.A.; Fischer, S. Effects of protonation on the hydrolysis of triphosphate in vacuum and the implications for catalysis by nucleotide hydrolyzing enzymes. *BMC Biochem.* **2016**, *17*, 1–13, doi:10.1186/s12858-016-0068-7.
33. Lutz, S.; Weber, P.; Focke, M.; Faltin, B.; Hoffmann, J.; Müller, C.; Mark, D.; Roth, G.; Munday, P.; Armes, N.; et al. Microfluidic lab-on-a-foil for nucleic acid analysis based on isothermal recombinase polymerase amplification (RPA). *Lab Chip* **2010**, *10*, 887–893, doi:10.1039/b921140c.
34. Formosa, T.; Alberts, B.M. Purification and Characterization of the T4 Bacteriophage *UvsX* Protein*. *J. Biol. Chem.* **1986**, *261*, 6107–6118.
35. Takahashi, S.; Brazier, J.A.; Sugimoto, N. Topological impact of noncanonical DNA structures on Klenow fragment of DNA polymerase. *Proc. Natl. Acad. Sci. U. S. A.* **2017**, *114*, 9605–9610, doi:10.1073/pnas.1704258114.
36. Zou, Y.; Mason, M.G.; Botella, J.R. Evaluation and improvement of isothermal amplification methods for point-of-need plant disease diagnostics. *PLoS One* **2020**, *15*, 1–19, doi:10.1371/journal.pone.0235216.
37. Vincent, M.; Xu, Y.; Kong, H. Helicase-dependent isothermal DNA amplification. *EMBO Rep.* **2004**, *5*, 795–800, doi:10.1038/sj.embor.7400200.
38. Zhang, X.; Li, Q.; Jin, X.; Jiang, C.; Lu, Y.; Tavallaie, R.; Gooding, J.J. Quantitative determination of target gene with electrical sensor. *Sci. Rep.* **2015**, *5*, 1–7, doi:10.1038/srep12539.

39. Mori, Y.; Nagamine, K.; Tomita, N.; Notomi, T. Detection of loop-mediated isothermal amplification reaction by turbidity derived from magnesium pyrophosphate formation. *Biochem. Biophys. Res. Commun.* **2001**, *289*, 150–154, doi:10.1006/bbrc.2001.5921.
40. Farb, J.N.; Morriscal, S.W. Functional complementation of UvsX and UvsY mutations in the mediation of T4 homologous recombination. *Nucleic Acids Res.* **2009**, *37*, 2336–2345, doi:10.1093/nar/gkp096.
41. Chen, G.; Chen, R.; Ding, S.; Li, M.; Wang, J.; Zou, J.; Du, F.; Dong, J.; Cui, X.; Huang, X.; et al. Recombinase assisted loop-mediated isothermal DNA amplification. *Analyst* **2020**, *145*, 440–444, doi:10.1039/C9AN01701A.
42. Notomi, T.; Okayama, H.; Masubuchi, H.; Yonekawa, T.; Watanabe, K.; Amino, N.; Hase, T. Loop-mediated isothermal amplification of DNA. *Nucleic Acids Res.* **2000**, *28*.
43. Nagamine, K.; Hase, T.; Notomi, T. Accelerated reaction by loop-mediated isothermal amplification using loop primers. *Mol. Cell. Probes* **2002**, *16*, 223–229, doi:10.1006/mcpr.2002.0415.
44. Chander, Y.; Koelbl, J.; Puckett, J.; Moser, M.J.; Klingele, A.J.; Liles, M.R.; Carrias, A.; Mead, D.A.; Schoenfeld, T.W. A novel thermostable polymerase for RNA and DNA loop-mediated isothermal amplification (LAMP). *Front. Microbiol.* **2014**, *5*, 395, doi:10.3389/FMICB.2014.00395/BIBTEX.
45. Markoulatos, P.; Siafakas, N.; Moncany, M. Multiplex polymerase chain reaction: A practical approach. *J. Clin. Lab. Anal.* **2002**, *16*, 47–51, doi:10.1002/jcla.2058.
46. Cai, S.; Jung, C.; Bhadra, S.; Ellington, A.D. Phosphorothioated Primers Lead to Loop-Mediated Isothermal Amplification at Low Temperatures. *Anal. Chem.* **2018**, *90*, 8290–8294, doi:10.1021/acs.analchem.8b02062.
47. Andreola, M.L.; Calmels, C.; Michel, J.; Toulmé, J.J.; Litvak, S. Towards the selection of phosphorothioate aptamers: Optimizing in vitro selection steps with phosphorothioate nucleotides. *Eur. J. Biochem.* **2000**, *267*, 5032–5040, doi:10.1046/j.1432-1327.2000.01557.x.
48. Di Giusto, D.; King, G.C. Single base extension (SBE) with proofreading polymerases and phosphorothioate primers: improved fidelity in single-substrate assays. *Nucleic Acids Res.* **2003**, *31*, doi:10.1093/nar/ngn007.
49. Venna, S.; Eckstein, F. Modified oligonucleotides: Synthesis and strategy for users. *Annu. Rev. Biochem.* **1998**, *67*, 99–134, doi:10.1146/annurev.biochem.67.1.99.
50. Rapley, R. Enhancing PCR amplification and sequencing using DNA-binding proteins. *Mol. Biotechnol.* **1994**, *2*, 295–298, doi:10.1007/BF02745882.
51. Zhang, Y.; Tanner, N.A. Isothermal Amplification of Long, Discrete DNA Fragments Facilitated by Single-Stranded Binding Protein. *Sci. Rep.* **2017**, *7*, 1–9, doi:10.1038/s41598-017-09063-x.
52. Singer, A.; Kuhn, H.; Frank-Kamenetskii, M.; Meller, A. Detection of urea-induced internal denaturation of dsDNA using solid-state nanopores. *J. Phys. Condens. Matter* **2010**, *22*, doi:10.1088/0953-8984/22/45/454111.
53. Martens, K.; Vos, R.; Stakenborg, T.; Lagae, L.; Heyns, M.; Severi, S.; Roy, W. Van; Santermans, S.; Gupta, M.; Hellings, G.; et al. BioFET Technology: Aggressively Scaled pMOS FinFET as Biosensor. *Tech. Dig. - Int. Electron Devices Meet. IEDM 2019, 2019-Decem*, 438–441, doi:10.1109/IEDM19573.2019.8993589.
54. Liu, R.; Chen, R.; Elthakeb, A.T.; Lee, S.H.; Hinckley, S.; Khraiche, M.L.; Scott, J.; Pre, D.; Hwang, Y.; Tanaka, A.; et al. High Density Individually Addressable Nanowire Arrays Record Intracellular Activity from Primary Rodent and Human Stem Cell Derived Neurons. *Nano Lett.* **2017**, *17*, 2757–2764, doi:10.1021/acs.nanolett.6b04752.
55. Dudina, A.; Seichepine, F.; Chen, Y.; Stettler, A.; Hierlemann, A.; Frey, U. Monolithic CMOS sensor platform featuring an array of 9'216 carbon-nanotube-sensor elements and low-noise, wide-bandwidth and wide-dynamic-range readout circuitry. *Sensors Actuators, B Chem.* **2019**, *279*, 255–266, doi:10.1016/j.snb.2018.10.004.
56. Frey, U.; Sedivy, J.; Heer, F.; Pedron, R.; Ballini, M.; Mueller, J.; Bakkum, D.; Hafizovic, S.; Faraci, F.D.; Greve, F.; et al. Switch-matrix-based high-density microelectrode array in CMOS technology. *IEEE J. Solid-State Circuits* **2010**, *45*, 467–482, doi:10.1109/JSSC.2009.2035196.
57. Li, D.C.; Lu, M.S.C. CMOS open-gate ion sensitive field effect transistors for femto-molar dopamine detection. *Proc. IEEE Sensors* **2010**, 419–423, doi:10.1109/ICSENS.2010.5690196.
58. Rani, D.; Pachauri, V.; Madaboosi, N.; Jolly, P.; Vu, X.T.; Estrela, P.; Chu, V.; Conde, J.P.; Ingebrandt, S. Top-Down Fabricated

- Silicon Nanowire Arrays for Field-Effect Detection of Prostate-Specific Antigen. *ACS Omega* **2018**, *3*, 8471–8482, doi:10.1021/ACSOMEGA.8B00990/ASSET/IMAGES/LARGE/AO-2018-00990A_0005.JPEG.
59. Lee, J.; Hong, M.H.; Han, S.; Na, J.; Kim, I.; Kwon, Y.J.; Lim, Y. beom; Choi, H.J. Sensitive and Selective Detection of HIV-1 RRE RNA Using Vertical Silicon Nanowire Electrode Array. *Nanoscale Res. Lett.* **2016**, *11*, 1–7, doi:10.1186/S11671-016-1504-8/FIGURES/6.
60. Gong, W.; Sencar, J.; Bakkum, D.J.; Jäckel, D.; Obien, M.E.J.; Radivojevic, M.; Hierlemann, A.R. Multiple single-unit long-term tracking on organotypic hippocampal slices using high-density microelectrode arrays. *Front. Neurosci.* **2016**, *10*, 537, doi:10.3389/FNINS.2016.00537/BIBTEX.
61. Bellando, F.; Garcia-Cordero, E.; Wildhaber, F.; Longo, J.; Guérin, H.; Ionescu, A.M. Lab on skin™: 3D monolithically integrated zero-energy micro/nanofluidics and FD SOI ion sensitive FETs for wearable multi-sensing sweat applications. *Tech. Dig. - Int. Electron Devices Meet. IEDM* **2018**, 18.1.1-18.1.4, doi:10.1109/IEDM.2017.8268413.
62. Duarte-Guevara, C.; Swaminathan, V.; Reddy, B.; Wen, C.H.; Huang, Y.J.; Huang, J.C.; Liu, Y.S.; Bashir, R. Characterization of a 1024 × 1024 DG-BioFET platform. *Sensors Actuators, B Chem.* **2017**, *250*, 100–110, doi:10.1016/j.snb.2017.04.107.
63. Tomar, S.; Lasne, C.; Barraud, S.; Ernst, T.; Guiducci, C. Integration of Ultra-Low Volume Pneumatic Microfluidics with a Three-Dimensional Electrode Network for On-Chip Biochemical Sensing. *Micromachines* **2021**, *12*, 762, doi:10.3390/mi12070762.
64. Waleed Shinwari, M.; Zhitomirsky, D.; Deen, I.A.; Selvaganapathy, P.R.; Jamal Deen, M.; Landheer, D. Microfabricated reference electrodes and their biosensing applications. *Sensors* **2010**, *10*, 1679–1715.
65. Unger, M.A. Monolithic Microfabricated Valves and Pumps by Multilayer Soft Lithography. *Science (80-.)*. **2000**, *288*, 113–116, doi:10.1126/science.288.5463.113.
66. Rabarot, M.; Bablet, J.; Ruty, M.; Kipp, M.; Chartier, I.; Dubarry, C. Thick SU-8 photolithography for BioMEMS. *Micromach. Microfabr. Process Technol. VIII* **2003**, 4979, 382, doi:10.1117/12.478244.
67. Ezkerra, A.; Ferrández, L.J.; Mayora, K.; Ruano-López, J.M. Fabrication of SU-8 free-standing structures embedded in microchannels for microfluidic control. *J. Micromechanics Microengineering* **2007**, *17*, 2264–2271, doi:10.1088/0960-1317/17/11/013.
68. Dellmann, L.; Roth, S.; Beuret, C.; Racine, G.A.; Lorenz, H.; Despont, M.; Renaud, P.; Vettiger, P.; de Rooij, N.F. Fabrication proces of high aspect ratio elastic structures for piezoelectric motor applications. In Proceedings of the International Conference on Solid-State Sensors and Actuators, Proceedings; 1997; Vol. 1, pp. 641–644.
69. Lau, K.H.; Giridhar, A.; Harikrishnan, S.; Satyanarayana, N.; Sinha, S.K. Releasing high aspect ratio SU-8 microstructures using AZ photoresist as a sacrificial layer on metallized Si substrates. *Microsyst. Technol.* **2013**, *19*, 1863–1871, doi:10.1007/s00542-013-1740-0.
70. Byun, I.; Coleman, A.W.; Kim, B. Transfer of thin Au films to polydimethylsiloxane (PDMS) with reliable bonding using (3-mercaptopropyl)trimethoxysilane (MPTMS) as a molecular adhesive. *J. Micromechanics Microengineering* **2013**, *23*, doi:10.1088/0960-1317/23/8/085016.
71. Yeo, H.G.; Jung, J.; Sim, M.; Jang, J.E.; Choi, H. Integrated piezoelectric ALN thin film with SU-8/PDMS supporting layer for flexible sensor array. *Sensors (Switzerland)* **2020**, *20*, doi:10.3390/s20010315.
72. Heyries, K.A.; Tropini, C.; VanInsberghe, M.; Doolin, C.; Petriv, O.I.; Singhal, A.; Leung, K.; Hughesman, C.B.; Hansen, C.L. Megapixel digital PCR. *Nat. Methods* **2011**, *8*, 649–651, doi:10.1038/nmeth.1640.
73. Zhu, Q.; Qiu, L.; Yu, B.; Xu, Y.; Gao, Y.; Pan, T.; Tian, Q.; Song, Q.; Jin, W.; Jin, Q.; et al. Lab on a Chip Digital PCR on an integrated self-priming compartmentalization chip †. **2014**, *14*, 1176, doi:10.1039/c3lc51327k.
74. Heyries, K.A.; Tropini, C.; VanInsberghe, M.; Doolin, C.; Petriv, O.I.; Singhal, A.; Leung, K.; Hughesman, C.B.; Hansen, C.L. Suppl - Megapixel digital PCR. *Nat. Methods* **2011**, *8*, 649–651, doi:10.1038/nmeth.1640.
75. Rohaizad, N.; Mayorga-Martinez, C.C.; Novotný, F.; Webster, R.D.; Pumera, M. 3D-printed Ag/AgCl pseudo-reference electrodes. *Electrochem. commun.* **2019**, *103*, 104–108, doi:10.1016/j.elecom.2019.05.010.
76. Ito, S.; Hachiya, H.; Baba, K.; Asano, Y.; Wada, H. Improvement of the silver/silver chloride reference electrode and its application to pH measurement. *Talanta* **1995**, *42*, 1685–1690, doi:10.1016/0039-9140(95)01628-7.

77. Kang, D.K.; Ali, M.M.; Zhang, K.; Huang, S.S.; Peterson, E.; Digman, M.A.; Gratton, E.; Zhao, W. Rapid detection of single bacteria in unprocessed blood using Integrated Comprehensive Droplet Digital Detection. *Nat. Commun.* **2014**, *5*, 1–10, doi:10.1038/ncomms6427.
78. Abasiyanik, M.F.; Wolfe, K.; Van Phan, H.; Lin, J.; Laxman, B.; White, S.R.; Verhoef, P.A.; Mutlu, G.M.; Patel, B.; Tay, S. Ultrasensitive digital quantification of cytokines and bacteria predicts septic shock outcomes. *Nat. Commun.* **2020**, *11*, 1–12, doi:10.1038/s41467-020-16124-9.
79. Wilson, D.H.; Rissin, D.M.; Kan, C.W.; Fournier, D.R.; Piech, T.; Campbell, T.G.; Meyer, R.E.; Fishburn, M.W.; Cabrera, C.; Patel, P.P.; et al. The Simoa HD-1 Analyzer: A Novel Fully Automated Digital Immunoassay Analyzer with Single-Molecule Sensitivity and Multiplexing. *J. Lab. Autom.* **2016**, *21*, 533–547, doi:10.1177/2211068215589580.
80. Diaz, L.A.; Bardelli, A. Liquid Biopsies: Genotyping Circulating Tumor DNA. *J Clin Oncol* **2014**, *32*, 579–586, doi:10.1200/JCO.2012.45.2011.
81. Hassibi, A.; Manickam, A.; Singh, R.; Bolouki, S.; Sinha, R.; Jirage, K.B.; McDermott, M.W.; Hassibi, B.; Vikalo, H.; Mazarei, G.; et al. Multiplexed identification, quantification and genotyping of infectious agents using a semiconductor biochip. *Nat. Biotechnol.* **2018**, *36*, doi:10.1038/nbt.4179.
82. Wang, X.; Shang, X.; Huang, X. Next-generation pathogen diagnosis with CRISPR/Cas-based detection methods. *Emerg. Microbes Infect.* **2020**, *9*, 1682–1691, doi:10.1080/22221751.2020.1793689.
83. Swank, Z.; Michielin, G.; Yip, H.M.; Cohen, P.; Andrey, D.O.; Vuilleumier, N.; Kaiser, L.; Eckerle, I.; Meyer, B.; Maerkl, S.J. A high-throughput microfluidic nanoimmunoassay for detecting anti-SARS-CoV-2 antibodies in serum or ultralow-volume blood samples. *Proc. Natl. Acad. Sci. U. S. A.* **2021**, *118*, doi:10.1073/PNAS.2025289118.
84. Goto, M.; Honda, E.; Ogura, A.; Nomoto, A.; Hanaki, K.I. Colorimetric detection of loop-mediated isothermal amplification reaction by using hydroxy naphthol blue. *Biotechniques* **2009**, *46*, 167–172.
85. Oscorbin, I.P.; Belousova, E.A.; Zakabunin, A.I.; Boyarskikh, U.A.; Filipenko, M.L. Comparison of fluorescent intercalating dyes for quantitative loop-mediated isothermal amplification (qLAMP). *Biotechniques* **2016**, *61*, 20–25, doi:10.2144/000114432/ASSET/IMAGES/LARGE/FIGURE3.JPEG.
86. Tomita, N.; Mori, Y.; Kanda, H.; Notomi, T. Loop-mediated isothermal amplification (LAMP) of gene sequences and simple visual detection of products. *Nat. Protoc.* **2008**, *35*, **2008**, *3*, 877–882, doi:10.1038/nprot.2008.57.
87. Ball, C.S.; Light, Y.K.; Koh, C.-Y.; Wheeler, S.S.; Coffey, L.L.; Meagher, R.J. Quenching of Unincorporated Amplification Signal Reporters in Reverse-Transcription Loop-Mediated Isothermal Amplification Enabling Bright, Single-Step, Closed-Tube, and Multiplexed Detection of RNA Viruses. *Anal. Chem* **2016**, *88*, 2021, doi:10.1021/acs.analchem.5b04054.
88. Men, Y.; Fu, Y.; Chen, Z.; Sims, P.A.; Greenleaf, W.J.; Huang, Y. Digital Polymerase Chain Reaction in an Array of Femtoliter Polydimethylsiloxane Microreactors. *Anal. Chem.* **2012**, *84*, 4262–4266, doi:10.1021/AC300761N.
89. R. Kubota; A. M. Alvarez; W.W. Su; D. M. Jenkins FRET-Based Assimilating Probe for Sequence-Specific Real-Time Monitoring of Loop-Mediated Isothermal Amplification (LAMP). *Biol. Eng. Trans.* **2011**, *4*, 81–100, doi:10.13031/2013.38509.
90. Tanner, N.A.; Zhang, Y.; Evans, T.C. Simultaneous multiple target detection in real-time loop-mediated isothermal amplification. *Biotechniques* **2012**, *53*, 81–89, doi:10.2144/0000113902.
91. Shoffner, M.A.; Cheng, J.; Hvichia, G.E.; Kricka, L.J.; Wilding, P. Chip PCR. I. Surface Passivation of Microfabricated Silicon-Glass Chips for PCR. *Nucleic Acids Res.* **1996**, *24*, 375–379, doi:10.1093/NAR/24.2.375.
92. Krishnan, M.; Burke, D.T.; Burns, M.A. Polymerase chain reaction in high surface-to-volume ratio SiO₂ microstructures. *Anal. Chem.* **2004**, *76*, 6588–6593, doi:10.1021/AC0488356/ASSET/IMAGES/LARGE/AC0488356F00005.JPEG.
93. Basu, A.S. Digital Assays Part I: Partitioning Statistics and Digital PCR. *SLAS Technol.* **2017**, *22*, 369–386, doi:10.1177/2472630317705680.
94. Kreutz, J.E.; Munson, T.; Huynh, T.; Shen, F.; Du, W.; Ismagilov, R.F. Theoretical design and analysis of multivolume digital assays with wide dynamic range validated experimentally with microfluidic digital PCR. *Anal. Chem.* **2011**, *83*, 8158–8168, doi:10.1021/AC201658S/SUPPL_FILE/AC201658S_SI_002.ZIP.
95. Accastelli, E.; Scarbolo, P.; Ernst, T.; Palestri, P.; Selmi, L.; Guiducci, C. Multi-wire tri-gate silicon nanowires reaching milli-

- pH unit resolution in one micron square footprint. *Biosensors* **2016**, *6*, 1–10, doi:10.3390/bios6010009.
96. Khan, Z.A.; Siddiqui, M.F.; Park, S. Current and emerging methods of antibiotic susceptibility testing. *Diagnostics* **2019**, *9*, doi:10.3390/diagnostics9020049.
 97. Nordmann, P.; Dortet, L.; Poirel, L. Rapid detection of extended-spectrum- β -lactamase-producing Enterobacteriaceae. *J. Clin. Microbiol.* **2012**, *50*, 3016–3022, doi:10.1128/JCM.00859-12.
 98. Sánchez-Clemente, R.; Igeño, M.I.; Población, A.G.; Guijo, M.I.; Merchán, F.; Blasco, R. Study of pH Changes in Media during Bacterial Growth of Several Environmental Strains. **2018**, 1297, doi:10.3390/proceedings2201297.
 99. Kohn, A.B.; Moroz, T.P.; Barnes, J.P.; Netherton, M.; Moroz, L.L. *Single-cell semiconductor sequencing*; 2013; Vol. 1048; ISBN 9781627035552.
 100. Villamil, C.; Calderon, M.N.; Arias, M.M.; Leguizamon, J.E. Validation of Droplet Digital Polymerase Chain Reaction for Salmonella spp. Quantification. *Front. Microbiol.* **2020**, *11*, doi:10.3389/fmicb.2020.01512.
 101. Liu, W.W.; Zhu, Y.; Feng, Y.M.; Fang, J.; Fang, Q. Droplet-Based Multivolume Digital Polymerase Chain Reaction by a Surface-Assisted Multifactor Fluid Segmentation Approach. *Anal. Chem.* **2017**, *89*, 822–829, doi:10.1021/acs.analchem.6b03687.
 102. Zarkadas, G.M.; Stergiou, A.; Papanastasiou, G. Silver electrodeposition from AgNo₃ solutions containing organic additives: Electrodeposition from binary water-methanol solvent systems in the presence of tartaric acid. *J. Appl. Electrochem.* **2004**, *34*, 607–615, doi:10.1023/B:JACH.0000021920.59845.4c.

Curriculum Vitae

Saurabh Tomar

Email: saurabhtomar@protonmail.ch

Phone: +41 789567713

Avenue du Tir Federal 92, Ecublens – 1024, Switzerland

EDUCATION

École Polytechnique Fédérale de Lausanne	Lausanne, Switzerland
<ul style="list-style-type: none"> • Doctoral Program in Microsystems and Microelectronics 	2017-present
École Polytechnique Fédérale de Lausanne	Lausanne, Switzerland
Institut Polytechnique de Grenoble	Grenoble, France
Politecnico di Torino	Turin, Italy
<ul style="list-style-type: none"> • Master in Micro and Nanotechnologies for Integrated Systems 	2013-2015
Indian Institute of Technology, Delhi	New Delhi, India
<ul style="list-style-type: none"> • Bachelor in Engineering Physics 	2009-2013

EXPERIENCE

École Polytechnique Fédérale de Lausanne	Lausanne, Switzerland
Doctoral Assistant with Prof. Carlotta Guiducci	06/2017 – present
My doctoral research is on nucleic acid amplification detection using silicon nanowire Ion Sensitive Field Effect Transistors (ISFETs). The interdisciplinary work has been at the intersection of microfluidics and CMOS for biosensing, where I:	
<ul style="list-style-type: none"> • Developed a process flow for a microfluidic design that eliminates post-processing of CMOS chips. • Troubleshoot various microfluidic packaging issues due to unorthodox nature of the process flow. • Developed RPA and LAMP based molecular assays for CMOS based biosensing. • Demonstrated real-time detection of DNA amplification in nanoliter-sized volume. 	
Stanford University	Stanford, USA
Visiting Student Researcher with Prof. Polly Fordyce	10/2019-12/2019
<ul style="list-style-type: none"> • Designed and validated a molecular diagnostic assay to detect sepsis causing fungal pathogens. • Used spectrally encoded beads to capture and detect amplified DNA of more than 25 pathogens. 	
École Polytechnique Fédérale de Lausanne	Lausanne, Switzerland
Research Assistant with Prof. Adrian Ionescu	02/2015 – 03/2016
<ul style="list-style-type: none"> • Worked on designing and fabrication of high-K charge trapping gate stack based vertical Tunnel FET non-volatile memory in class 100 cleanroom. • Performed extensive cleanroom metrology to maintain fidelity of 30 steps long process flow. • Performed extensive electrical characterization on the memory devices to measure I-V curves, variations in threshold voltage shift, program/erase speed, endurance and retention. 	
National Chiao Tung University	Hsinchu, Taiwan
Intern with Prof. Yiming Li	06/2014 – 08/2014
<ul style="list-style-type: none"> • Performed TCAD simulation of Gate-All-Around Silicon Nanowire MOSFET for 10nm technology node to see the effect of channel shape on the transfer characteristics. • I-V characteristics of channels with varying ellipsoidal cross section were simulated, in both single channel and multi-channel configuration. 	

TECHNICAL SKILLS

Cleanroom: 6+ years of experience in class 100 cleanroom (CMi) involving fabrication on SOI wafers.

- Thin Film: Atomic Layer Deposition, Evaporation, Sputtering, Rapid Thermal Processing.
- Photolithography: Mask fabrication, Photoresist coating, Exposure and Development tools.
- Etching: Deep RIE, Dry etch, Wet Etch, Ion Beam Etch.
- Meteorology: SEM, EDX, Ellipsometer, FIB, AFM, Profilometer, Optical Microscopy.
- Miscellaneous: Stencil lithography, PDMS, SU-8 process, Electrochemical deposition/etching

Characterization: Strong experience in DC/AC electrical characterization tools for semiconductor devices.

- Semiconductor parameter analyzer, LCR meter, Function generator, Switching matrix (Agilent).
- Semi-automated and manual probe station (Cascade Microtech, Summit 12000, Karl Suss PM8).
- Cryogenic probe system (SUSS MicroTec) - 77K-400K under normal and high vacuum.

Simulation/Programming Tools:

- CAD – L-edit
- EDA suite – Cadence Virtuoso (Full Custom, Semi-Custom and Verification).
- Device Modeling – Synopsys Sentarus, COMSOL, Silvaco, Ansys.
- Languages – Python, VHDL, C, Java.

INVITED TALK

- Invited talk as junior scientist on “Multiplexed Nucleic Acid Amplification Detection on Silicon Chips” at Frontiers in NanoBio Engineering and Medicine – 2018 at EPFL.

PATENTS

- Currently an EU patent application on microfluidic design and manufacturing process filed.

LANGUAGES

- HINDI: Mother Tongue
- ENGLISH: Fluent spoken and written (C1)
- FRENCH: Beginners Level (A2)

OTHER ACTIVITIES

- I like sports climbing and Olympic Weightlifting.